MAJOR AND TRACE ELEMENT GEOCHEMISTRY OF BASALTS FROM THE EXPLORER AREA, NORTHEAST PACIFIC OCEAN

by

BRIAN LLOYD COUSENS
B. Sc., McGill University, 1979

A THESIS SUBMITTED IN PARTIAL FULFILMENT OF
THE REQUIREMENTS FOR THE DEGREE OF
MASTER OF SCIENCE

in

THE FACULTY OF GRADUATE STUDIES
(Department of Geological Sciences)

We accept this thesis as conforming
to the required standard

THE UNIVERSITY OF BRITISH COLUMBIA

April 1982

In presenting this thesis in partial fulfilment of the requirements for an advanced degree at the University of British Columbia, I agree that the Library shall make it freely available for reference and study. I further agree that permission for extensive copying of this thesis for scholarly purposes may be granted by the head of my department or by his or her representatives. It is understood that copying or publication of this thesis for financial gain shall not be allowed without my written permission.

Department of Geological Sciences.

The University of British Columbia
2075 Wesbrook Place
Vancouver, Canada
V6T 1W5

Date April 2nd, 1982

ABSTRACT

Fifty fragments of young, fresh basalts from the Explorer Ridge, Paul Revere Ridge (Fracture Zone), Dellwood Knolls, and the J. Tuzo Wilson Knolls have been analysed for 12 major and minor elements, as well as 11 trace elements, by X-ray fluorescence spectrometry. Rare earth element concentrations in 25 of the samples have been determined by instrumental neutron activation, and Sr^{87}/Sr^{86} ratios have been obtained for 11 of the basalts.

The Explorer Ridge basalts have major element compositions similar to most mid-ocean ridge basalts (MORB), and can be classified as ferrobasalts, similar to those of the southern Juan de Fuca Ridge. The incompatible minor and trace elements K, Ti, Rb, Zr, and Nb are weakly to strongly enriched in the Explorer samples, with respect to MORB, part of which is the result of crystal fractionation. The observed trace element and light rare earth element (LREE) enrichment of many of the samples, particularly those from Explorer Deep, suggest that a weak hotspot may exist beneath the Explorer Deep. The adjacent ridge segments, Explorer Rift and the Southern Explorer Ridge, are erupting basalts both enriched and depleted in incompatible elements, which could be an indicator of a chemically heterogenous mantle source, or may be the result of intermittent injection of enriched magmas from the postulated hotspot beneath Explorer Deep into areas producing normal MORB. The enriched basalts do not have significantly different Sr^{87}/Sr^{86} ratios from the depleted basalts. All the samples fall within the range of values typical for Juan de Fuca and Gorda Ridge basalts, and East Pacific Rise tholeiites in general. Thus, although the source areas for the 2 basalt types may differ chemically, they are similar radiogenically, unlike other hypothetically plume-influenced areas such as the Mid-Atlantic Ridge at 45° N and the FAMOUS area.

The basalts from the northwest and southeast Dellwood Knolls appear to be related by crystal fractionation, based on major element analysis. However,

the very different REE patterns and Sr^{87}/Sr^{86} ratios exhibited by the two knolls suggest that they have different mantle sources, one typically depleted (northwest knoll) and one chemically and radiogenically enriched (southeast knoll).

In terms of their major and trace element chemistry, the J. Tuzo Wilson Knolls basalts are typical of late-stage volcanism on ocean islands associated with mantle plumes. The hawaiites strongly resemble alkali basalts dredged from several seamounts in the Pratt-Welker Chain, which are co-latitudinal with the J. Tuzo Wilson Knolls on a small circle about the Pacific-Hotspot pole of rotation. Geochronological evidence questions the hypothesis that the mantle plume responsible for Pratt-Welker volcanism is also the source for the J. Tuzo Wilson basalts. The existence of a second mantle plume, 300 km southeast of the first, would explain minor chemical and physiographical differences between the Knolls and the other Pratt-Welker seamounts, as well as the evidence for two phases of volcanism on the southeastern seamounts of the chain. A second plume also explains the coeval volcanism of Bowie Seamount and the J. Tuzo Wilson Knolls.

Recent geophysical evidence suggests that the J. Tuzo Wilson Knolls are also part of the Explorer-Dellwood spreading system. Although the JTW basalts are plume-type basalts chemically, the situation appears to be somewhat analagous to other ridge segments where plumes are coincident with the ridge itself.

TABLE OF CONTENTS

Table of Contents, continued.

LIST OF TABLES

LIST OF PLATES AND FIGURES

List of Plates and Figures, continued.

ACKNOWLEDGEMENTS

I first thank R.L. Chase and R.L. Armstrong for guidance in this project. Stanya Horsky, Rob Berman, and Graham Nixon assisted with analytical procedures and computer programming, as well as discussion of results. Discussions with W.K. Fletcher, R.P. Riddihough, R.G. Currie, and R.D. Hyndman were also helpful. E. Montgomery carefully prepared photographs for the manuscript.

R.L. Chase, Arnie Thomlinson, Guy Beland, Ken Hansen, and others involved with sea-floor study at the University of British Columbia, created the UBC basalt collection, from which samples for this study were selected. The cooperation of the officers and crews of the CSS PARIZEAU, CNAV ENDEAVOUR, and CSS HUDSON, is appreciated by all concerned.

R.L. Chase, R.L. Armstrong, and K.C. Mc Taggart critically reviewed the thesis manuscript.

Collection of the basalts studied in this paper has involved grants from the following agencies to R.L. Chase, and jointly to R.L. Chase, J.W. Murray, and E.V. Grill: the Defense Research Board of Canada; the National Research Council and the Natural Science and Engineering Research Council of Canada; Energy, Mines, and Resources Canada; the Ministry of Energy, Mines, and Petroleum Resources of British Columbia; Placer Development Ltd.; Cominco Ltd; and the University of British Columbia.

Funding for this project was in the form of a university grant to R.L. Chase, as well as grants from EMR and NSERC.

INTRODUCTION

The Juan de Fuca-Gorda Ridge system, the northern extension of the East Pacific Rise in the northeast Pacific, is one of the most extensively studied ocean ridge systems in the world (Kay et al., 1970; Moore, 1970; Barr and Chase, 1974; Vogt and Byerly, 1976; Clague and Bunch, 1976; Wakeham, 1977; Liias et al., 1982), but the basalt geochemistry of the spreading segments north of the Sovanco Fracture Zone (Figure 2) has received relatively little attention. This is the first study of basalt geochemistry on the Explorer Ridge, and partially completes a project initiated in 1970 by A.G. Thomlinson, but not finished. This paper also presents trace element data for the Dellwood Knolls spreading segment, and the J. Tuzo Wilson Knolls.

Several questions concerning basalt chemistry of the Explorer area can be addressed:

(i) Are Explorer basalts chemically similar to other mid-ocean ridge basalts (MORB)? Where do they fit in the Melson et al. (1976) classification of ocean ridge tholeiites? Do the basalts resemble those from the northern Juan de Fuca (Barr and Chase, 1974) or the southern Juan de Fuca Ridge (Wakeham, 1977), or are they chemically distinct from both?

(ii) Do any familiar geochemical patterns exist within the Explorer-Dellwood system? If so, what process(es) can explain them?

(iii) If the J. Tuzo Wilson Knolls are the surface expression of a mantle plume or hotspot, is there evidence for magma mixing of the plume basalts with ocean ridge basalts, in the form of chemical gradients, as has been observed on the Reykjanes Ridge (Schilling, 1973) or on the Azores Platform (Schilling, 1975)?

(iv) Is there any chemical evidence to suggest that the J. Tuzo Wilson Knolls are part of a spreading ridge, as is indicated by geophysical observations?

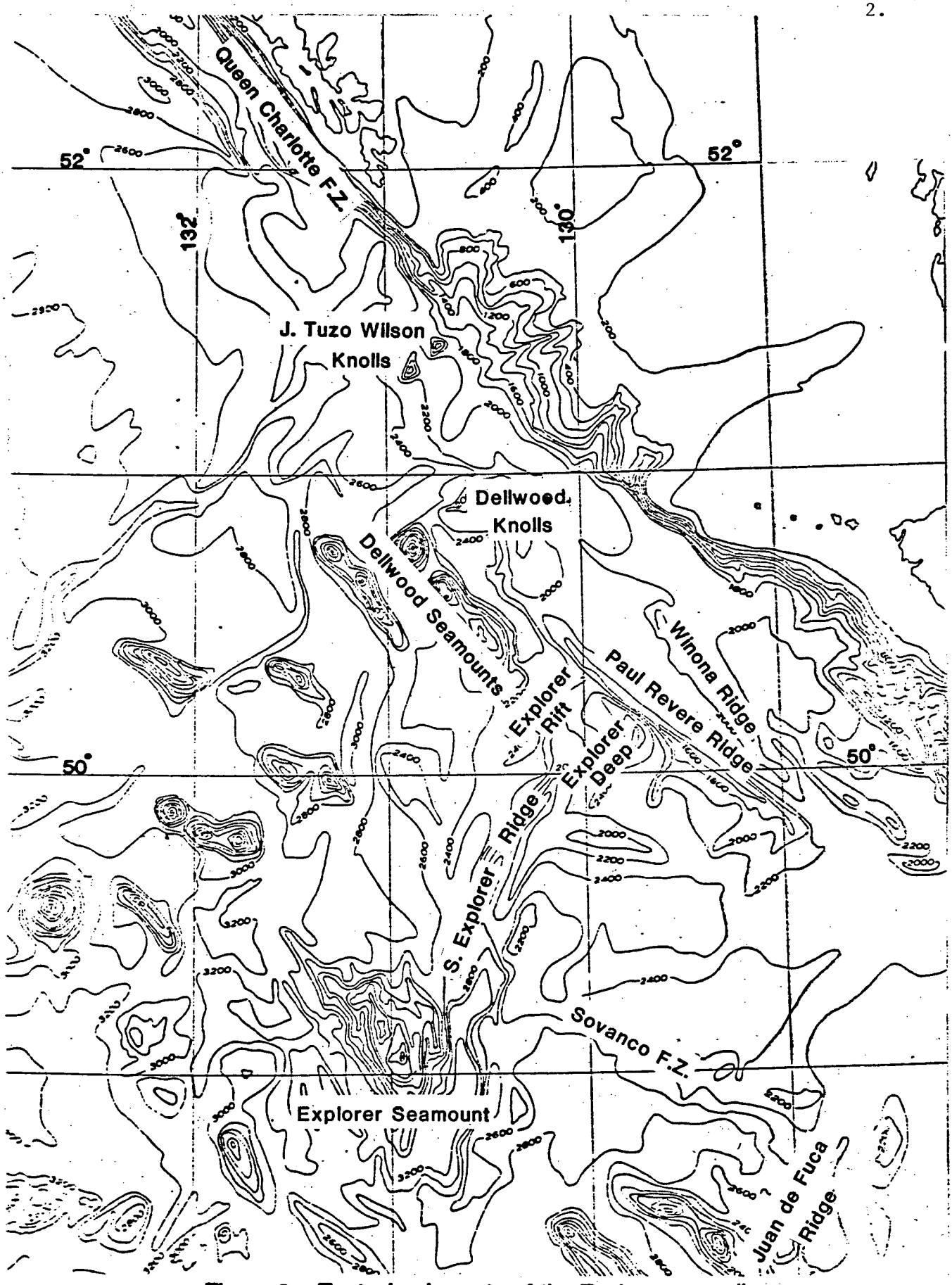

Figure 2 : Tectonic elements of the Explorer spreading area.

Physiography and Tectonic History

The spreading segments of the Explorer area are physiographically variable. The southern Explorer Ridge (Figure 2) does not possess a well-developed axial trough, similar to most fast-spreading ridges, although seismic reflection profiles (CSP) do show faulting in the central ridge area. The southern end of the ridge is very poorly expressed bathymetrically. In contrast, the Explorer Deep and Explorer Rift are well-developed, graben-like rift zones, that lack high flanking walls. To the northeast, they are abruptly terminated by the Revere-Dellwood Fault Zone. The Dellwood Knolls are two heavily-faulted volcanic ridges with peaks, 400 to 500 meters above the seafloor, separated by the disturbed, sediment-filled, Dellwood Spreading Zone (Bertrand, 1972). The Knolls terminate to the southwest at the Revere-Dellwood transform. CSP data reveals that the Knolls terminate before the continental rise to the east, and that the intervening sedimentary pile is heavily faulted. The J. Tuzo Wilson Knolls (JTW) are two irregularly-shaped, 500 meter high, NE-SW elongate peaks, aligned northeast-southwest. CSP profiles (Chase, 1977) indicate that the steep-sided knolls penetrate a thick sedimentary blanket.

The magnetic anomaly pattern of the Juan de Fuca Ridge area (Raff and Mason, 1961) was used by Wilson (1965) and Vine and Wilson (1965) to demonstrate sea-floor spreading. A magnetic-anomaly-based tectonic model for recent plate interactions in the Juan de Fuca-Explorer area was first developed by Riddihough (1977), and has been revised by Davis and Riddihough (1982). Figure 4 illustrates sequence of events in the evolution of the ridge:

4 Ma BP

The Pacific-America-Explorer triple junction lies near the Brooks Peninsula. Predominantly right lateral transform motion with a small component of convergence occurs between the Pacific and America plates along the margin northwest of the junction. Nearly normal convergence

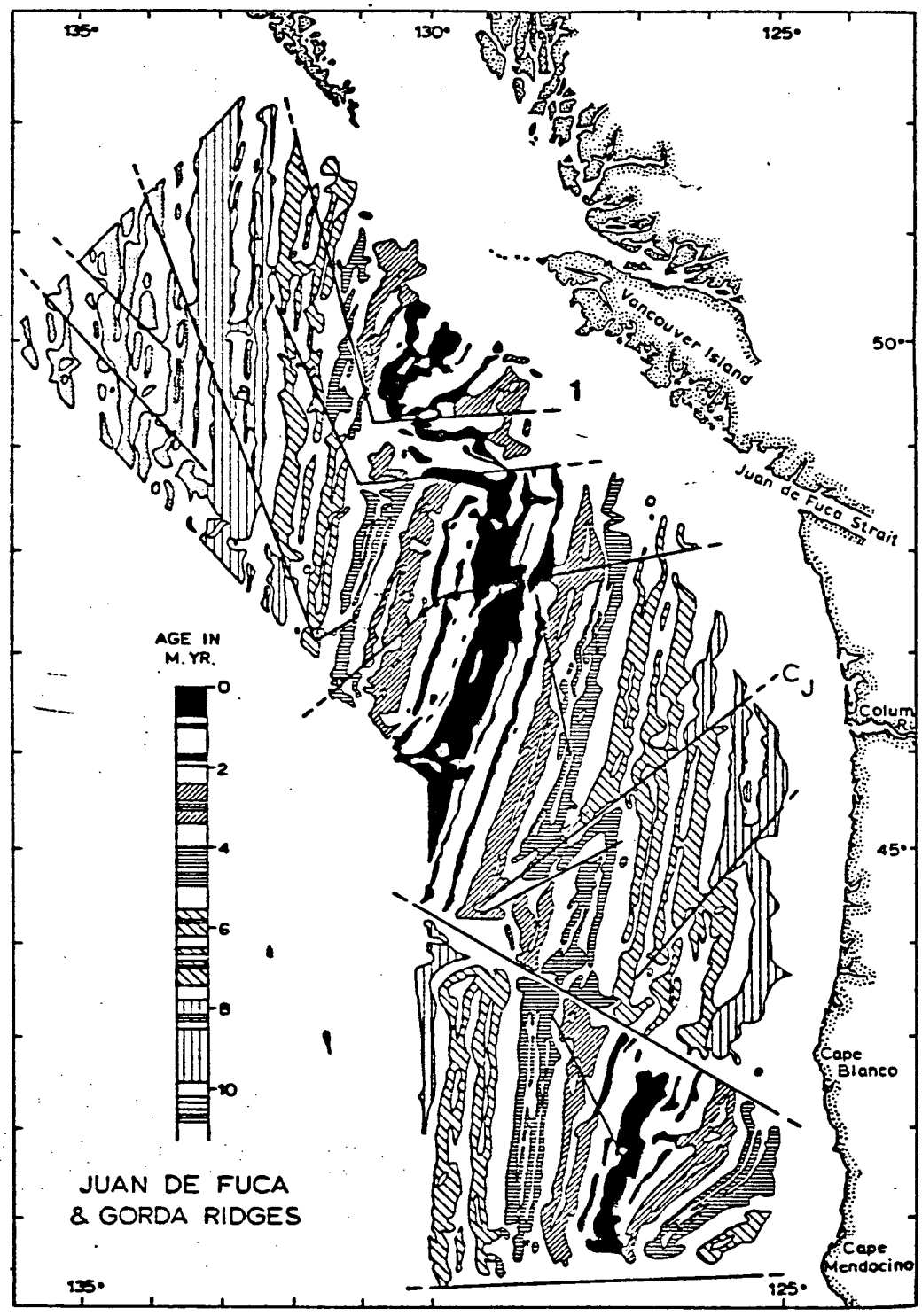

Figure 3 : Raff and Mason (1961) magnetic anomaly map of the Juan de Fuca area. Straight lines are pseudofaults as proposed by Vine (1968), and are interpreted to be a result of ridge propagation (Hey, 1977). Brunhes anomaly in black.

occurs along the margin to the southeast of the junction. Rapid sedimentation near the base of the continental margin causes magnetization of the crust to be reduced. A small left lateral transform is initiated on the ridge (this will become the Paul Revere transform).

3 Ma BP

The lengthening left lateral fracture zone migrates northwards, and along with the ridge system, acts as a sediment barrier, possibly shortening the length of the section of ridge which produces poorly magnetized crust.

1.5-2.0 Ma BP

Flexural stresses associated with the interaction of the Pacific plate at the margin (including convergence and sediment loading) cause normal faulting near and along the inactive trace of the fracture zone, which is now within 80 km of, and subparallel to, the margin. A Winona Basin lithospheric block becomes partly decoupled from the Pacific Plate; assymmetric subsidence of the Winona Basin and uplift of the Paul Revere Ridge begins.

1 Ma BP

Spreading on the section of the ridge off northern Vancouver Island stops and transfers to a new postion in old crust near the western end of the fracture zone (Dellwood Knolls). A Winona lithospheric block is thus fully isolated and ceases to move with the Pacific Plate. This critical change in configuration may have been caused by the resistance to the 5-6 cm/yr Pacific Plate partial strike-slip interaction between the small, partly decoupled Winona Basin block, and the continent.

1 Ma BP to present

Spreading on the Explorer Ridge migrates northwestwards by assymmetric spreading, eventually splitting and jumping to its most recent position (Explorer Rift). The Winona block continues to tilt and subside and the thickening sediment fill continues to deform as a result of convergence with the continent.

(from Davis and Riddihough, 1982)

The History of the Explorer spreading area has been one of gradual breakup of a single ridge into several smaller segments. This has been

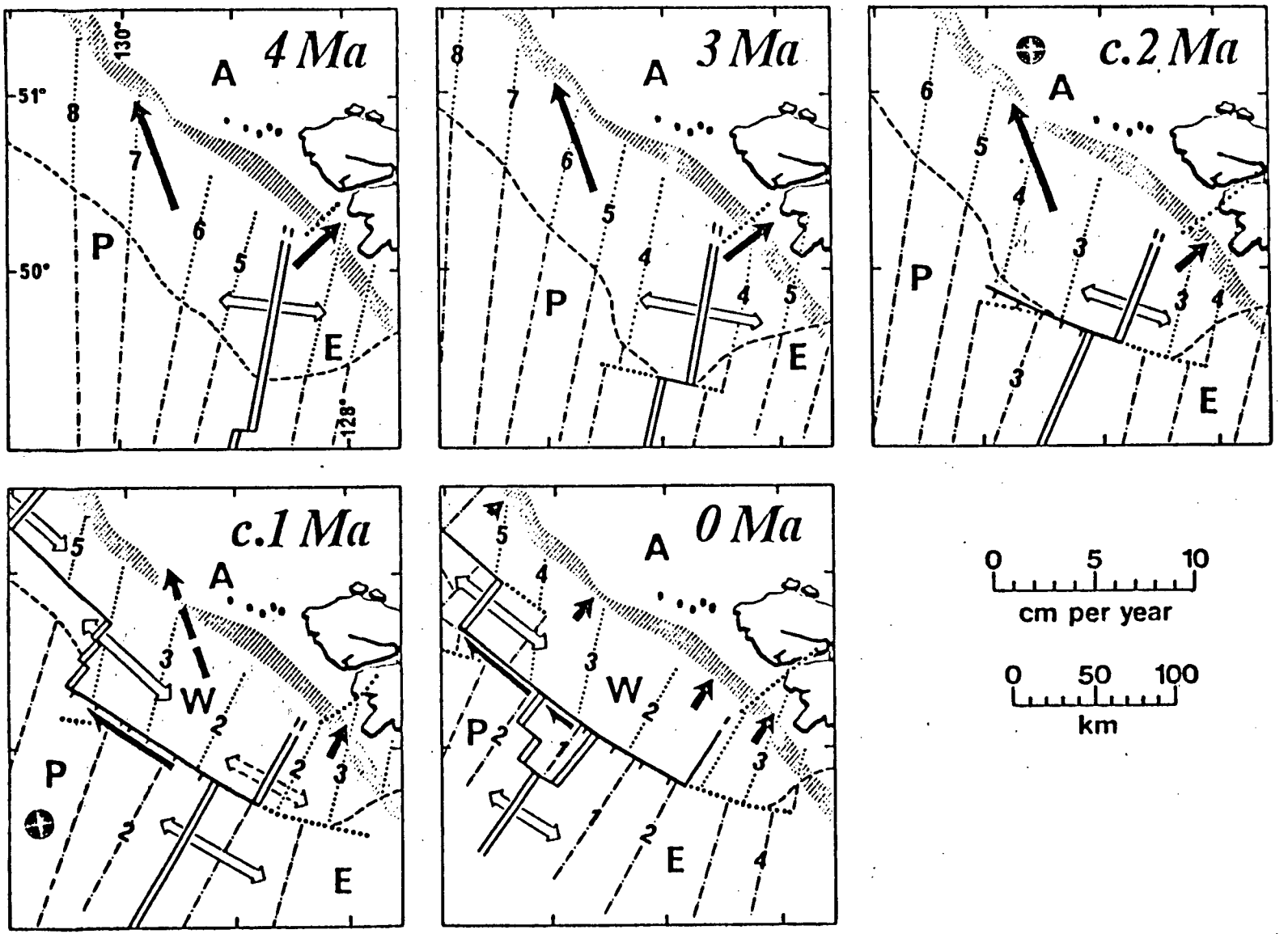

Figure 4 : Tectonic analysis and history of the Explorer area. Davis & Riddihough (1982).

accompanied by clockwise rotation of the direction of spreading, such that it is presently parallel to the margin. The Explorer Plate now moves independently of the Juan de Fuca Plate (Riddihough, 1977). The reason for the rotation of the ridge segments is probably related to the relatively unstable subduction regime east of the ridge. Relatively young crust is being subducted, and as such, is still hot and bouyant, resulting in increased resistance to subduction. By rotating, the subduction rate is lowered to a minimum, and less work is required.

Even though spreading "jumped" from Explorer Deep to Explorer Rift during the last million years, both rifts are seismically active, and fresh basalts have been dredged from each one in more than one location.

Previous Work

Bertrand (1972) completed the initial petrologic and tectonic analysis of the Dellwood Knolls, although his chemical and petrologic data applied to only two successful dredge hauls. The Dellwood basalts are chemically intermediate between tholeiitic and alkali basalt. Thick manganese encrustations on the basalt fragments suggest that the basalts from the southeast knoll are older than basalts from the northwest knoll. The more differentiated nature of the southeast knoll basalts indicate that they were erupted further away from the spreading center. It appears that the southeast knoll has ceased activity, while the northwest knoll is still active. Suggested ages for the knolls are 0.2-1 Ma for the northwest knoll, and 1-2 Ma for the southeast knoll (Bertrand, 1972).

Trace element contents and Sr isotope data for Dellwood Knolls sample 70-25-2D-8 were obtained by Armstrong and Nixon (1980). The values were similar to those of normal MORB.

Chase (1977) published major element data on the J. Tuzo Wilson Knolls

basalts, based on two dredge hauls from the southwest peak. The basalts are hawaiites, similar to late-stage alkalic volcanic rocks found on ocean islands associated with mantle plumes, or "hotspots". The JTW Knolls lie on the same Pacific-Hotspot colatitude as the seamounts in the Pratt-Welker Seamount Chain, which includes Bowie Seamount and Kodiak Seamount. Assuming the rate of rotation about the PCFC-HSPT pole of Minster et al.(1974), Chase concluded that the hotspot responsible for the Pratt-Welker Chain is presently beneath the JTW area. A K-Ar date of 54,000 yrs was obtained for one of the basalt fragments (Table 1).

A recent geochronological study of the Pratt-Welker Chain (Turner et al., 1980) suggests, however, that the hotspot lies 250-300 km northwest of the JTW area, based on a K-Ar date from Bowie Seamount of 74,000 yrs. Interestingly, two phases of volcanism, spaced 10 million years apart, have been identified on the southeastern seamounts of the chain.

Geophysical evidence indicates that the JTW Knolls may be the newest segment of spreading ridge on the Explorer-Dellwood system (Keen and Hyndman, 1979; R.D. Hyndman, personal communication). Seismicity suggests that a transform fault exists between the Dellwood and JTW Knolls.

Several geophysical surveys have been performed over the Explorer area. These include magnetic, bathymetric, gravity, heat flow, and seismic reraction studies (Srivastava et al.,1971; Tiffin and Seeman, 1975; Malacek and Clowes, 1976; Hyndman et al.,1978; Riddihough et al.,1980).

Sample Collection

Basalts from the Explorer Ridge and the Paul Revere Fracture Zone (Figure 1) were collected by A.G. Thomlinson and R.L. Chase between 1970 and 1972, as part of a Ph. D. program that was not completed. Fresh basalts from Explorer Rift (1977) and Explorer Deep (1979) were collected by G. Beland and K. Hansen, along with R.L. Chase, in the course of sedimentological and bathymetric

TABLE 1

K-Ar Analytical Data and Age Determination for

J. Tuzo Wilson Knolls

SAMPLE: 73-26-2-1C

POSITION: 51° 24′ 30″ N latitude, 131° 02′ W longitude.

MATERIAL ANALYSED: Basalt- whole rock

POTASSIUM CONTENT: (%K): 2.025±0.023% (average of 2 analyses)

Ar^{40r}/total Ar^{40}: 0.0079

Ar^{40r} (10^{-5}cc STP/g): 4.366×10^{-4}

Ar^{40r}/K^{40}: 3.161×10^{-6}

APPARENT AGE: 55,000±100% yrs.

Constants used: $\lambda_\varepsilon = 0.581 \times 10^{-10}\,yr^{-1}$

$\lambda_\beta = 4.962 \times 10^{-10}\,yr^{-1}$

$K^{40}/K = 1.167 \times 10^{-4}$

Ar^{40r} = radiogenic Ar^{40}

ANALYST: J. Harakel, for R.L. Chase.

studies of the two rift zones. In addition to the samples from the southwest J. Tuzo Wilson Knoll, dredged by R.L. Chase in 1973, fresh pillow basalts were collected by D.L. Tiffin of the Geological Survey of Canada (sample "73").

Figure 1 (~~in pocket~~ p. 10a) shows the locations of all dredge hauls from which samples for this study were selected. The latitudes, longitudes, and depths of recovery of the dredge stations are listed in Table 2.

DREDGE HAUL LOCATIONS from the EXPLORER RIDGE

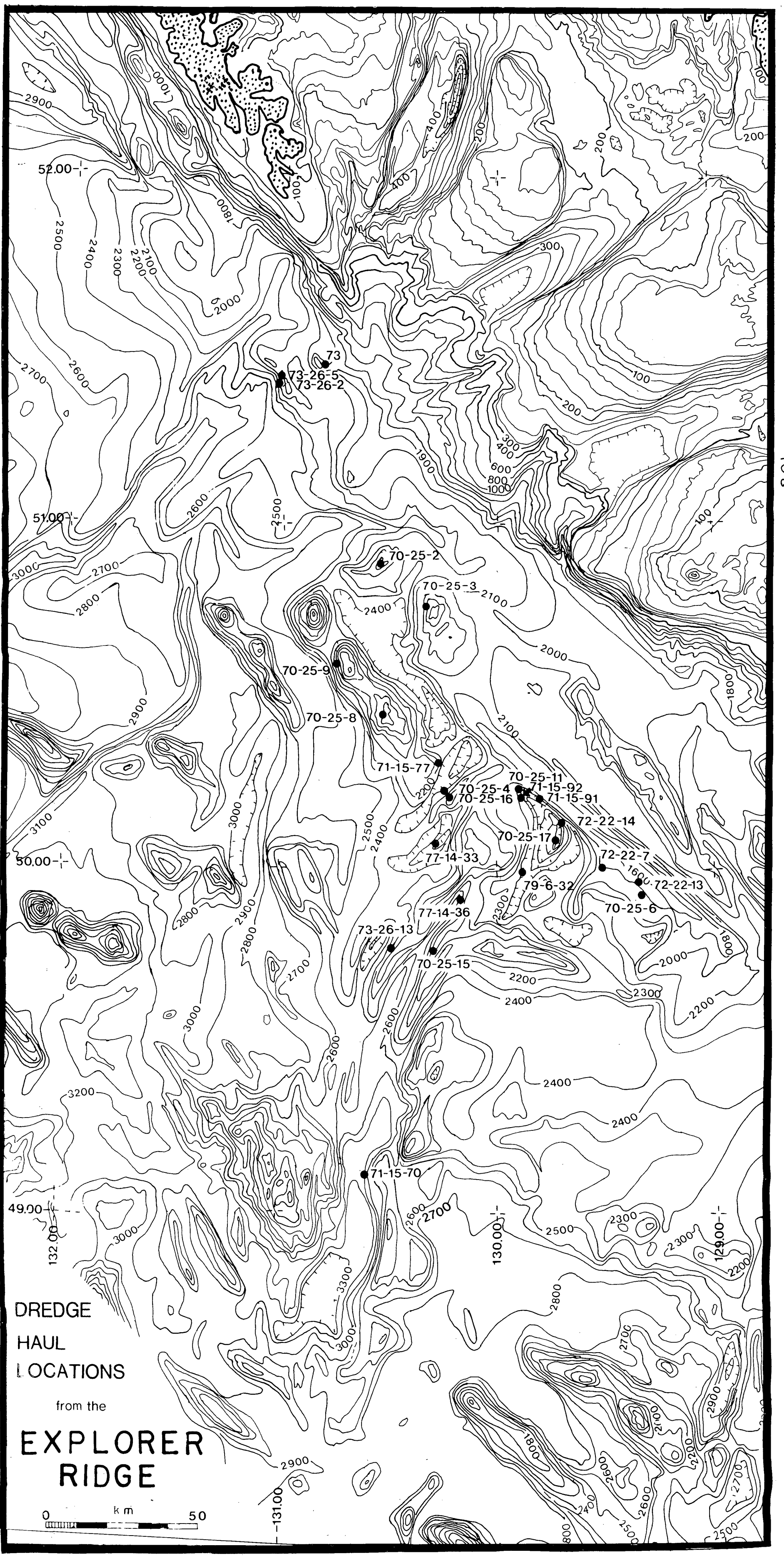

TABLE 2

Locations and Depths of Dredge Hauls

Each UBC dredge haul has a six-digit descriptor, of which the first two digits indicate the year of collection, the third and fourth digits the cruise number, and the fifth and sixth digits the station number of the dredge. Other digits appended to this are fragment numbers.

DREDGE HAUL	TOPOGRAPHIC FEATURE	NAVIGATION SYSTEM	LATITUDE (°N)	LONGITUDE (°W)	DEPTH RANGE (meters)
67-6-12	Bowie Smt	radar transponder	53° 19′	135° 38′	100-120
73-26-2	JTW Knolls	Radar	51° 24′ 30″	130° 02′	1883-1682
73-26-5	JTW Knolls	Radar	51° 25′ 30″	131° 01′	?
"73"	JTW Knolls	?	51° 28′ 30″	130° 51′	?
70-25-2D	Dell. Kn.	Satnav	50° 53′ 40″	130° 33′	1940-1554
70-25-3D	Dell. Kn.	Satnav	50° 46′ 38″	130° 25′ 12″	1875-1509
70-25-8D	Dell. Smt.	Satnav	50° 27′ 12″	130° 32′ 30″	1475-1300
70-25-9D	Dell. Smt.	Satnav	50° 36′	130° 45′ 30″	1800-1500
71-15-77	Ex. Rift	?	50° 18′ 24″	130° 17′ 18″	2460-2300
70-25-4	Ex. Rift	Satnav	50° 13′ 54″	130° 15′ 06″	2500
70-25-16	Ex. Rift	?	50° 13′	130° 14	2100-1900
77-14-33	Ex Rift	Loran A	50° 04′ 42″	130° 17′ 48″	2675
70-25-11	P. Revere R.	Satnav	50° 14′ 18″	129° 54′ 42″	2300-2200
71-15-92	P. Revere R.	Loran A	50° 12′ 48″	129° 54′	2600-2420
71-15-91	P. Revere R.	Satnav	50° 12′ 29″	129° 48′ 42″	2050-1975
72-22-7	P. Revere R.	Satnav	50° 00′ 25″	129° 31′ 30″	1800
70-25-17	Ex. Deep	Satnav	50° 05′ 30″	129° 44′ 30″	3200-2400
79-6-32	Ex. Deep	Loran C	49° 59′ 24″	129° 53′ 06″	2465-2375
77-14-36	S. Ex. Ridge	Loran A	49° 55′ 12″	130° 10′ 48″	2450-2130
73-26-13	S. Ex. Ridge	?	49° 46′ 30″	130° 30′	2200-2148
70-25-15	S. Ex. Ridge	?	49° 46′	130° 18′	2100-2000
71-15-70	S. Ex. Ridge	?	49° 07′	130° 36′ 30″	2540

BASALT PETROGRAPHY

The basalt samples studied are fragments of glassy pillow lavas, and other flows, dredged from the sea floor. Fragments were chosen for analysis based on apparent freshness.

The initial assessment of freshness was confirmed under the microscope. With few exceptions, all the samples are very fresh, with unaltered olivine and plagioclase phenocrysts, and no apparent alteration minerals. Four samples show red staining, apparently due to oxidation of iron-bearing minerals, most notably spinel. Four others display minor olivine alteration, at phenocryst edges and along fractures. As was expected, the somewhat older rocks of the Paul Revere Ridge show a slightly higher degree of alteration than do the basalts of the active volcanic areas.

The dominant phenocryst phases are olivine and plagioclase. Pyroxene only rarely occurs as phenocrysts, which is a common feature of oceanic basalts (Bryan, 1972). Increasing crystallization of magnesian olivine increases the FeO/MgO ratio of the residual liquid, until the olivine-plagioclase-pyroxene eutectic is reached. In oceanic basalts, the high rate of cooling generally does not allow phenocryst pyroxene to crystallize. Phenocrysts are not abundant in the Explorer, Dellwood, or JTW Knolls basalts, rarely exceeding 10% by volume of the samples. Plagioclase microphenocrysts are common to all areas except the JTW Knolls, suggesting that the ridge magmas had a somewhat longer period of crystallization after extrusion than did the seamount basalts. Commonly, the phenocrysts are glomeroporphyritic.

The phenocrysts exhibit excellent quench and fast-growth textures, as described by Bryan (1972). Olivines are in places euhedral or anhedral, but most commonly are subhedral and skeletal (Plate 2-A,B,C). Plagioclase phenocrysts have glass inclusions (Plate 2), and are generally normally zoned. The Dellwood basalts have plagioclase phenocrysts with An contents exceeding 80%,

and olivines with Fo contents of 90%, which are out of equilibrium with the bulk composition of the rock (Bertrand, 1972). The Explorer basalts show the same petrographic features; the phenocrysts are probably also more anorthitic and forsteritic than would be predicted from the bulk chemistry of the basalts.

Texturally, the majority of the basalt fragments studied are hyalopilitic or hyalophitic, consisting of plagioclase, olivine, and rare pyroxene phenocrysts, in a glassy to fan-sherulitic groundmass (Plate 2-A,B,C). The mineralogical composition of the fan-spherulites is not distinguishable optically, but is probably a combination of plagioclase and pyroxene (Bryan, 1972). Less commonly, the basalts exhibit intergranular or intersertal texture, and in 3 cases, the basalts are holocrystalline (Plate 3). These fragments may be from the centers of pillows, or from more massive lava flows (Bryan, 1972). One sample (Plate 2-D) shows fan-sperulitic texture: radial clusters of elongate plagioclase and pyroxene crystals, often with cross-cutting "lantern string" (Bryan, 1972) olivine crystals, and only minor amounts of fan-spherulitic matrix. This texture probably reflects a slower rate of cooling than that experienced by the hyalopilitic basalts.

The Explorer basalts studied are rarely vesicular. In some samples, a vesicular zone is found about 1 cm below the pillow surface. The vesicularity decreases quickly in both directions away from this zone. Vesicles rarely occupy more than 5% of the rock by volume, reflecting the low volatile content and depth of extrusion of the basalts. In contrast, the JTW and Dellwood Knolls samples are very vesicular. Some JTW basalts have elongated vesicles up to 5 cm in length and 1 cm in width, and have high dissolved volatile contents ($H_2O \sim 1.1\%$, $CO_2 \sim 0.6\%$). The Dellwood basalts do not have similar high volatile contents.

In summary, the Explorer, Dellwood, and JTW basalts are petrographically very similar, with uniform texture and phenocryst assemblages. The dominant pheno-

cryst phases are olivine and plagioclase, but these rarely occupy more than 10-15% by volume of the rock. They commonly show glomeroporphyritic texture. Most of the samples selected are hyalopilitic basalts, and alteration is generally minor.

Appendix 1 contains petrographic details for the J. Tuzo Wilson Knolls, Dellwood Knolls and Seamounts, and Explorer Ridge basalts.

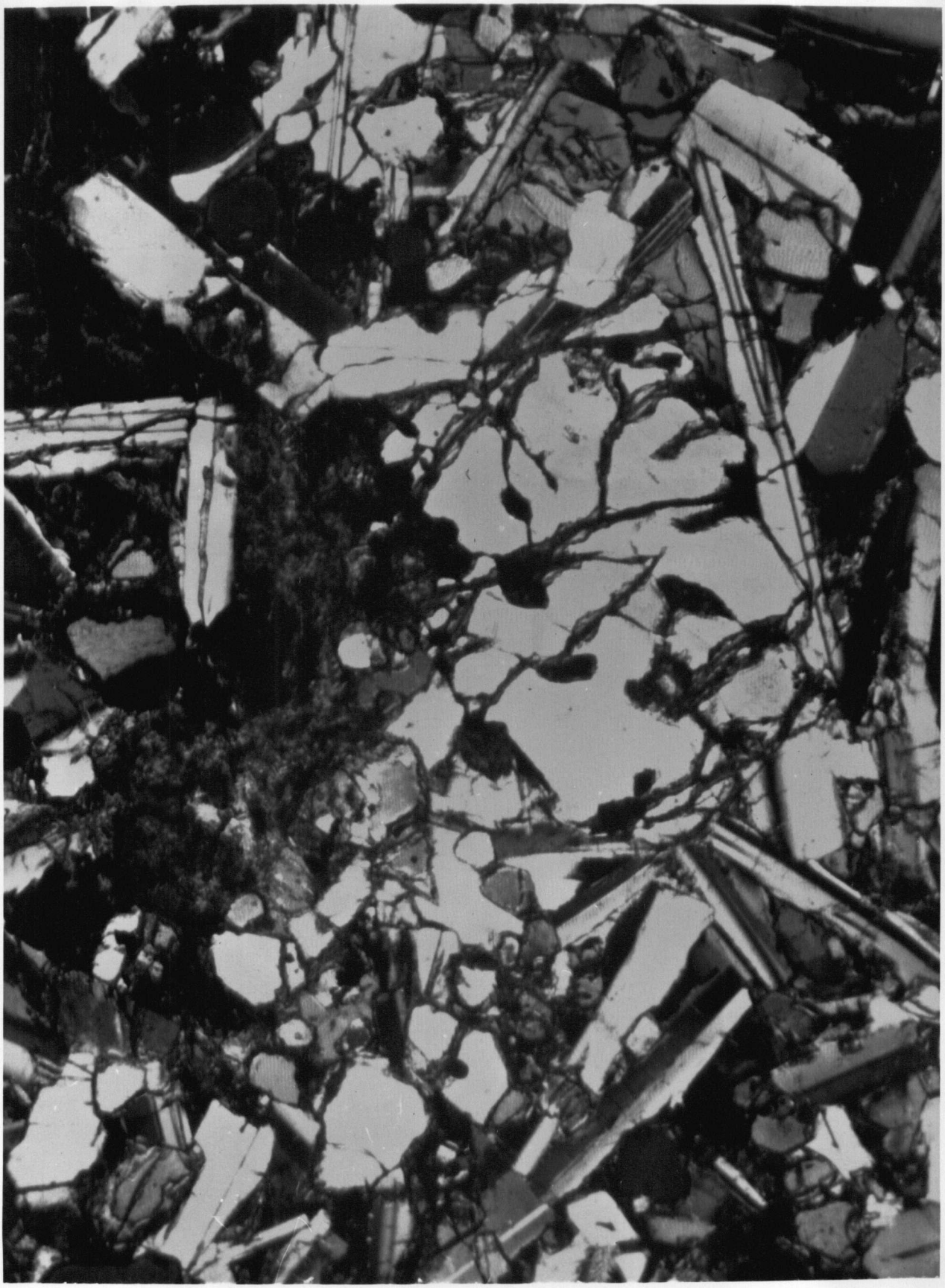

Intergranular basalt. Olivine altered along fractures, groundmass alteration extensive. Mag. 35x. 71-15-91-1.

PLATE 2

A. Skeletal, quenched olivine and plagioclase phenocrysts in a hyalopilitic matrix. Mag 25x. 77-14-36-X.

B. Quenched olivine phenocrysts in a hyalopilitic matrix. Mag. 25x. 77-14-36-G.

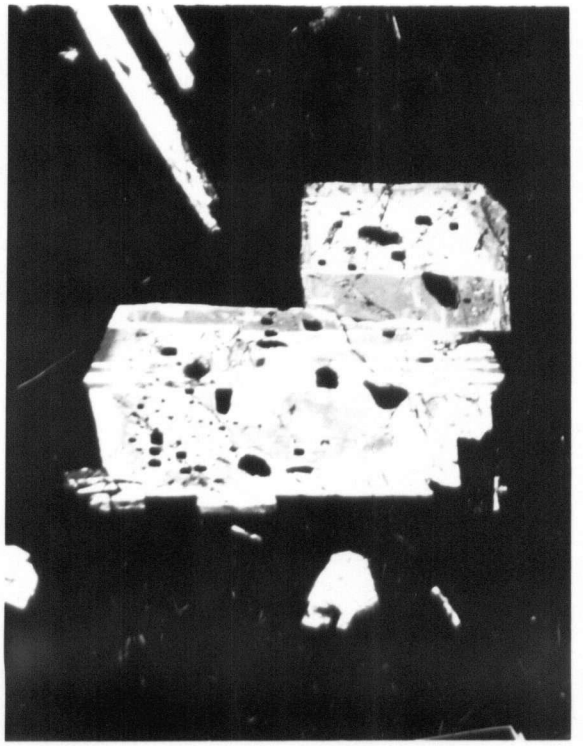

C. Zoned plagioclase phenocryst with glass inclusions. Mag. 35x. 77-14-33-B.

D. Fan-spherulitic basalt. Mag. 100x. 77-14-36-36.

Holocrystalline basalt. Radial pyroxene and plagioclase crystals with olivine phenocrysts. Mag. 30x. 77-14-36-35.

MAJOR ELEMENTS

(i) Analytical Procedure

Each basalt fragment selected for analysis was first crushed in a custom built hydraulic rock splitter, then ground to a fine powder in a Rockland Cr-steel ring mill. Ten grams of powder were then formed into a 3.1 cm-diameter, 1.2 cm-thick pellet, with a boric acid backing.

Major element oxide concentrations were determined by X-ray fluorescence spectroscopy, on a Phillips PW-1410 spectrometer, using the pressed powder method of Brown et al. (1973). This method has been refined by Peter van der Heyden, Stanya Horsky, and W.K. Fletcher, of the Department of Geological Sciences at the University of British Columbia. This procedure uses mass absorption coefficients from the Handbook of Spectroscopy (1974) to correct for matrix effects in both standards and unknowns. Also, instrument drift and sample backgrounds are monitored and corrected for.

XRF operating conditions for the major element analysis are listed in Appendix 4, along with a brief description of the computer program used for the data reduction. For a more complete description of the program, see van der Heyden (1982).

The major element composition of all the samples studied is listed in Appendix 2.

(ii) Precision and Accuracy

Appendix 2 contains precision data for the seven standards used for the calibration curves, along with precision estimates for the unknowns. The mean (average of the seven standards) percent deviation for each element (the difference between the "recommended values" (Abbey, 1980) and the values calculated using the working curves) is nearly equal to, or is less than, the precision of data used to generate the "recommended values" (Flanagan, 1973;

S. Berman, personal communication to S. Horsky).

Precision estimates for the unknowns were also calculated, using the method of Howarth and Thompson (1976). Duplicate analyses of several of the unknowns were carried out, after which the difference between the two runs for each unknown was plotted against the mean of the two runs. Precision lines indicate the 90 and 99% probability limits of any replicate point falling below the lines, given a specified precision (95% confidence limits) in the data. These precisions are maximum values, assuming there are no extraordinary points. An example of two of the precision plots (Fe_2O_3 and MgO) are shown in Appendix 3.

Table 3 presents duplicate major element analyses , using different analytical procedures, for 3 basalts: 70-25-2D-8 from the Dellwood Knolls; 73-26-2-1 and 73-26-5-1, both from the JTW Knolls. It is evident that the pressed pellet analyses yield somewhat lower SiO_2 and Al_2O_3 values, and higher values for Fe_2O_3, MgO, and CaO. The most obvious result of this is that the samples appear to be more silica undersaturated using the pressed powder analysis.

(iii) Results

The Explorer basalts, with the exception of the JTW samples, plot within the field of abyssal tholeiites (Miyashiro et al., 1970) on an AFM diagram, as shown in Figure 5. The cluster of points falls between the Hawaiian tholeiite and Hawaiian alkali basalt differentiation trends. The transitional to tholeiitic nature of the basalts is further emphasized in a silica variation diagram (Figure 6). The Explorer basalts appear to be slightly enriched in alkali metals compared to the Gorda and Juan de Fuca Ridges. However, this may be due to differences in analytical procedure rather than to true chemical differences. The JTW hawaiites plot as a distinct group on both diagrams, due to their significantly higher alkali metal contents. They do not outline any differentiation trend on the AFM diagram, but lie along an SiO_2 and alkali enrichment path.

Figures 7 and 8 compare the concentrations of the major element oxides

TABLE 3

Duplicate Analyses of Explorer Area Basalts

by Different Analytical Methods

SAMPLE:	70-25-2D-8				73-26-2-1B		73-26-5-1B	
METHOD:	Atom. Absor.	Fused Disk	Fused Disk	Press. Pel.	Fused Disk	Press. Pel.	Fused Disk	Press. Pel.
ANALYST:	W. Bertrand (1972)	R.L. Chase	Armstrong & Nixon, 1980	B. Cousens (1982)	R.L. Chase	B. Cousens (1982)	R.L. Chase	B. Cousens (1982)
SiO_2	46.10	47.77	47.87	47.33	49.63	48.75	51.11	50.12
TiO_2	1.24	1.21	1.19	1.30	2.27	2.40	1.52	1.73
Al_2O_3	16.30	16.81	17.38	16.91	17.30	15.87	17.87	16.16
Fe_2O_3*	9.20	9.48	9.24	10.23	9.03	9.28	6.90	7.62
MnO	0.12	0.15	0.16	0.16	0.15	0.16	0.14	0.17
MgO	8.76	8.57	8.76	9.50	4.53	5.06	5.08	6.78
CaO	11.00	11.79	11.89	12.36	8.03	8.00	8.15	8.57
Na_2O	3.20	2.46	2.39	2.29	4.52	5.18	4.82	4.95
K_2O	0.19	0.20	0.14	0.22	2.57	2.46	2.20	2.02
P_2O_5	no data	0.08	0.13	0.09	0.91	0.66	0.79	0.58
$H_2O^+ + CO_2$	0.80	>1.03	1.00	0.80	>1.44	2.77	>0.66	1.79
TOTAL	96.90	98.75	99.61	101.19	99.86	100.60	99.03	100.48

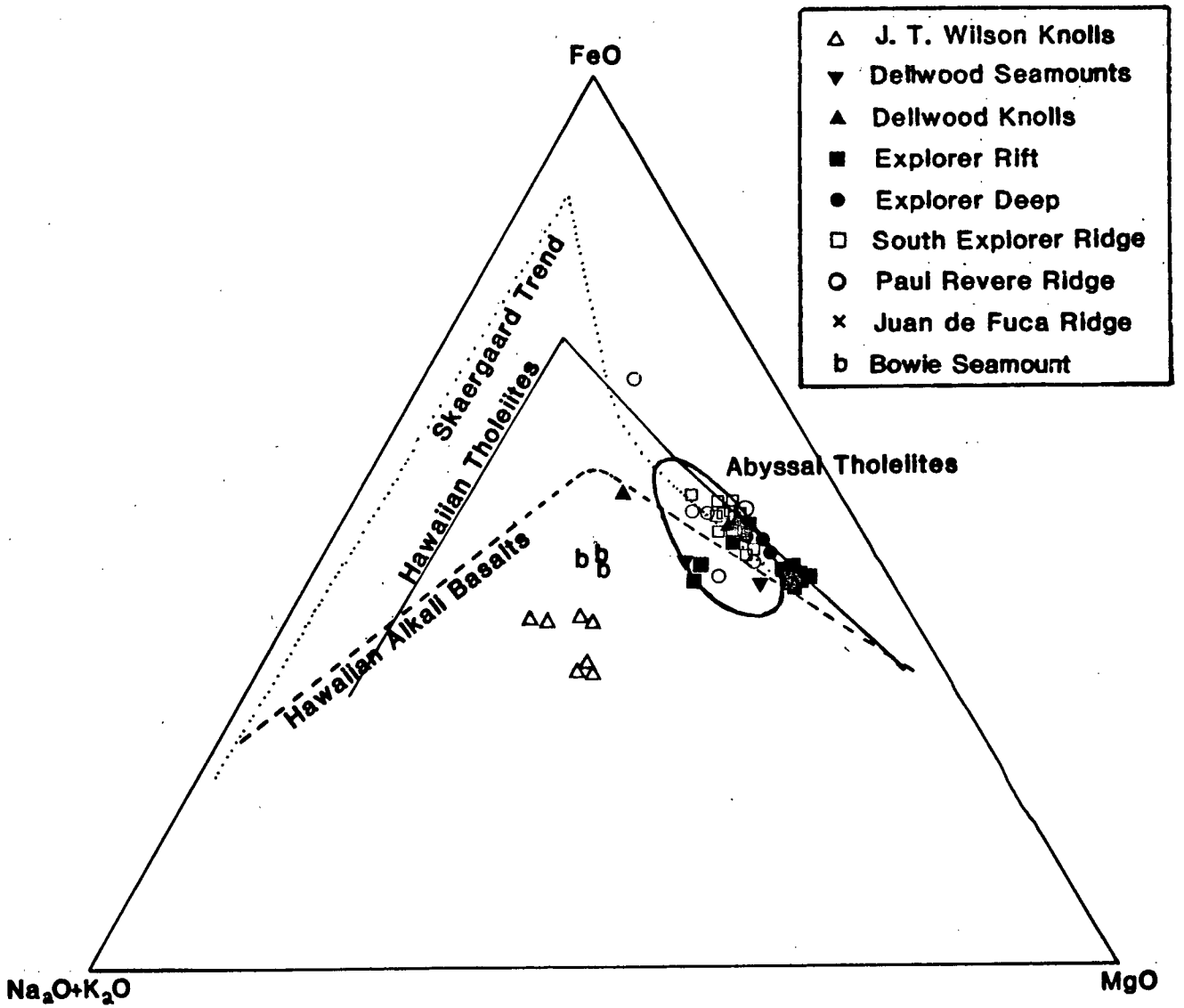

Fig. 5: AFM diagram for Explorer area basalts. Differentiation trends from MacDonald and Katsura (1964). Abyssal tholeiite field from Miyashiro et al.(1970).

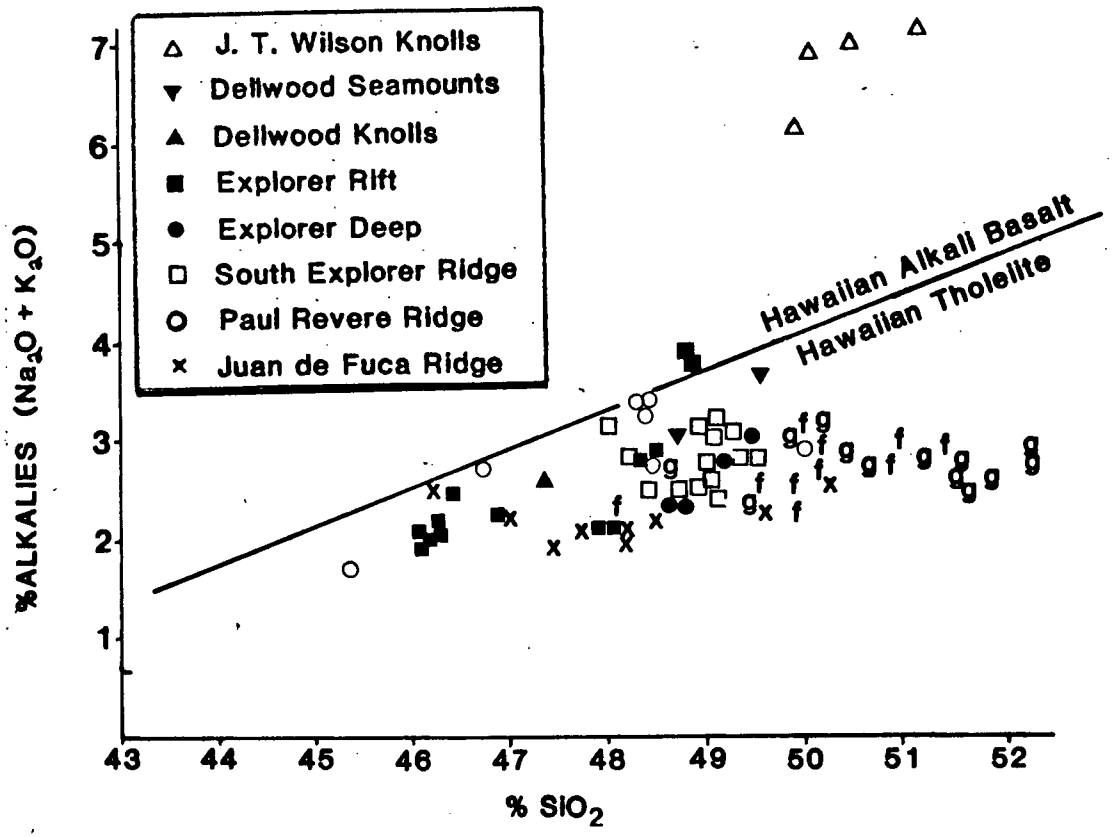

Figure 6 : Silica variation diagram for Explorer area basalts. Tholeiite/alkali basalt boundaryfrom MacDonald and Katsura (1964). Juan de Fuca basalts: x- Barr & Chase (1974). f and g- Wakeham (1977).

Al_2O_3, FeO^t, CaO and TiO_2, relative to MgO, in Explorer basalts, with those of other MORB. In all cases, the Explorer rocks plot within the field of MORB whole rock analyses, and generally plot near or within the field of MORB glass analyses. This suggests that phenocryst composition is not influencing the whole rock chemistry significantly. It is notable that although Explorer CaO and Al_2O_3 contents plot in the middle of the MORB range, FeO^t and TiO_2 plot in the high range, significantly higher than the northern Juan de Fuca Ridge analyses.

The Explorer tholeiites somewhat resemble the "average" chemical composition of basalts from the southern Juan de Fuca Ridge (Melson et al., 1976). Similar high values for FeO^t, TiO_2, K_2O and P_2O_5 are encountered, but MgO contents are significantly higher than the southern Juan de Fuca "average". Using a Melson et al. (1976) classification, the Explorer basalts most resemble low titanium members of the FETI group, more accurately termed ferrobasalts. Picritic basalts, similar to those found on Gorda Ridge (Wakeham, 1977) and on northern Juan de Fuca Ridge (Barr and Chase, 1974), are present in the Explorer Rift and along the Paul Revere Ridge. The JTW Knolls basalts do not fit into any catagory of Melson et al. (1976), and they do not report any analysis of ocean ridge volcanic rocks with similar chemistry.

Figure 9 is a ternary diagram of the system plagioclase-pyroxene-olivine, with phase boundaries from the simpler system anorthite-diopside-forsterite superimposed on it. As has been previously noted for most MORB (Thompson et al., 1980; Basaltic Volcanism Study Project, 1981), the Explorer basalts cluster along the plagioclase-olivine cotectic. This correlates well with the occurrence of olivine and plagioclase phenocrysts in the rocks, and with the lack of pyroxene phenocrysts.

It is notable that in Figures 7 to 9, the JTW basalts plot within the field of MORB whole rock analyses, although they more resemble Bowie Seamount alkali

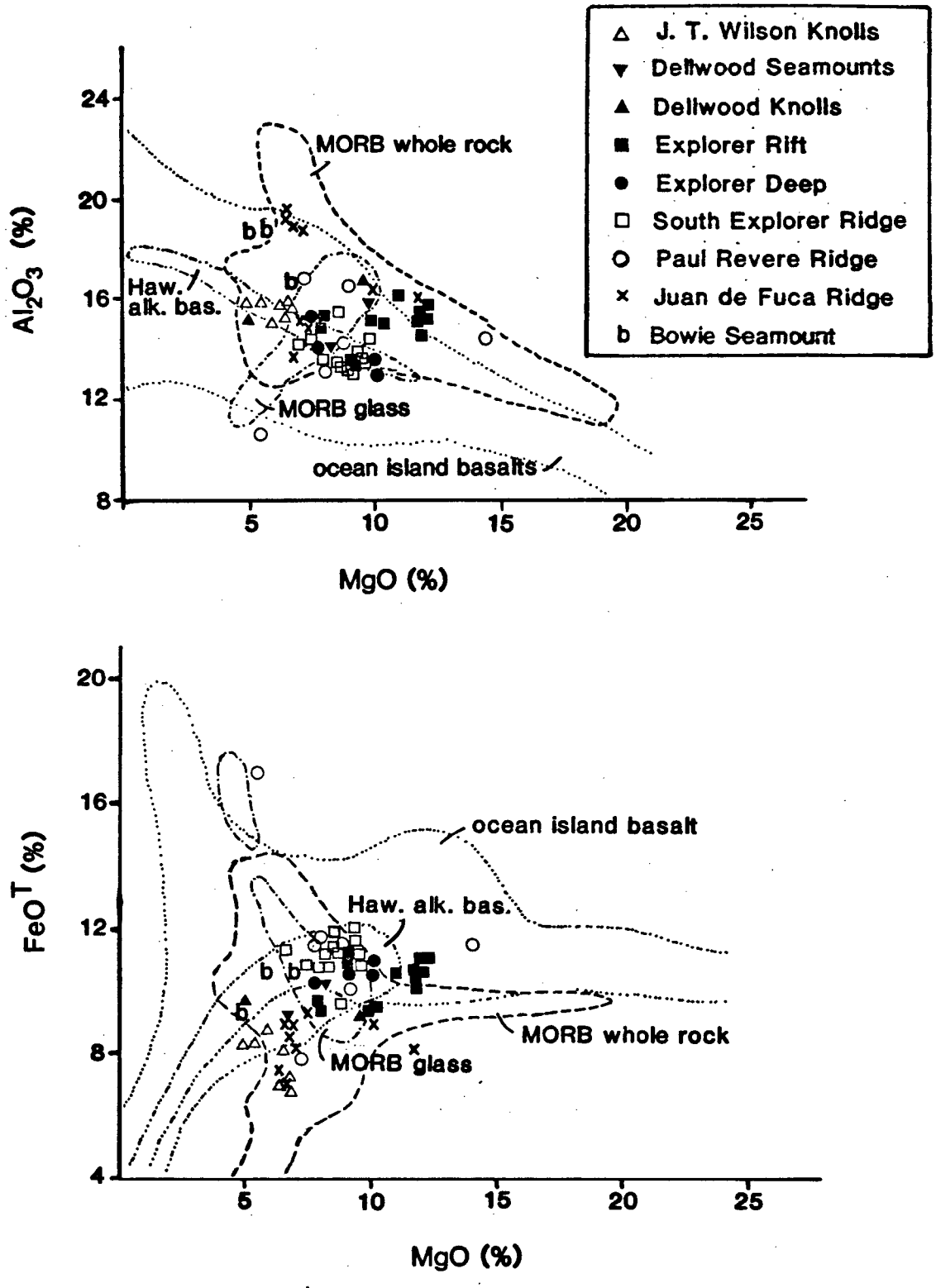

Figure 7 : MgO-variation diagram for FeO and Al_2O_3 in Explorer basalts. MORB glass, MORB whole rock, ocean island basalt, and Hawaiian alkali basalt fields from Basaltic Volcanism Study Project (1981). Juan de Fuca basalts: Barr and Chase (1974).

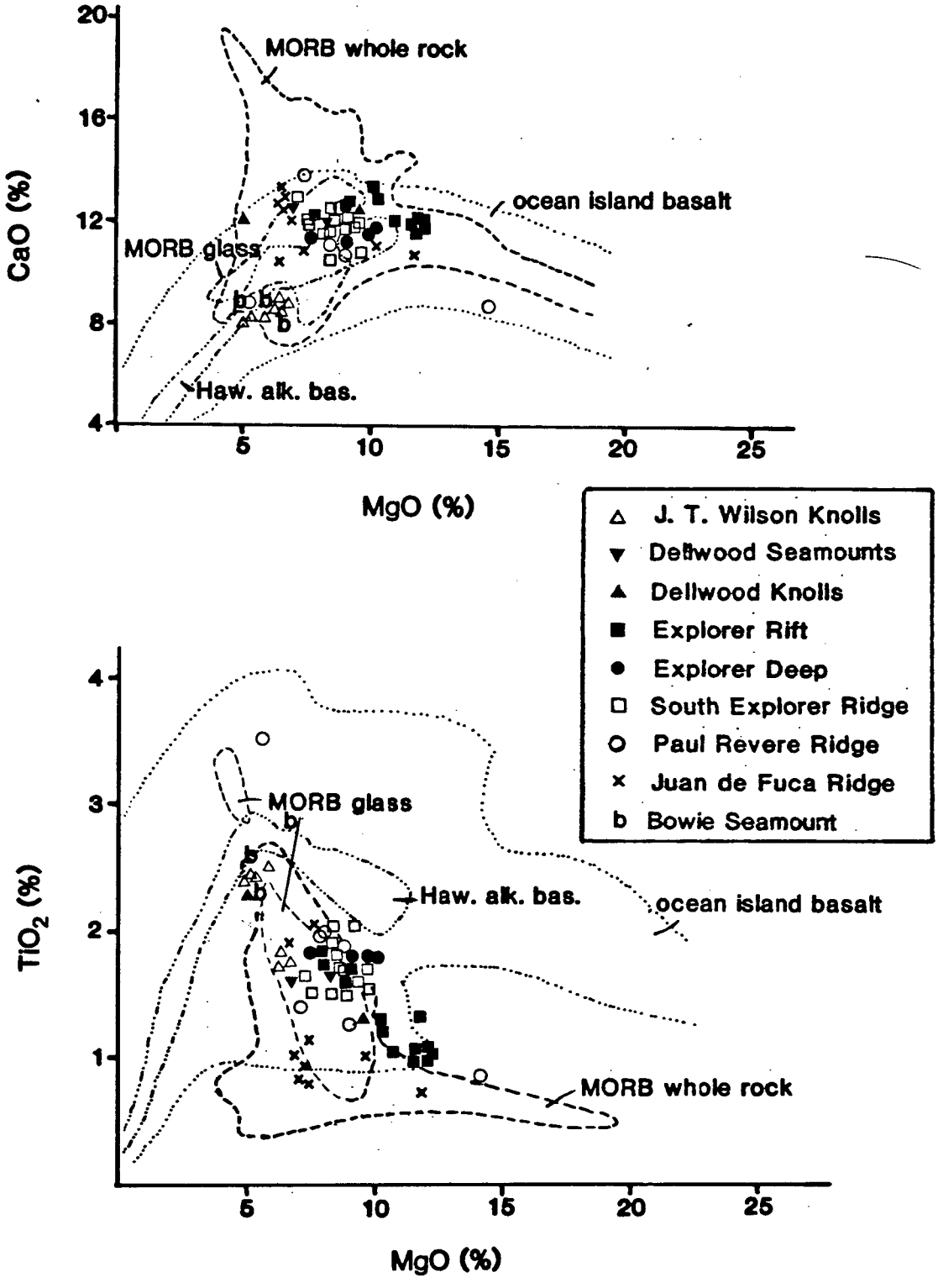

Figure 8 : MgO-variation diagram for CaO and TiO_2 in Explorer basalts. Basalt fields and data sources as in Figure 7 .

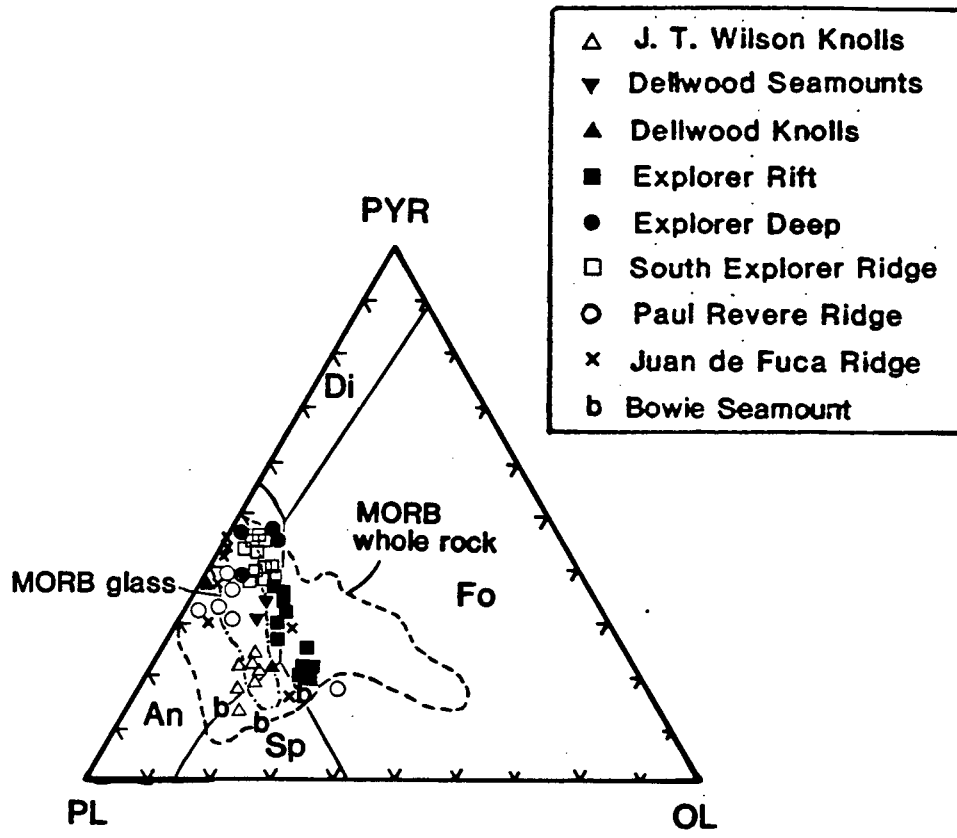

Figure 9 : CIPW-normative triangle diagram of the plagioclase-olivine-pyroxene system. Basalt fields and data sources as in Figure 7. Phase boundaries after Osborn and Tait (1952) for simplified system An-Di-Fo.

basalts (part of the Pratt-Welker Seamount Chain) than Explorer tholeiites.

The incompatible major elements, titanium and potassium, are present in weakly to strongly enriched concentrations in Explorer basalts, compared to MORB (Figure 10). Average K_2O is especially high in the Explorer Deep samples. In these elements, the Explorer rocks are similar to basalts from the FAMOUS area. The levels of Na_2O, K_2O, and TiO_2 in the Explorer basalts are higher than those found on the northern Juan de Fuca Ridge (Barr and Chase, 1974), and K_2O contents are generally higher than those of the southern Juan de Fuca and Gorda Ridges (Kay et al., 1970; Wakeham, 1977). K_2O and Na_2O are highly enriched in the JTW hawaiites, substantially above levels typical of MORB.

The high concentrations of incompatible major elements could be the result of crystal fractionation, minor "plume source" influence, smaller degrees of partial melting of the mantle source, or differences in the chemistry of the mantle source. To test the influence of fractionation, K_2O and TiO_2 are plotted against the magnesium ratio, 100 $(Mg/Mg+Fe^{2+})$, as illustrated in Figure 11. The observed negative correlation between the two oxides and the magnesium ratio is due, at least in part, to fractionation. In several cases, basalts from the same dredge haul (e.g. 70-25-16, 79-6-32, 71-15-92, and 70-25-4) appear to be directly related by this process. However, the general scatter of points is appreciable. There is substantial variability in the K_2O content of basalts from the same ridge segment, with similar magnesium ratios, notably from Explorer Rift and the Southern Explorer Ridge. It is also notable that whereas the highly differentiated FETI basalts from the Galapagos Rise (Byerly, 1980) and the southern Juan de Fuca Ridge rarely have K_2O greater than 0.3%, several Explorer area samples exceed this value. Thus, fractionation alone cannot explain the variation in K_2O in the basalts.

The occurrence of relatively unfractionated basalts (magnesium ratio of 68 to 72) in the Explorer Rift is somewhat puzzling. This spreading segment is the result of a ridge "jump" from Explorer Deep within the last 1Ma BP. It is

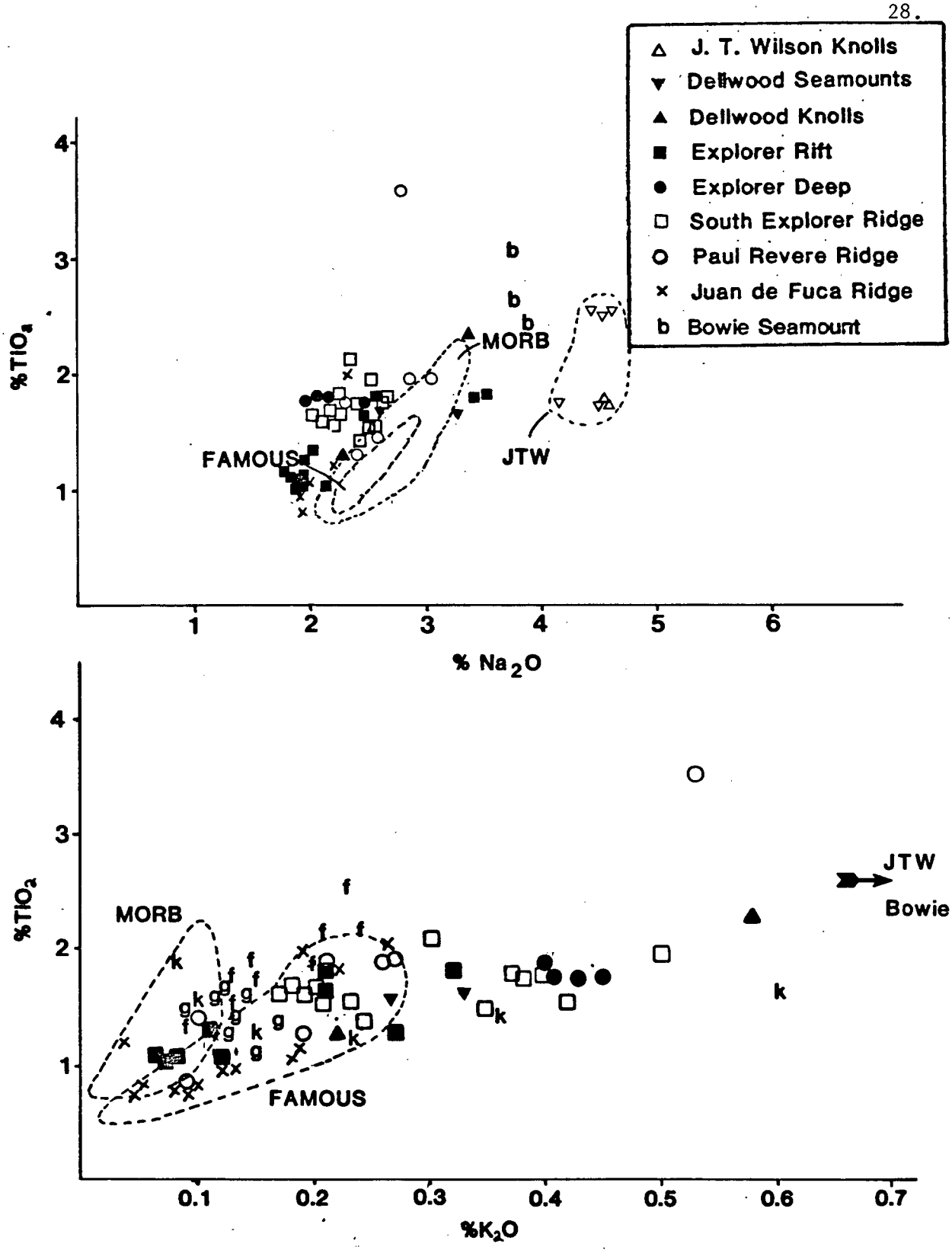

Figure 10 : Plots of TiO_2 vs. Na_2O and K_2O. JTW basalts plot off-scale on K_2O diagram. MORB and FAMOUS fields from compilation in Thompson et al. (1980). Juan de Fuca basalts: x- Barr & Chase (1974). k- Kay et al.(1970). f and g- Wakeham (1977).

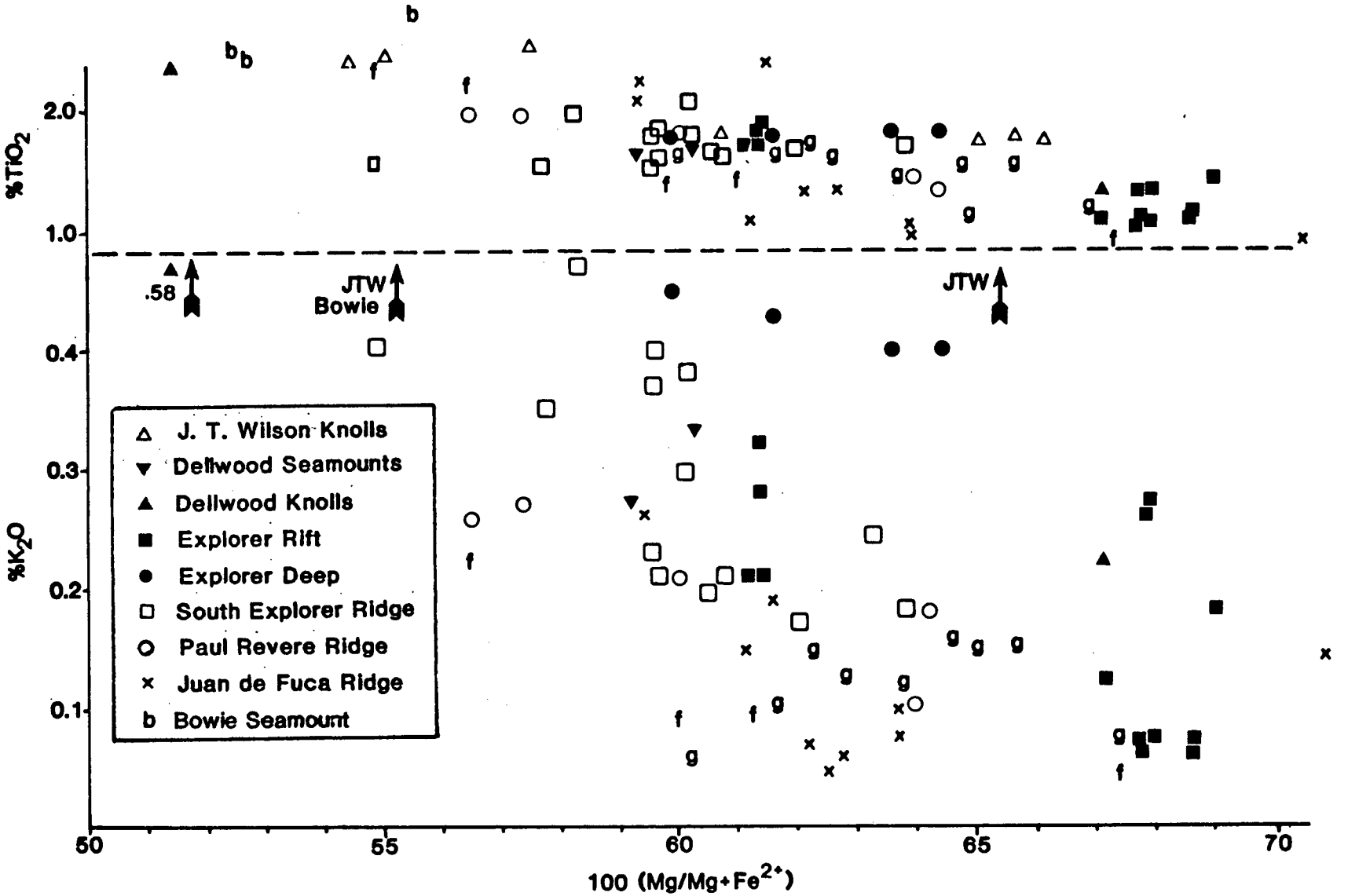

Fig. 11: Magnesium ratio variation diagram for K_2O and TiO_2. J. Tuzo Wilson samples plot off the K_2O diagram (>1.0%) Juan de Fuca basalts: x- Barr (1974) and Chase , f- Wakeham (1977). Gorda basalts: g- Wakeham (1977).

rifting relatively older and cooler crust (1.3-2.1 Ma). Thus, a high degree of low-pressure crystal fractionation would be expected, similar to that seen at propagating ridge tips (Clague and Bunch, 1976; Byerly, 1980), such as the Galapagos Rise. It appears that the greater age and consequent coolness of the rifted crust has little effect on the chemistry of the Explorer Rift rocks, contrary to what was expected.

In general, the abundance of relatively unfractionated basalts in the Explorer area is greater than the ocean ridge average, as shown in the frequency histogram in Figure 12. Almost half of the Explorer basalts studied have magnesium ratios of 62 or greater, while only one quarter of MORB lie in this range. The Explorer distribution is wieghted by the numerous unfractionated samples from Explorer Rift, but nevertheless, the Explorer system produces less fractionated basalts than the average ocean ridge.

CIPW normative compositions for all the Explorer area samples studied are listed in Appendix 2.

It is immediately apparent that the JTW, Dellwood Knolls, and Explorer Rift basalts are nepheline normative, while the Southern Explorer Ridge, Explorer Deep, and Paul Revere Ridge basalts are olivine-hypersthene normative. The JTW Knolls samples are hawaiites and mugearites, with relatively large amounts of nepheline and orthoclase in the norm.

Figure 13 is a plot of the system An-Ne-Ol-Hy-Q, and it demonstrates a general trend of increasing silica saturation, progressing southward along the ridge system. This correlates well with the age of the spreading segments involved. The youngest segments, including the Dellwood Knolls and Explorer Rift, are largely nepheline normative, while the older segments progress through olivine tholeiite to quartz tholeiite in composition. This is probably a reflection of the lower temperature gradient, and consequent higher pressure of magma generation, experienced at a newly initiated rift. This results in a more alkalic magma (Presnall et al., 1979).

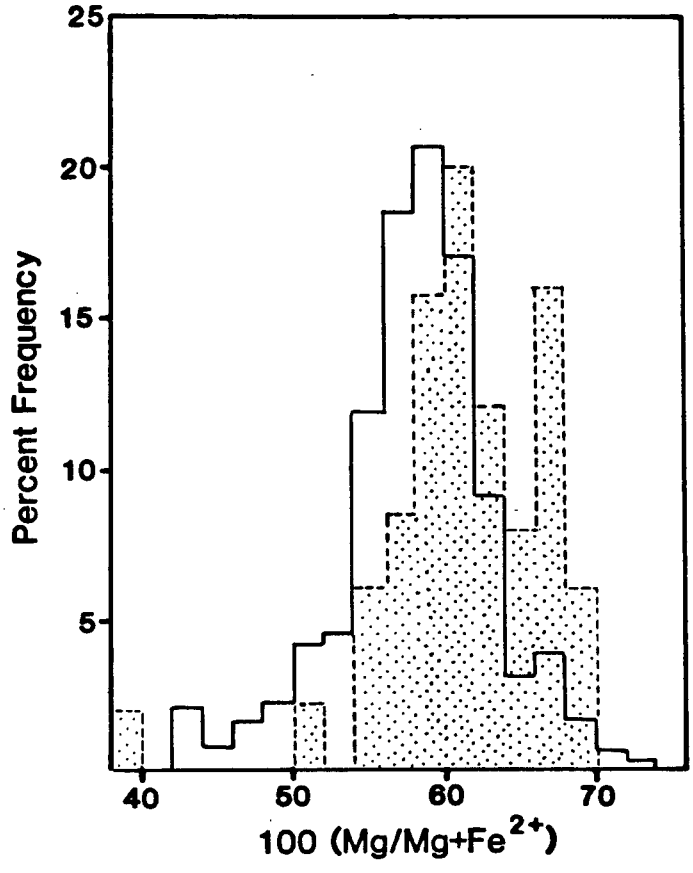

Figure 12: Frequency histogram of Mg ratios in ocean floor basalts (solid line) and Explorer Area basalts (stipled area). Ocean floor data from Basaltic Volcanism Study Project (1981).

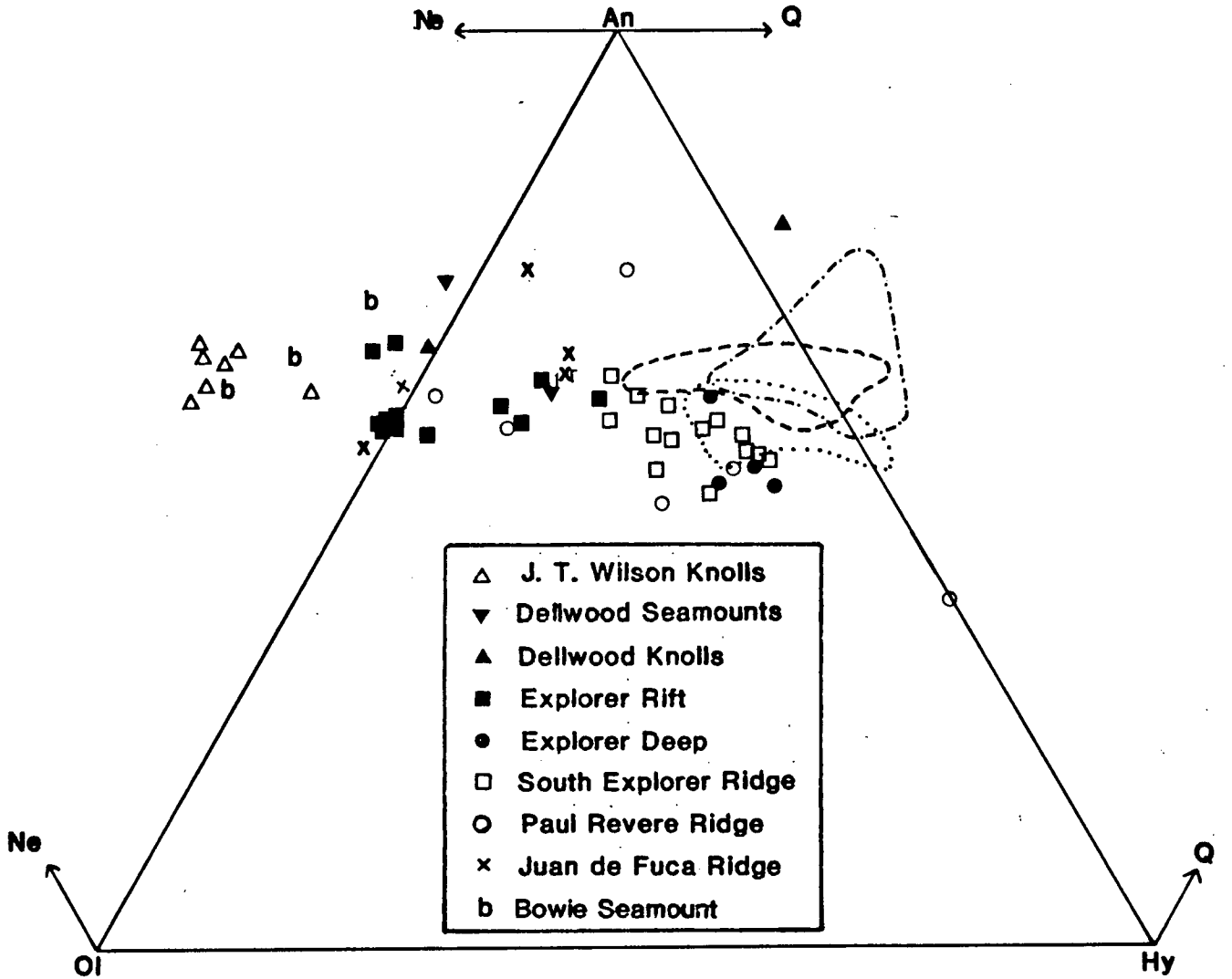

Figure 13: Normative triangle for the system An-Ne-Ol-Hy-Q. Juan de Fuca basalt fields: dashed line: Barr & Chase (1974). dotted line: Kay et al.(1970). "x": Moore (1970). dot-dashed line: Wakeham (1977).

TRACE ELEMENTS

(i) Analytical Procedure

The concentrations of barium, cerium, chromium, niobium, neodymium, nickel, rubidium, strontium, vanadium, yttrium, and zirconium were determined by X-ray fluorescence analysis of pressed powder pellets. The pellets used in the major element analysis were also used for the trace element determinations. Rb and Sr data were reduced by the method of Feather and Willis (1976). Ba, Ce, Cr, Nb, Nd, Ni, V, Y, abd Zr data were reduced by the traditional peak measurement-background subtraction method, including interference correction and mass absorption adjustment, using computer programs written by R. G. Berman of the University of British Columbia. La/Sm_{ef} ratios were determined by neutron activation analysis, performed by J.-G. Schilling at the University of Rhode Island.

XRF operating conditions for all trace element analyses are listed in Appendix 4.

The trace element data for all the samples studied are listed in Appendix 2.

(ii) Precision and Accuracy

With the exception of Ba and Ce, the observed precisions for analyses of standards used to create the working curves is better than 5 ppm (one standard deviation). In view of the uncertainty of the "recommended values" (Abbey, 1980), this level of precision is acceptable.

The precision for analyses of unknowns was estimated using the method of Howarth and Thompson (1976), following the same procedure discussed in the previous chapter. An example of a precision plot is presented in Appendix 3, and the precisions of both standards and unknowns are listed in Appendix 2. Ba Precision is poor due to low intensities, while Ce precision is poor due to the interference of Nd, for which no correction pellet was available.

(iii) Results

Compared to other ocean ridge systems, the Explorer basalts have high concentrations of Ba (Fig. 14), Rb, Nb, Sr, and Zr (Pearce and Cann, 1973; Sun, 1980; Engel et al., 1965). Figure 15 is a magnesium ratio variation diagram for these five elements. All except Sr are highly incompatible, and exhibit negative correlations with the magnesium ratio, although, as with K_2O, a considerable scatter of points is evident. This indicates that, as previously suggested, crystal fractionation can account for much of the chemical variation seen in the Explorer basalts, but another process must be influencing the chemistry to produce the observed scatter. Explorer Deep shows abnormally high concentrations of Rb, Nb, and Zr, which cannot be explained by fractionation.

The ferromagnesian elements, Ni and Cr, correlate positively with the magnesium ratio, as depicted in Figures 16 and 17. Nickel follows the predicted pattern due to its removal from the magma by olivine (Sato, 1977). Cr also shows signs of removal by chromian spinel, although only a few samples have been analysed for this element. None of the basalts, except the holocrystalline rocks, have large numbers of phenocrysts, and this should not be an influence on the data. The nickel diagram shows some scatter, similar to that seen in previous magnesium ratio diagrams.

Figure 17 also shows variations in V concentration with increasing fractionation. V acts as an incompatible element until titanomagnetite or clinopyroxene begin to crystallize, whereupon it readily enters the crystal lattices of these two phases. The pattern in figure 17 shows a steady linear increase as the magnesium ratio decreases, similar to the behavior of TiO_2. This indicates that neither magnetite nor clinopyroxene are crystallizing phases in the Explorer area, as was noted in thin-section (Clague et al., 1981).

It is evident from Figures 15 to 17 that the least fractionated basalts are found in the Dellwood Knolls and the Explorer Rift. Ni contents and the magnes-

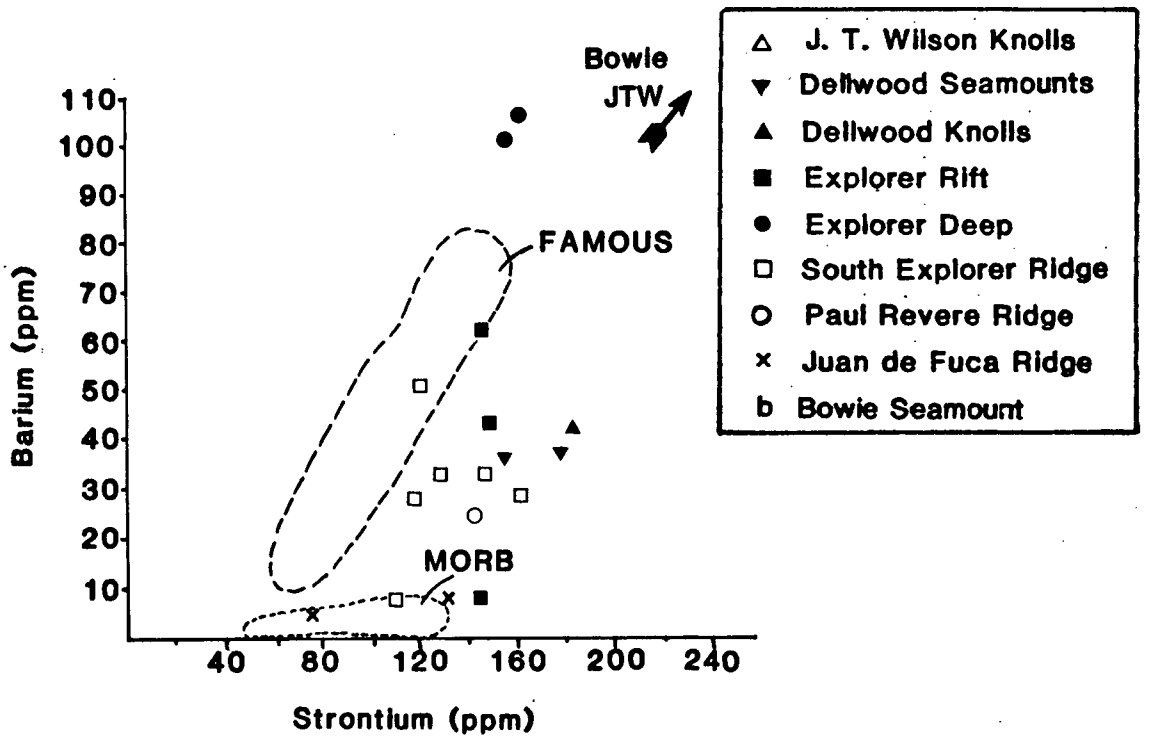

Figure 14: Plot of Ba vs. Zr . MORB and FAMOUS fields from Thompson et al.(1980). Juan de Fuca basalts from Armstrong and Nixon (1980). J. Tuzo Wilson and Bowie basalts plot above the scale.

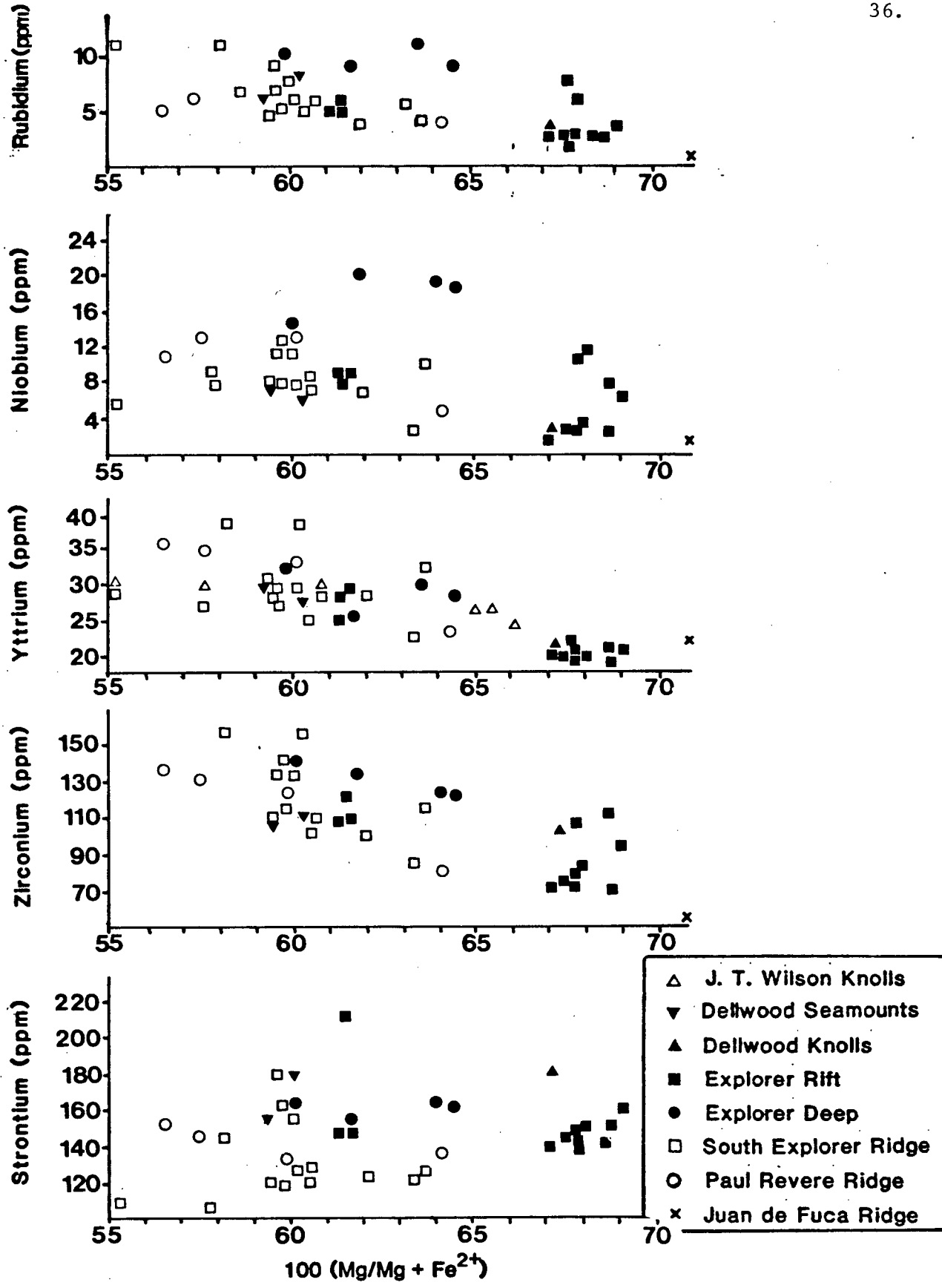

Figure 15: Magnesium ratio variation diagram for Rb, Nb, Y, Zr, and Sr. JTW basalts plot off the diagrams, except for Y.

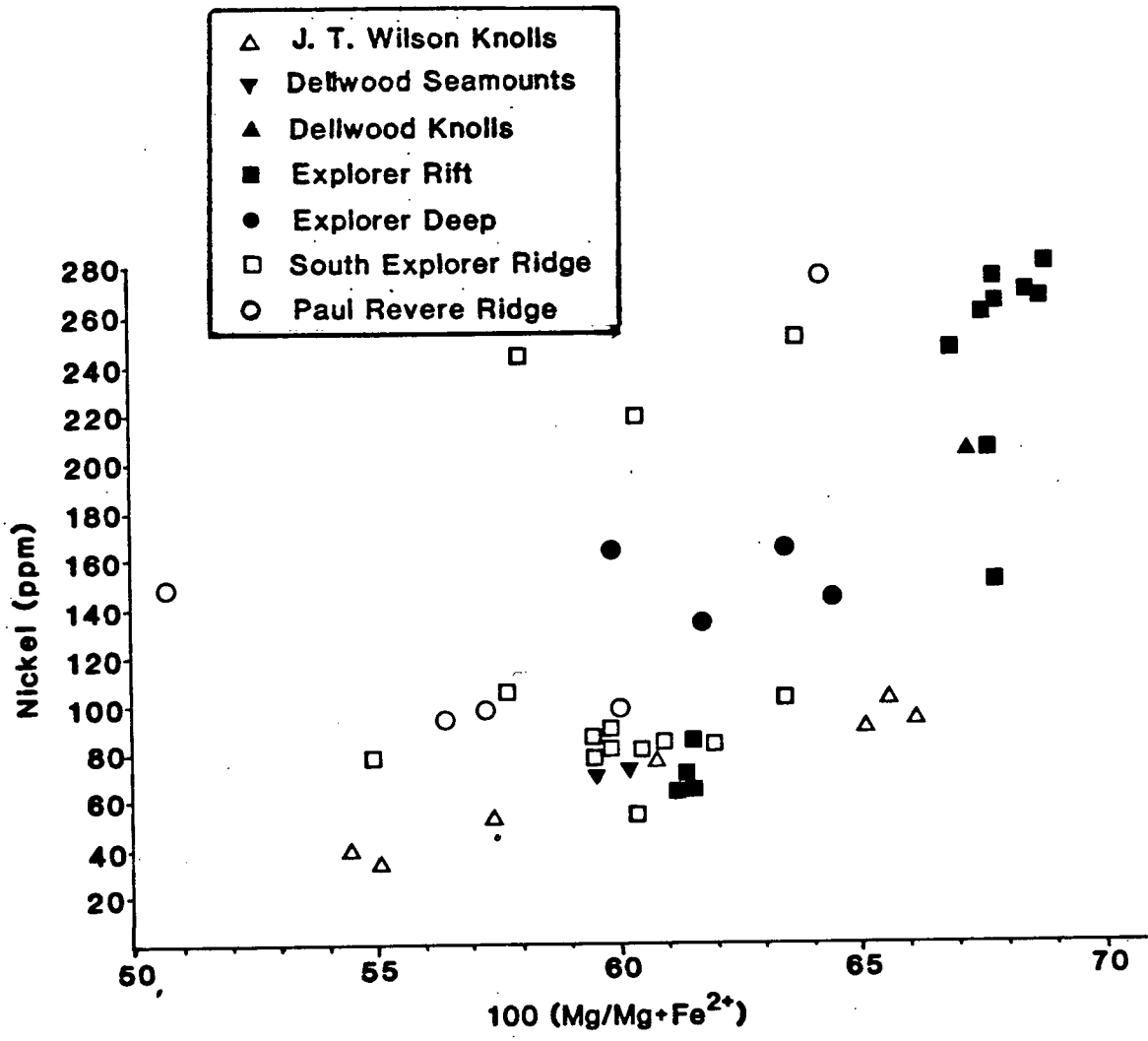

Figure 16: Magnesium variation diagram for Ni.

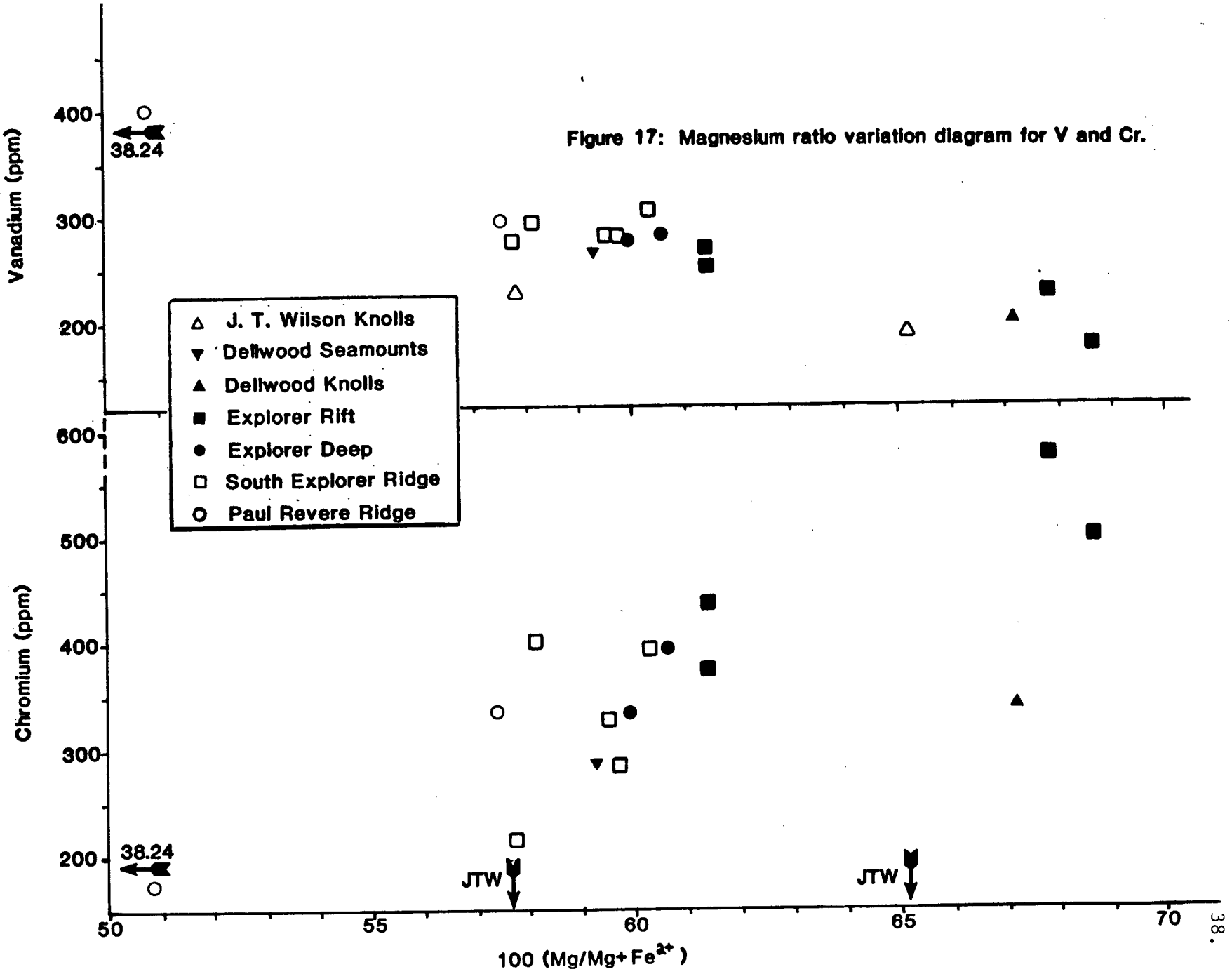

Figure 17: Magnesium ratio variation diagram for V and Cr.

ium ratio are high, while incompatible element levels are low. The most "evolved" (fractionated) basalts are from the Southern Explorer Ridge, which is the oldest of the ridge segments. This suggests that the newer segments have not yet developed a large magma chamber, in which magma can reside for a period of time, to allow fractionation to occur.

The JTW basalts are highly enriched in every incompatible trace element with respect to typical MORB, and strongly resemble basalts dredged from the co-linear Pratt-Welker Chain (Engel et al., 1965; Table 4). The observed trace element levels are similar to those of an "average" ocean island alkali basalt.

In terms of rare earth element patterns (Figure 18), the Explorer area is anomalous, in that two-thirds of the samples analysed show light rare earth element (LREE) enrichment. This is not characteristic of normal ocean ridge tholeiites, which generally exhibit LREE depletion (Schilling, 1971; Sun et al., 1979). The observed La/Sm_{ef} ratios resemble those of plume-influenced MORB, typical of the FAMOUS area and the Mid-Atlantic Ridge at 45°N (Sun et al., 1979; White et al., 1976). Kay et al. (1970) and Wakeham (1977) report light REE depletion in all samples from the Gorda and southern Juan de Fuca Ridges, with only one exception.

Basalts from Explorer Deep, with high levels of other incompatible elements, are LREE enriched. Explorer Rift and the Southern Explorer Ridge again show a range of La/Sm_{ef} values, from LREE depleted (0.59) to LREE enriched (1.73). It is notable that the northwest Dellwood Knoll has a La/Sm_{ef} ratio of 0.81, but the southeast knoll has a ratio of 1.49. The JTW Knolls exhibit extreme enrichment in the LREE , above the levels for major mantle plumes (e.g. Iceland, Azores, Jan Mayen). Such a high level of enrichment has been encountered in an olivine tholeiite dredged from a single volcanic cone on a short segment of spreading ridge in the Tadjura Trough, at the west end of the Gulf of Aden (Schilling, personal communication).

Erlank and Kable (1976) use the Zr/Nb ratio to measure the degree of de-

TABLE 4

Trace Element Concentrations in Oceanic Basalts

	MORB AVERAGE*	OCEAN ISLAND AVERAGE*	BOWIE SEAMOUNT PV-50*	BOWIE SEAMOUNT 67-6-12†	J. TUZO WILSON 73-26-2-1†
Ba	14 ±7	498 ±136	420		361
Cr	297 ±73	67 ±57	170	335	25
Nb	3	72 ±9	82		87
Ni	97 ±19	51 ±33	76	86	38
Rb	1.2	33 ± ?	33	41	36
Sr	130 ±25	815 ±375	1100	670	590
V	292 ±57	252 ±32	260		232
Y	43 ±10	54 ±7	48		31
Zr	95 ±35	333 ±48	350	338	396
FeO^t/MgO	1.20	1.99	1.72	1.80**	1.63

Sources: * - Engel et al. (1965), except Nb and Rb, which are from Sun (1980).
** - Herzer (1971)
† - this study

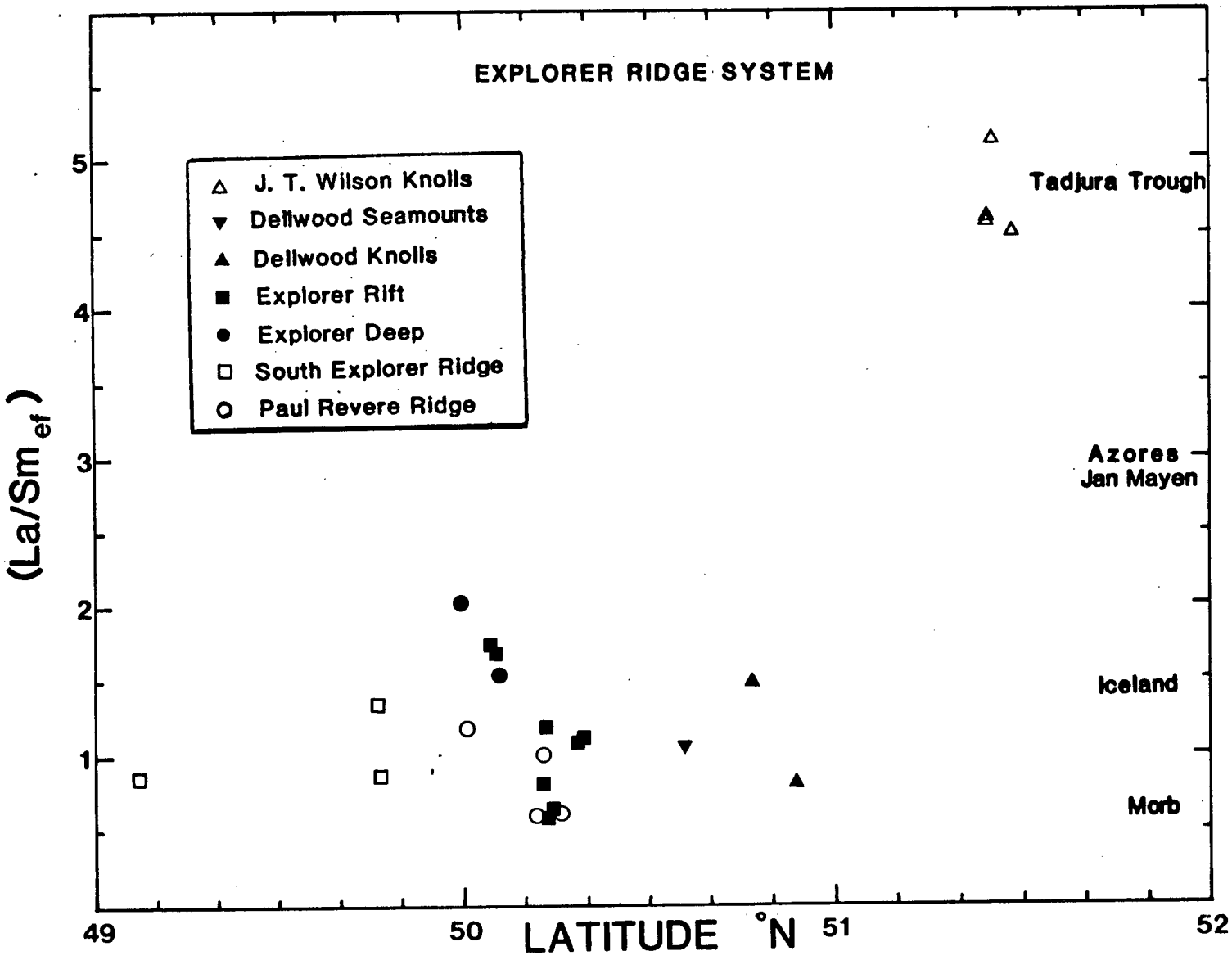

Figure 18 : Latitudinal variation in the La/Sm ratio, normalized to chondrites, for the Explorer system. Average values for MORB and typical ocean island basalts indicated on right side of diagram.

pletion of the magma-generating mantle source. The Explorer area basalts have low to transitional Zr/Nb ratios compared to MORB, varying from 6 to 30 (Figure 19). Explorer Deep and the JTW Knolls have the lowest ratios, which are typical of ocean island plume basalts. The same patterns noted for the REE in Explorer rocks are evident in the Zr/Nb ratios. Liias et al. (1981) report Zr/Nb ratios of approximately 25 for one hundred and twenty four samples, from fifty-two dredge hauls, from the Juan de Fuca Ridge. This is thought to be the first occurrence of intermediate Zr/Nb ratios along such an extended ridge segment (400 km). Thus, the Explorer basalts have somewhat atypical Zr/Nb ratios for MORB, but are similar to, or lower than, those of Juan de Fuca Ridge basalts. The mantle source of Explorer basalts appears to be undepleted relative to most ocean ridge systems.

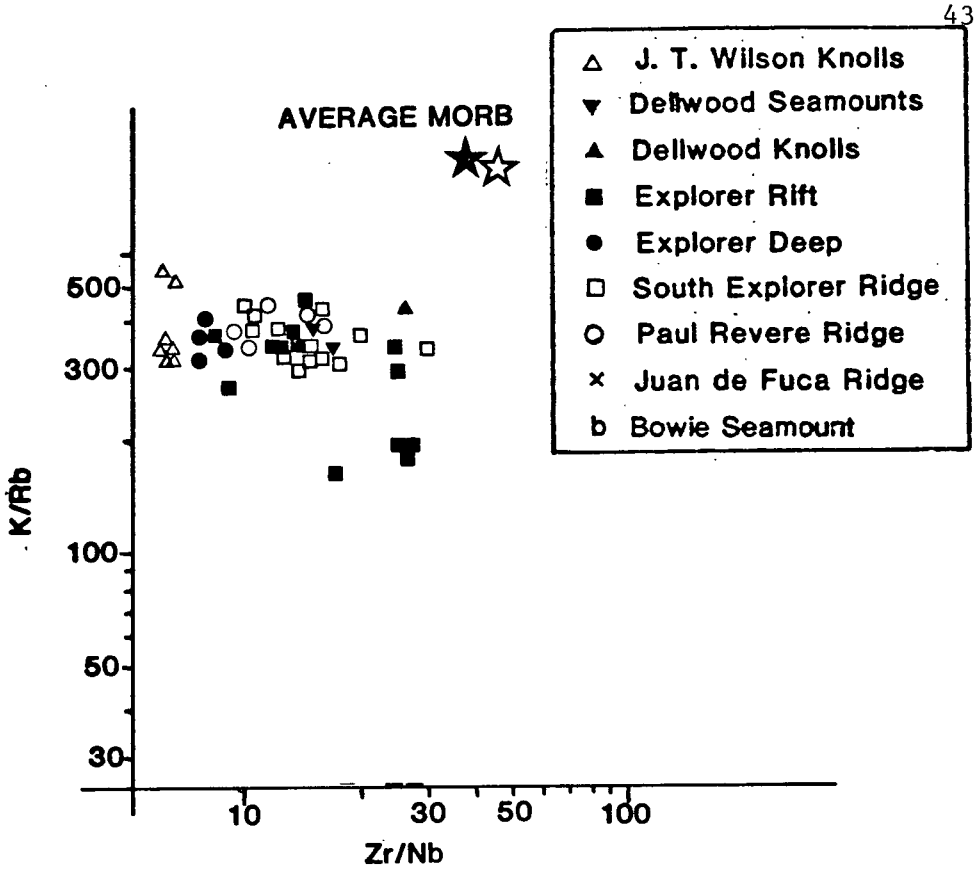

Figure 19: Zr/Nb diagram (Erlank & Kable, 1976) for Explorer area basalts. Closed star: Average MORB, Erlank and Kable, 1976. Open star: Average MORB, Sun, 1980.

STRONTIUM ISOTOPES

(i) Analytical Procedure

Seven basalts from the Explorer-Dellwood system, three JTW Knolls hawaiites, and one alkali basalt from Bowie Seamount have been analysed for $^{87}Sr/^{86}Sr$ ratios, using a VG Isomass 54R mass spectrometer. Data acquisition is automated using a Hewlett-Packard HP-85 computer. Experimental data has been adjusted so that the NBS standard $SrCO_3$ (SRM987) gives a $^{87}Sr/^{86}Sr$ ratio of .71020±2. Samples were unspiked, and were prepared using standard ion-exchange techniques.

$^{87}Sr/^{86}Sr$ ratios for the basalts are listed in Appendix 2.

(ii) Precision and Accuracy

For each sample, between 6 and 15 separate data blocks were completed, and machine 1σ precisions range from ±.00002 to ±.00015. The average 1σ precision is .00006, although true reproducability is probably ±.00010 (R.L. Armstrong, personal communication). Three of four duplicate analyses do fall within .00010 of each other.

(iii) Results

The spreading ridge basalts have $^{87}Sr/^{86}Sr$ ratios ranging from .70232 to .70254. They fall within the range of analyses from the Juan de Fuca and Gorda Ridges (Figure 20), which is between .7023 and .7027 (Sun et al., 1979). Three other analyses from the northwest Dellwood Knoll, northern Juan de Fuca Ridge (71-23-3), and Explorer Seamount (69-6-4), also fall within the range of the Explorer analyses (Nixon and Armstrong, 1980).

It is notable that the Explorer samples enriched in incompatible elements (79-6-32-39, 77-14-33-A, 70-25-15-3) have similar isotopic ratios to the incompatible-element-depleted basalts (70-25-4-62, 77-14-36-X), and thus their mantle sources appear to be similar isotopically.

However, the northwest Dellwood Knoll basalt is significantly less radiogenic than the southeast Knoll basalt. This, combined with the LREE enrich-

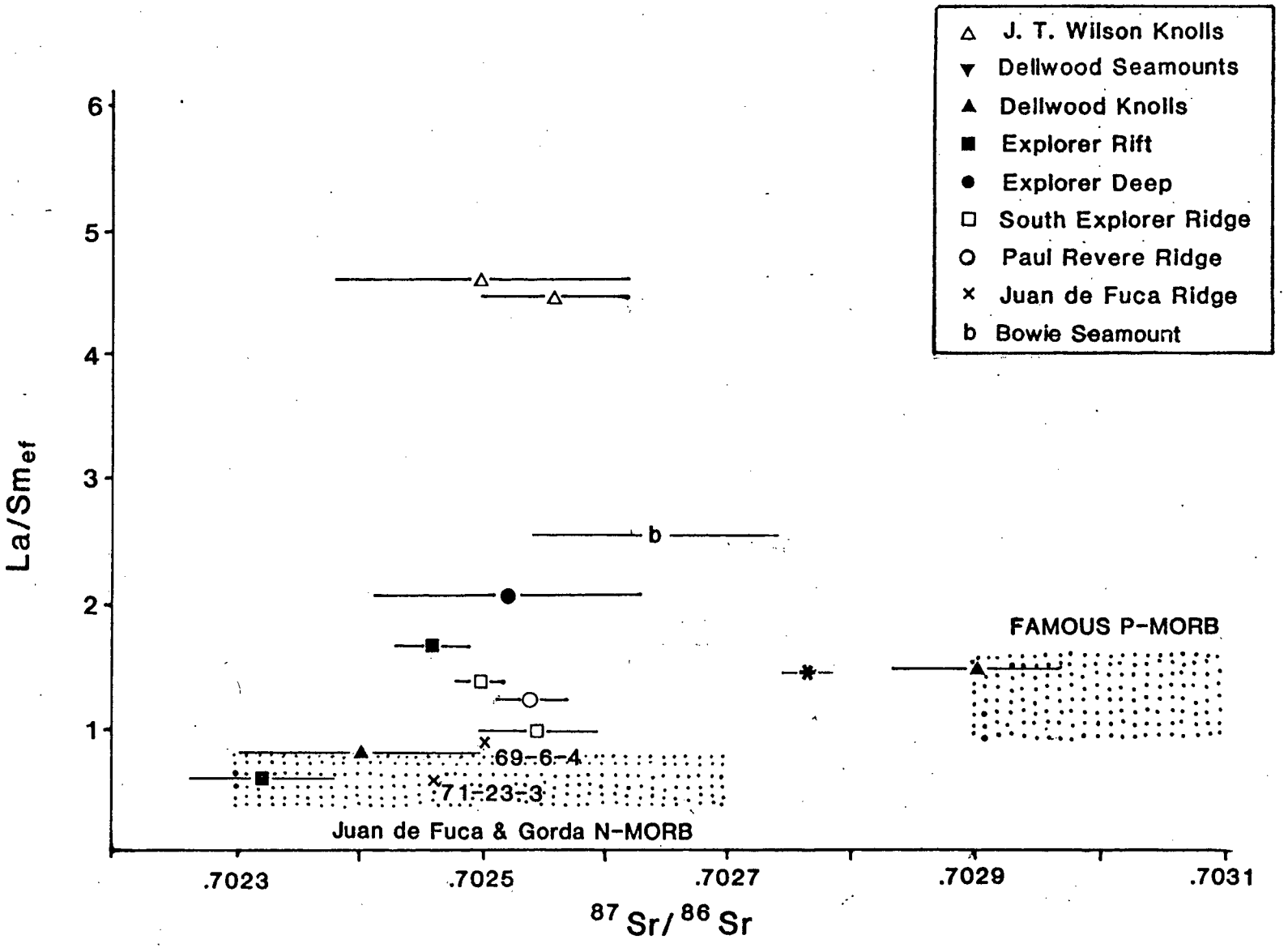

Figure 20: La/Sm $_{ef}$ vs. $^{87}Sr/^{86}Sr$ for Explorer,Dellwood, JTW, and Bowie basalts. Juan de Fuca and NW Dellwood Knoll analyses from Nixon and Armstrong (1980). Error bars are precisions determined from within-run variation of the measured ratio for each sample. Reference fields from Sun et al, (1979). Asterisk: leached sample 70-25-3D-1.

ment of the southeast Knoll, suggests that the mantle sources for the basalts from the two adjacent knolls are different. To ensure that the observed difference in $^{87}Sr/^{86}Sr$ ratios is not due to alteration by seawater of sample 3D-1, a leached subsample (following an HCl-leaching procedure described in Zhou and Armstrong, 1982, in press) was run through the mass spectrometer, yielding a slightly lower ratio of .70267. This is still significantly different from the northwest Knoll value of .70240, which if subjected to the leaching process, would probably also be reduced (R.L. Armstrong, personal communication).

The JTW and Bowie Seamount alkali basalts appear to be distinct from the Explorer basalts, as indicated in Figure 20. They fall within the range of $^{87}Sr/^{86}Sr$ values obtained from the other Pratt-Welker seamounts, although the observed ratios are somewhat lower than the Pratt-Welker average (.7032-.7039) and the ocean island basalt average (Forbes et al., 1982; Sun et al., 1979).

DISCUSSION

Explorer Ridge and Propagating Rifts

In terms of major element chemistry, the Explorer area ridge basalts can be classified as ferrobasalts, or as MORB bordering on ferrobasalt (Melson et al., 1976). This is characteristic of many other segments of the fast-spreading East Pacific Rise, and is considered to be the result of low-pressure crystal fractionation (Clague and Bunch, 1976). The results of this study are consistent with the findings of Vogt and Byerly (1976), who suggest that the observed high magnetic relief over the Explorer area (Figure 21) could be due to high Fe-Ti basalts, similar to those dredged from the southern Juan de Fuca Ridge. The FeO^t and TiO_2 contents of the Explorer basalts are very similar to those of the Juan de Fuca and Galapagos Ridges, and one sample (72-22-7-1) from the Paul Revere Ridge resembles the extreme FETI basalts that are associated with both areas.

FETI basalts are associated with propagating rifts (Hey et al., 1980; Byerly, 1980), an example of which is the southern Juan de Fuca Ridge. Figure 3 is a magnetic anomaly map for the Juan de Fuca area, showing several magnetic "pseudofaults" which are interpreted to be features of major ridge propagation sequences (Hey, 1977). If the V-shaped pseudofault marked "1" is the result of ridge propagation, it implies that the Explorer Ridge has propagated southwest to its present southwestern termination at the Sovanco Fracture Zone in the recent past. As is characteristic of other propagating rifts, the ridge segment is oriented obliquely to the Sovanco F.Z. (Hyndman et al., 1978). Another feature of propagators is that the highest FeO^t and TiO_2 contents are found at the tip of the propagating segment. Samples 71-15-70-1/8, from the extreme southwest end of the Southern Explorer Ridge, have among the highest FeO^t (12.0%) and TiO_2 (2.1%) contents of all the samples studied. At the northeast end of

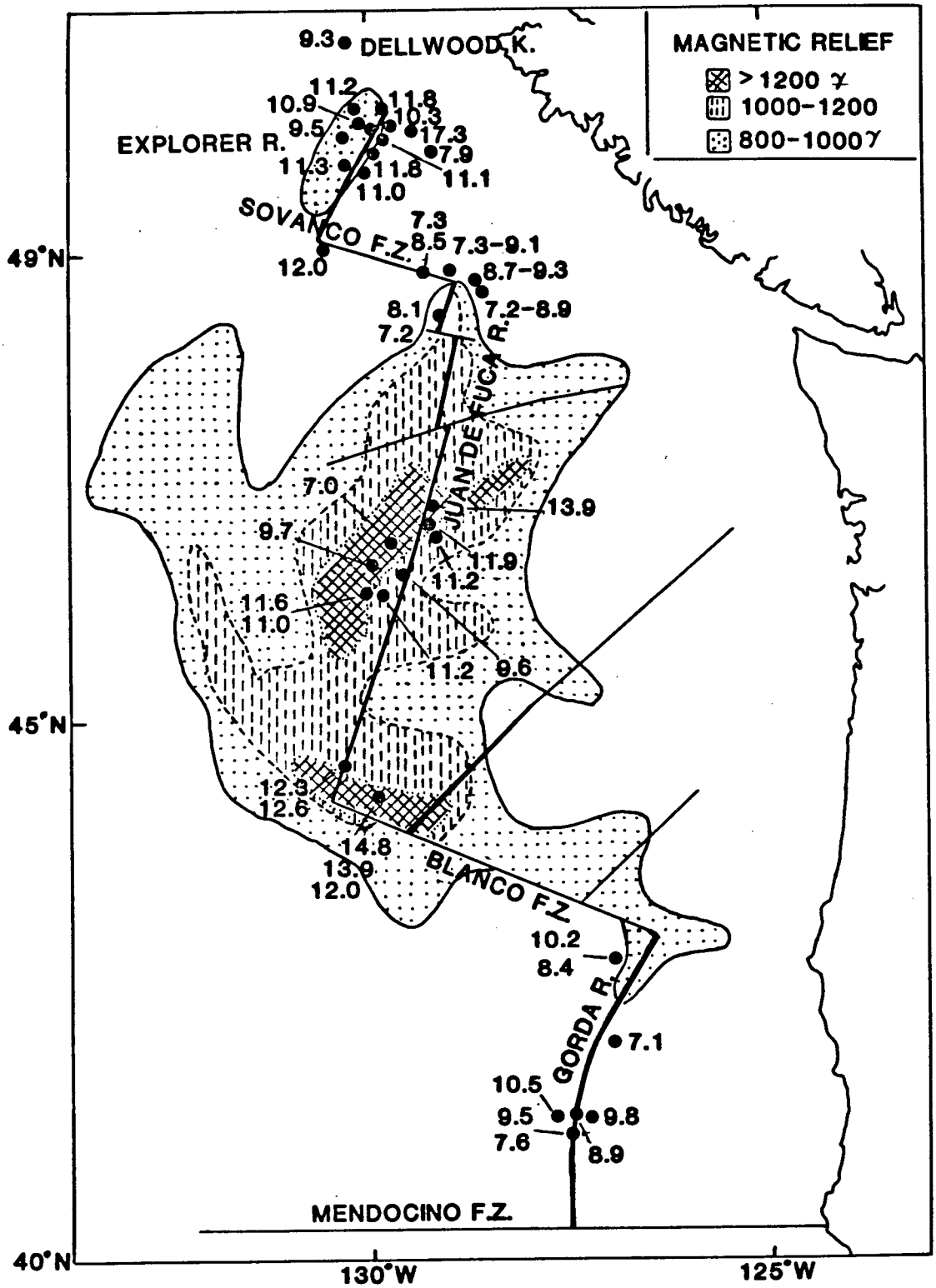

Figure 21: Map of magnetic relief and FeO content along the Juan de Fuca system. Total iron expressed as FeO. Dots mark dredge sites. Magnetic relief and Juan de Fuca FeO data from Vogt and Byerly (1976).

Explorer Deep, Paul Revere Ridge (fracture zone) samples 71-15-92-8 and 72-22-7-1 have very high FeO^t (11.8-17.3%) and TiO_2 (1.95-3.53%) contents, which could be interpreted as evidence for an older, northeasterly propagator (Figure 20). However, sampling is at present insufficient to make a definitive conclusion concerning the propagating rift theory as it applies to the Explorer area. A detailed magnetic and bathymetric survey of the Southern Explorer Ridge is also lacking, the south end of which is extremely interesting in terms of this theory.

Explorer Deep, Explorer Rift, and the Southern Explorer Ridge

Much of the chemical variation within the Explorer-Dellwood system can be explained by low-pressure crystal fractionation (Figures 11, 15-17). However, all the plots show considerable scatter, suggesting that some other process is influencing the basalt chemistry. As well, the LREE enrichment measured in many of the samples cannot be explained by fractionation (Schilling, 1971).

Explorer Deep basalts have exceptionally high concentrations of K_2O, Ba, Nb, and Rb, as well as an anomalous LREE-enriched rare earth pattern. Figure 22, after Sun (1980), illustrates the normalized pattern of incompatible trace elements. Explorer Deep basalts, and some of the Explorer Rift rocks, have the characteristics of plume-influenced MORB, or P-MORB (Sun et al., 1979), where ocean ridge basalt magmas are augmented by an incompatible-element-rich phase, such as a plume magma. The Azores Platform and the Reykjanes Ridge are areas where this process has been documented (White et al., 1976; Schilling, 1973).

Explorer Deep is presently a 400-meter deep graben however, with no obvious topographic expression of a plume nearby. There are many small seamount chains trending away from the ridge, such as the Dellwood Seamounts, which probably originated at Explorer Deep between 2.8 and 4.5 Ma BP. In the past, therefore, we have evidence for above-average volumes of magma generation in the Explorer Deep area. In addition, the average sea floor depth in the Ex-

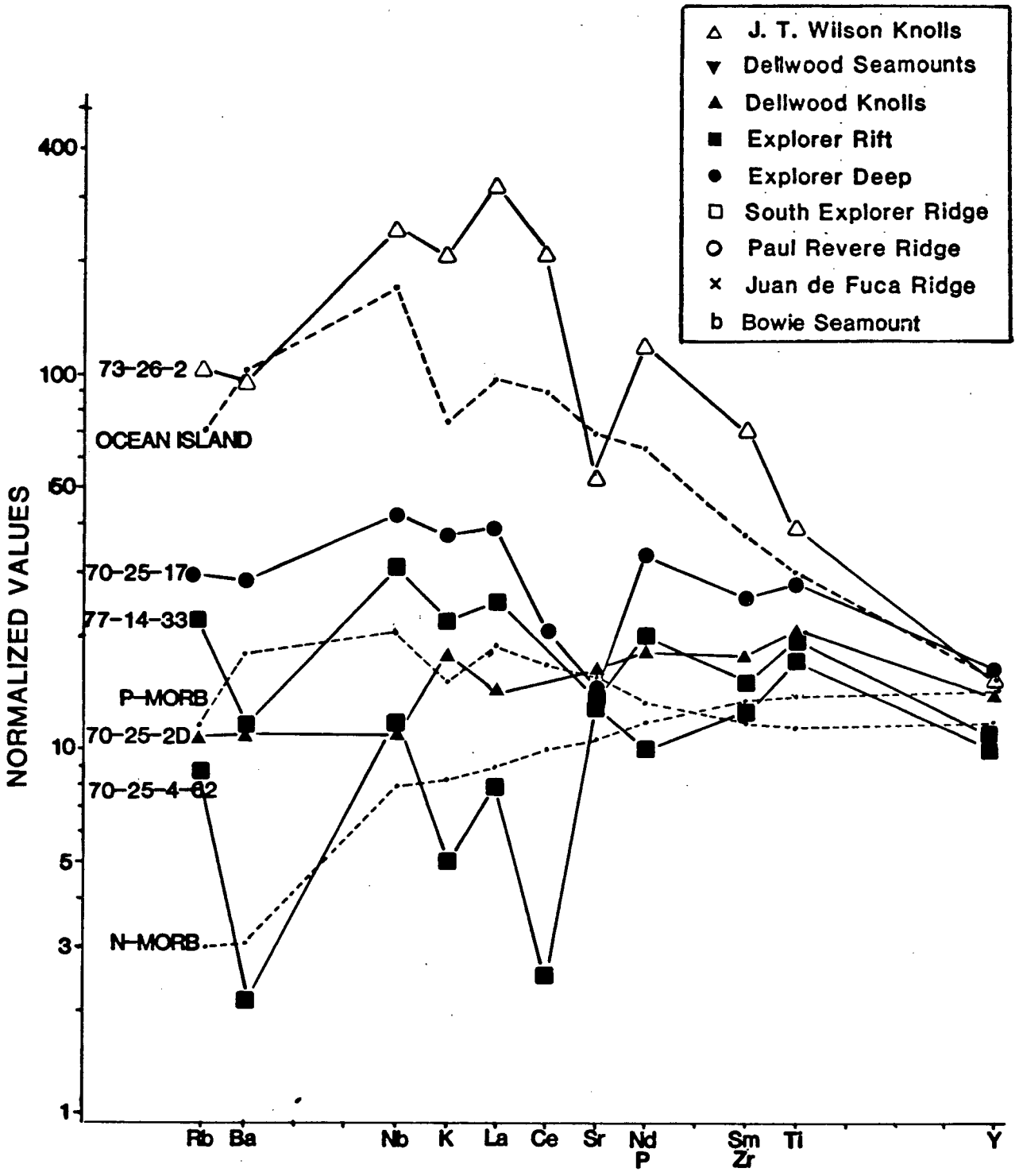

Figure 22: "Sun diagram" (Sun, 1980) showing variations in incompatible element concentrations relative to chondrites for Explorer area basalts, average normal MORB,(N-MORB), plume-enriched MORB (P-MORB), and ocean island basalts.

plorer Deep is slightly shallower than the average depth of the northern Juan de Fuca Ridge (2200 meters and 2400 meters, respectively). For the Explorer Ridge as a whole, the average depth increases from 2200 meters near Explorer Deep, to 2800 meters at the Sovanco Fracture Zone. The shallower depth of the Explorer Deep area may reflect the presence of a broad hotspot zone centered beneath it.

It should be noted that a plume model is not required to explain the anomalous chemistry of Explorer Deep. A smaller degree of partial melting of the mantle source would also explain the high levels of incompatible elements without effecting the major element chemistry (O'Hara, 1977). The Sr^{87}/Sr^{86} ratios for the Explorer Deep basalts are not different from the other more typical MORB from the Explorer system, and suggests that the above explanation may be more suitable for this case. Other plume-influenced areas, such as the FAMOUS area and the Mid-Atlantic Ridge at 45°N, exhibit anomalously high Sr^{87}/Sr^{86} ratios compared to Atlantic MORB (White et al., 1978).

An alternate explanation for the shallower depths of Explorer Deep is flexure of the crust caused by oblique subduction of the Pacific and Explorer Plates beneath the American Plate. This process is probably responsible for the tilting of the Paul Revere Ridge and compression in the Winona Basin (Davis and Riddihough, 1982). The Oshawa Rise, an elongate basement high extending southeast from Bowie Seamount (Figure 23), is thought by Silver et al. (1974) to mark the passage of the Pacific Plate over a hotspot. However, this feature may also represent flexure due to subduction (C. Yorath, personal communication).

The three other ridge segments display a large degree of chemical variation. Three dredge hauls from Explorer Rift, within 15 km of each other, recovered three different basalt types. Type 1 is a differentiated, incompatible element enriched basalt (71-15-77). Type 2 is a relatively undifferentiated, incompatible element depleted basalt (70-25-4 and 70-25-16-1). Type 3 is also relatively undifferentiated, but is weakly enriched in incompatible

elements (77-14-33). The incompatible element patterns of Type 2 and Type 3 are shown in Figure 22. Even within a single dredge haul, 70-26-16, basalts of Types 1 and 2 were recovered. This variability cannot be related to fractionation. It could be an indicator of a heterogenous mantle source beneath Explorer Rift, especially since no appreciable difference in Sr isotopes is observed between the Type 2 and 3 basalts.

Alternately, if a hotspot does exist beneath Explorer Deep, feeder dykes could extend northwards to Explorer Rift, and at times produce basalts enriched in incompatible elements with respect to other magmas erupted in the same rift. Note that in Figure 22, the pattern of sample 77-14-33 lies between the Explorer Deep pattern and 70-25-4-62, as if mixing of the latter two magmas could produce the pattern of 77-14-33.

Basalts from the Southern Explorer Ridge show the same variability in incompatible element concentrations without much change in the degree of fractionation. Although all the samples have moderate to high levels of K_2O and trace elements, and similar magnesium ratios, their La/Sm_{ef} ratios vary from 0.85 to 1.35. Thus, although the Southern Explorer Ridge tholeiites appear to be more fractionated than the Explorer Rift basalts, the same heterogeneity affects both ridge segments. Unfortunately, sample coverage of the Southern Explorer Ridge is irregular, mostly from the northern end; only one sample is from the southern end. More samples are needed to give even coverage, but these do not exist at present.

Dellwood Knolls

The geology of the Dellwood Knolls has been studied in detail by Bertrand (1972) and Riddihough et al. (1977). Both studies indicate that the northwest knoll (sample 70-25-2D-8) is presently active seismically and volcanically, while the southeast knoll (sample 70-25-3D-1) ceased activity approximately 1 Ma

BP. Chemically, the knolls are very different. Based on major element data, sample 3D-1 is a more fractionated basalt, that could have had a parent magma of similar composition to sample 2D-8 (Figure 5, 11).

The only new data presented in this study from the Dellwood Knolls are selected trace element contents, La/Sm_{ef} ratios, and Sr^{87}/Sr^{86} ratios for both 3D-1 and 2D-8. The rare earth and Sr isotope data suggest that 2D-8 could not be a parent magma for 3D-1. The more radiogenic nature and LREE enrichment of 3D-1 indicate that it had a very different mantle source from 2D-8. As with Explorer Deep, a plume influence may be responsible for the chemical variation in the Dellwood area.

J. Tuzo Wilson Knolls

The conflicting evidence as to the origin of the J. Tuzo Wilson Knolls makes this an interesting part of this study. In the origional study of the Knolls, Chase (1977) considered them to be the expression of the mantle plume which had probably created the Pratt-Welker Seamount Chain (also called the Bowie-Kodiak Seamount Chain). As shown in Figure 23, the JTW Knolls lie on the trend (colatitude) of the Pratt-Welker Chain, and lie only 60 km northwest of the Dellwood spreading segment. One aim of this study is to determine if, as with other ridges with nearby hotspots, magma mixing of the two types of basalt is occurring, resulting in a chemical gradient from the JTW Knolls south through the Dellwood-Explorer system. Examples of areas where this gradation from ocean island basalt composition to MORB is observed include the Reykjanes Ridge, the Galapagos Rise, and the Azores Platform (Schilling, 1973; Schilling et al., 1976; White et al., 1978).

It is immediately obvious that no smooth chemical gradient exists that could be due to simple magma mixing. In terms of alkali metals, incompatible elements, and especially the La/Sm_{ef} data, the JTW Knolls are distinctly different from the Dellwood and Explorer segments. It is possible that the magma

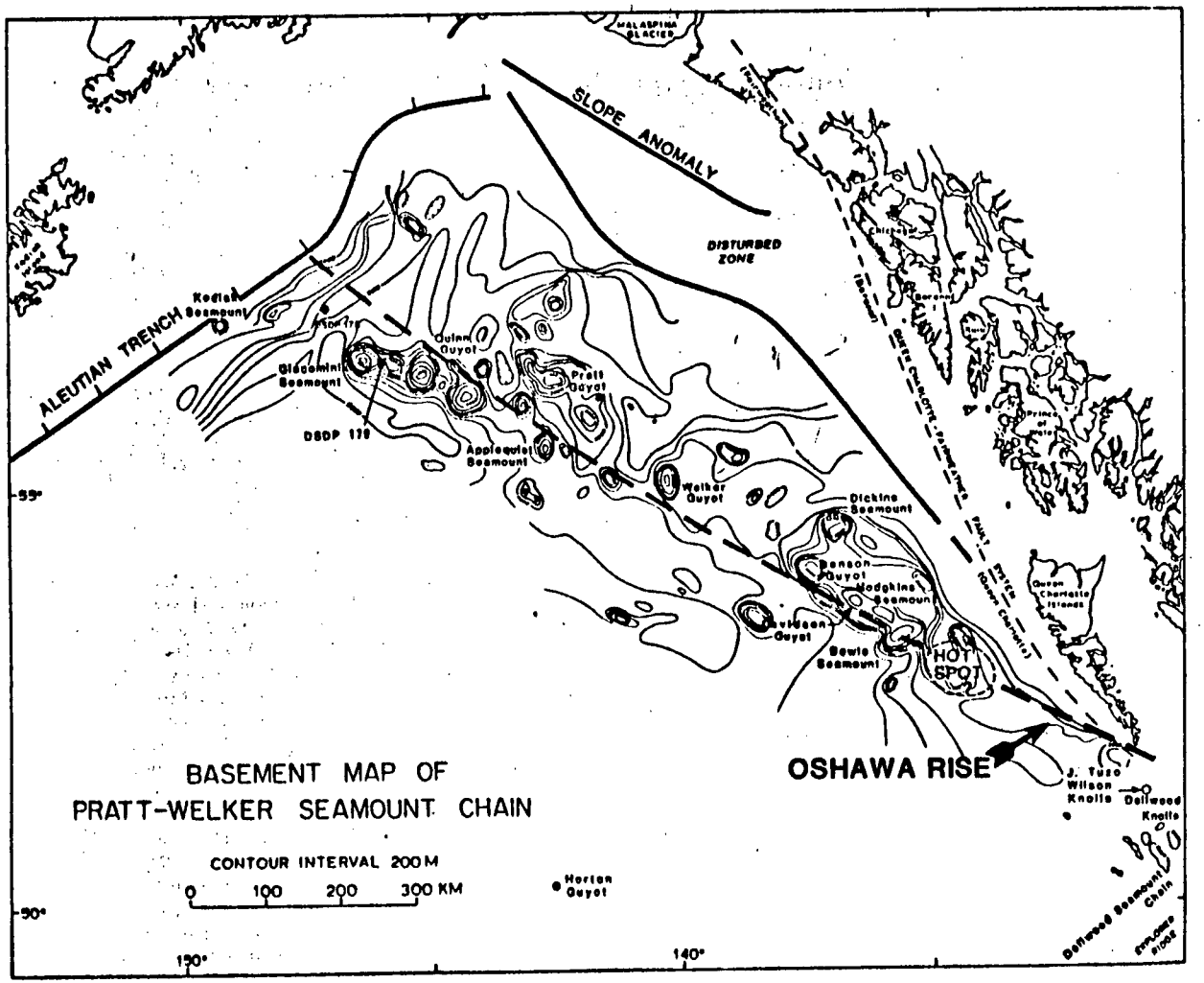

Figure 23: Simplified bathymetric map of the Gulf of Alaska, showing locations of the Pratt-Welker Seamounts. Dashed line describes a small circle about the Pacific-Hotspot pole of rotation. Map from Turner et al.(1980).

TABLE 5

Alkali Basalt Composition of Pratt-Welker Seamounts, J. Tuzo Wilson Knolls, and "Average" Ocean Isalnd Basalt.

	Kodiak	Giacomini	Hodgekins	Bowie	JTW	"Average"
SiO_2	44.08	47.62	45.33	45.40	50.12	47.41
TiO_2	3.16	2.42	3.53	2.60	1.78	2.87
Al_2O_3	16.60	16.42	15.50	18.50	16.16	18.02
Fe_2O_3*	13.25	13.82	13.72	11.86	7.62	10.67
MnO	0.16	0.14	0.23	0.19	0.17	0.16
MgO	2.43	1.65	6.77	5.90	6.78	4.79
CaO	7.59	8.13	8.50	8.50	8.57	8.65
Na_2O	4.01	4.79	4.30	3.80	4.95	3.99
K_2O	1.69	1.81	2.36	1.90	2.02	1.66
P_2O_5	1.14	1.84	0.73	0.70	0.58	0.92
H_2O^+	1.83	1.51	0.20	0.40	1.17	0.79
SUM	98.11	99.89	99.91	98.59	100.48	100.54
FeO^t/MgO	4.86	7.48	1.81	1.80	1.42	1.99
La/Sm_{ef}	2.4-3.5	2.0	1.2-2.0		4.5-5.1	2.5
Source:	Forbes and Hoskin, 1969.	Forbes et al., 1969.	Engel and Engel, 1964.	Herzer, 1971.	this study	Engel et al., 1965.
K-Ar age:	23.4 Ma	20.8 Ma	2.8 Ma	>75,000 yrs.	55,000 yrs.	

(all age data from Turner et al.(1980), except JTW from this study.)

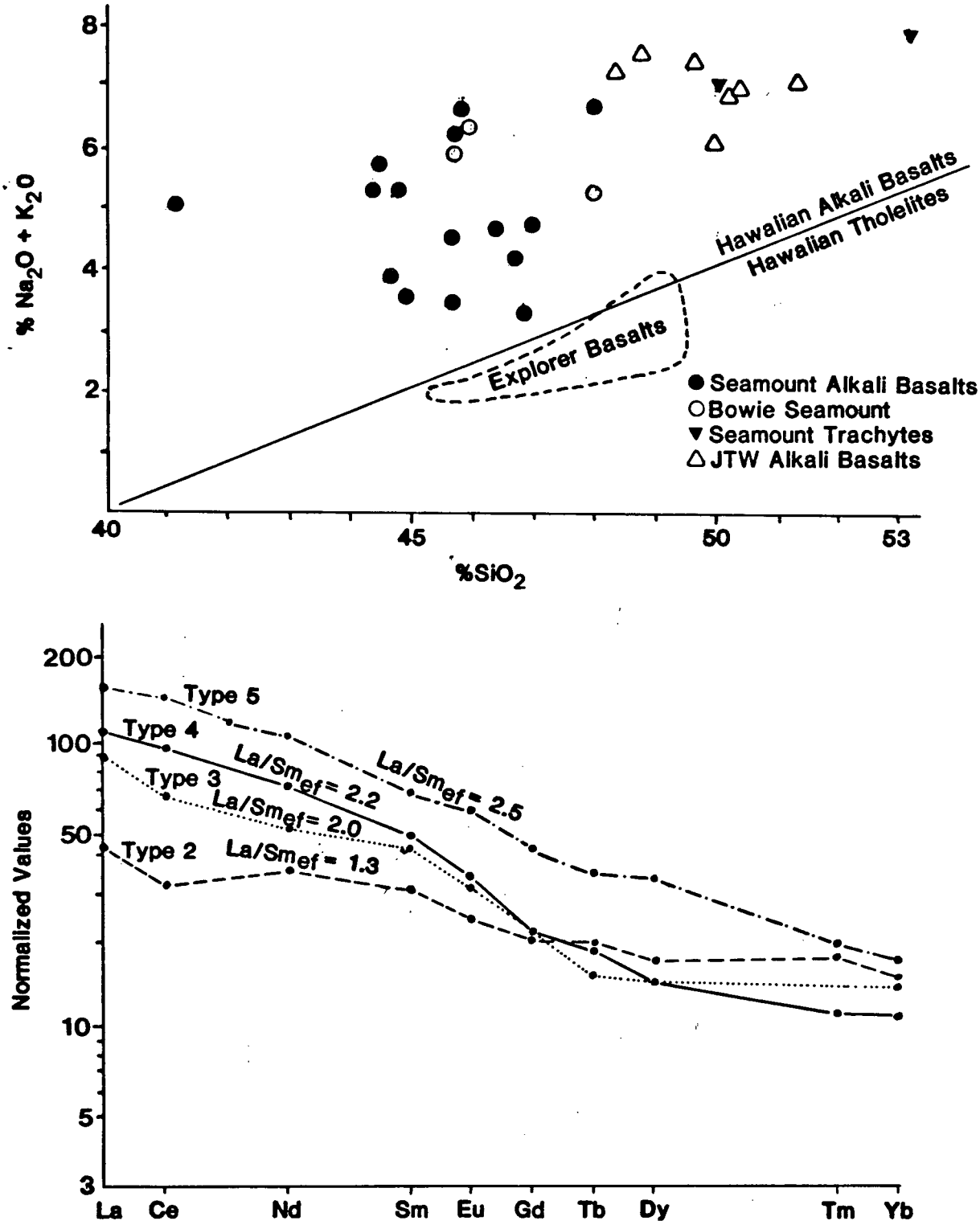

Figure 24: Silica variation diagram and chondrite-normalized rare-earth patterns for the Pratt-Welker Seamount magma types. Data from Forbes et al.(1982), and Bowie Seamount data from Herzer,(1971), Engel & Engel (1964).

source for the JTW Knolls is not very big, and that the spreading segments are too far away for mixing to occur. Iceland, the Galapagos Islands, and the Azores all rise above sea level, and must have higher magma production rates. All lie closer to or on the ridge segment whose chemistry they influence. Another factor to consider is the effect of fracture zones on magma movement. These faults truncate ridge segments and form an effective barrier to magmas migrating along the ridge magma chamber. This is exemplified at the tip of a propagating rift, which is separated from the dying rift by a transform fault. Sharp changes in basalt chemistry are seen from one end of the fault to the other (Schilling et al., 1976). Thus, due to the smaller rate of magma production, young age, the 60 km separation, and poor magma conductivity along transform faults, magma from JTW Knolls is not observed at the Dellwood Knolls.

In terms of major and trace element chemistry, the JTW hawaiites closely resemble the "average" composition of ocean island basalts (Engel et al., 1965) as shown in Tables 4 and 5. As well, the JTW basalts compare closely with the major element analyses from seamounts in the Pratt-Welker chain, such as Bowie, Kodiak, Giacomini and Hodgkins (Herzer, 1971; Forbes et al., 1969; Forbes and Hoskin, 1969; Engel and Engel, 1964), data from which are included in Table 5. However, there are minor differences between the JTW Knolls and the other seamounts, illustrated in Figure 24. The JTW alkali basalts are enriched in silica and total alkalies with respect to the Pratt-Welker alkali basalts, as is evident in the silica variation diagram. JTW hawaiites also have lower FeO^t/MgO ratios, suggesting that the enrichment is not simply the result of crystal fractionation. The La/Sm_{ef} ratios are also different. Ratios for the Pratt-Welker Chain seamounts range from 1.3 (transitional basalt) to 3.5 (trachyte), although most are between 1.8 and 2.4 (Forbes et al., 1982). The values are consistent throughout the chain. The JTW basalts exhibit a higher degree of LREE enrichment, with La/Sm_{ef} ratios of 4.5 to 5.1 .

Another difference between the JTW Knolls and the Pratt-Welker seamounts

is physiography. Except for Kodiak and JTW, all the seamounts are guyots that extended above sea level at some time in their history. The JTW Knolls have only 400-500 meters of relief above the thick sedimentary pile they are penetrating.

Chase (1977) calculated that the colatitude of the JTW Knolls, relative to the Pacific-Hotspot pole of rotation, lies within the range of colatitudes for the Pratt-Welker seamounts. The JTW area is connected to the seamount chain by a broad topographic rise, the Oshawa Rise, which Silver et al.(1974) attributed to the passage of the Pacific Plate over a mantle plume. From this, and the similar chemistries, Chase concluded that the JTW Knolls represented the present location of the Pratt-Welker mantle plume. The rate of rotation of the Pacific Plate about the PCFC-HSPT pole, 0.83°/Ma, of Minster et al.(1974) was then used to estimate the ages of the Pratt-Welker seamounts, assuming a zero age for JTW, as shown in Table 6. The K-Ar dates from Kodiak, DSDP Hole 178, and Giacomini Seamount match the estimated ages well. The southeastern seamounts all have significantly younger K-Ar dates than Chase's estimates, however.

A recent geochronological and bathymetric study of the Pratt-Welker Chain disputes the idea that the mantle plume that created the chain presently lies near the JTW Knolls (Turner et al., 1980). Bowie Seamount has a magnetic age of 0.72 Ma or less, and tephra from a small, late-stage pinnacle yields a whole-rock age of 75,000 ±100,000 yrs. Morphological considerations suggest that the latest stage of volcanism on Bowie must have occurred within the last 18,000 yrs. Turner et al.(1980) therefore conclude that the mantle plume presently sits only 40-130 km southeast of Bowie Seamount (Figure 23). Yet sample 73-26-2-1C from the JTW knolls has a K-Ar age of ~54,000 yrs, and has a distinct ocean island chemical affinity. Consequently, we must explain two seamounts of similar age and chemistry that are 300 km apart.

The existence of a second hotspot, lying on the same colatitude as the

TABLE 6

Position and Age Data for the Pratt-Welker Seamounts*

	J.T. Wilson	Bowie	Hodgekins	Dickens	Giacomini	DSDP 178	Kodiak
Co-latitude about PCFC-HSPT Pole (deg):	37.1	37.4	37.4	36.9	38.8	38.6	39.4
Angular Distance from JTW about PCFC-HSPT Pole (deg)	0	5.5	6.1	7.8	16.6	17.6	18.9
Calculated Age (Myr)	0	6.7	7.4	9.4	20.0	21.2	22.8
K/Ar Age (Myr)	<0.1	0.1±0.1	2.65±0.2 13.2±2.0†	3.7±0.2	19.9±1.0	22-23	22.6±1.1
Fission Track Age (Myr)	-	-	-	4.2±1.4†	19.3±3.8 19.8±1.9†	-	25.3±4.3 21.6±2.2† 30.1±2.2†
Age of Underlying Crust from Magnetic Anomaly Identification	<10	18	19	20	46	47	50

* - Table taken from Chase (1977).

† - Data from Turner et al. (1980).

first, but 300 km southeast of it, more LREE-enriched and less prolific in magma generation, could explain the differences between the JTW and Pratt-Welker seamounts. Turner et al. (1980) suggest that the southeastern seamounts have experienced two phases of volcanism, one near-ridge, and one plume. As shown in Figure 25, the near-ridge phase from Denson, Davidson, and Hodgekins seamounts have K-Ar ages approximately 4 Ma younger than the crust they are penetrating. The JTW Knolls are presently intruding crust of 4.6 to 5.4 Ma in age, and thus could represent a hotspot responsible for the near-ridge phase. It must be noted, however, that a progression line drawn through the JTW and "near-ridge" seamount basalts in Figure 25 would have a steeper slope, and smaller rotation rate, than the progression line for the alkali basalts. This would imply that the proposed JTW plume is not fixed, and is moving in a direction similar to the rotation of the Pacific Plate about the PCFC-HSPT pole of rotation.

The near-ridge phase basalts from Denson, Davidson, and Hodgkins Seamounts are chemically different from JTW basalts. The former are transitional between alkali basalt and tholeiite (K_2O>.25%, La/Sm_{ef}=1.3, Type 2 in Figure 24). The latter are hawaiites (Type 4, Figure 24). This probably reflects the normal ocean island chemical cycle. Many ocean islands are largely made up of transitional to tholeiitic basalts (e.g. Hawaii), which is the dominant magma type through most of the active life if a seamount. Alkali basalts are typical of the late stage of activity, and volumetrically form only a small part of an ocean island.

It could be argued that a second hotspot is not necessary to explain the simultaneous volcanism of the two seamounts, Bowie and JTW, 300 km apart, citing the Hawaiian hotspot as an example. Coeval tholeiitic volcanism has occurred on Waianae and Niihau, and Nihoa is not much older than Kauai. Thus, the length of crust affected by the plume at any one time is in the order of 200-400 km (Dalrymple et al., 1973). However, the average rate of hotspot pro-

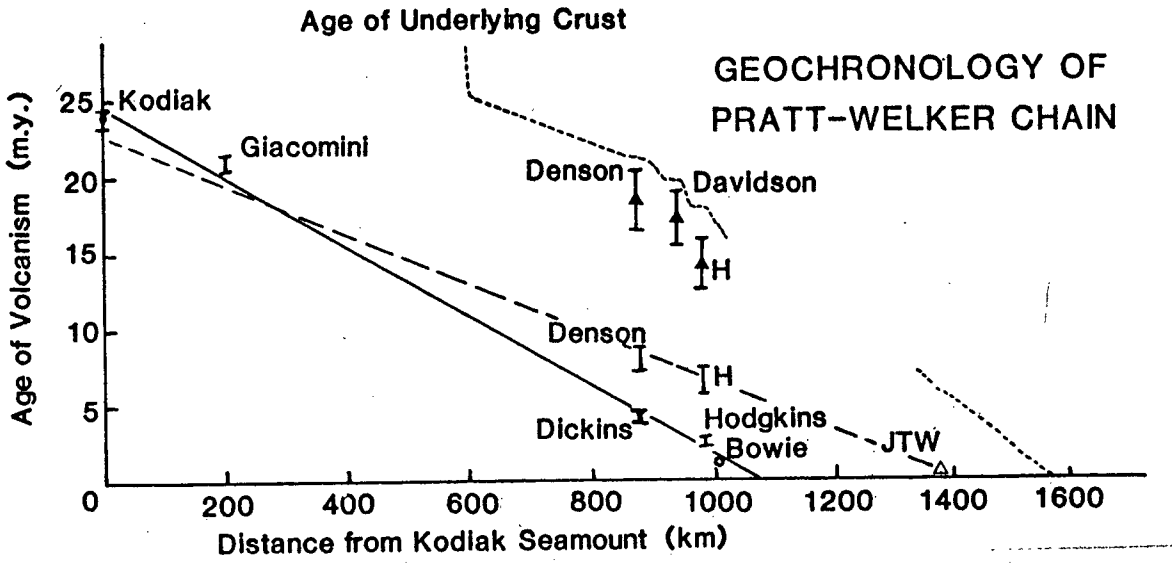

Figure 25: K-Ar and fission track ages of the Pratt-Welker seamounts plotted against distance from Kodiak Seamount. Solid line indicates trend of alkali basalts. Dashed line indicates age of oceanic crust. From Turner et al.(1980). Long dashed line is age progression of chain from Chase (1977, Table 6). Transitional basalts marked by solid triangles.

gression on the Hawaiian chain is 12.5 cm/yr (Dalrymple et al., 1973), which is much faster than the 4.4 cm/yr rate calculated for the Pratt-Welker Chain (Turner et al., 1980). It would be expected, therefore, that the length of crust effected by the hotspot at one time would be longer in the Hawaiian chain than in the Pratt-Welker chain. Thus, the existence of a second plume better explains the data.

Other theories, besides the plume or hotspot, have been used to explain seamount chains, such as the propagating crack (Turcotte and Oxburgh, 1973), and the longitudinal roll (Richter, 1973). Neither hypothesis requires that there be an age progression along the chain, nor do they explain the chemical cycle exhibited by the seamounts.

Geophysical evidence suggests that the JTW Knolls are the topographic expression of a new spreading segment, initiated less than 1 Ma BP. (Hyndman et al., 1978; Riddihough et al., 1980; R. Hyndman, personal communication). Ocean-bottom seismometers have recorded seismic activity along a proposed transform fault between the Dellwood and JTW Knolls, lying parallel to, and 25 km southwest of, the continental margin (Figure 26). As well, seismic reflection profiles from the NW Dellwood Knoll to the continental margin show a 20 to 25 km gap between the fault-truncated Knoll and the fault-bounded continental slope (Figure 27). CSP Profiles from the JTW area reveal that the pre-existing sedimentary pile has been uplifted and pushed 20-25 km away from the new spreading center. Heat flow values from the surrounding sediments range from 4.7 to 8.3 μcal $cm^{-2}sec^{-1}$, which are typical of other spreading centers. Magnetic data is not very good close to the continental slope due to thermal blanketing by thick sediments, but a broad, elongate positive anomaly is present over the proposed spreading center (Figure 28). The Knolls are intruding crust between 4.5 and 5.3 Ma in age, as indicated by extrapolated magnetic anomalies (Riddihough et al., 1980). The proposed rate of spreading is 5.5 cm/yr, which is the measured rate of relative motion along the Queen

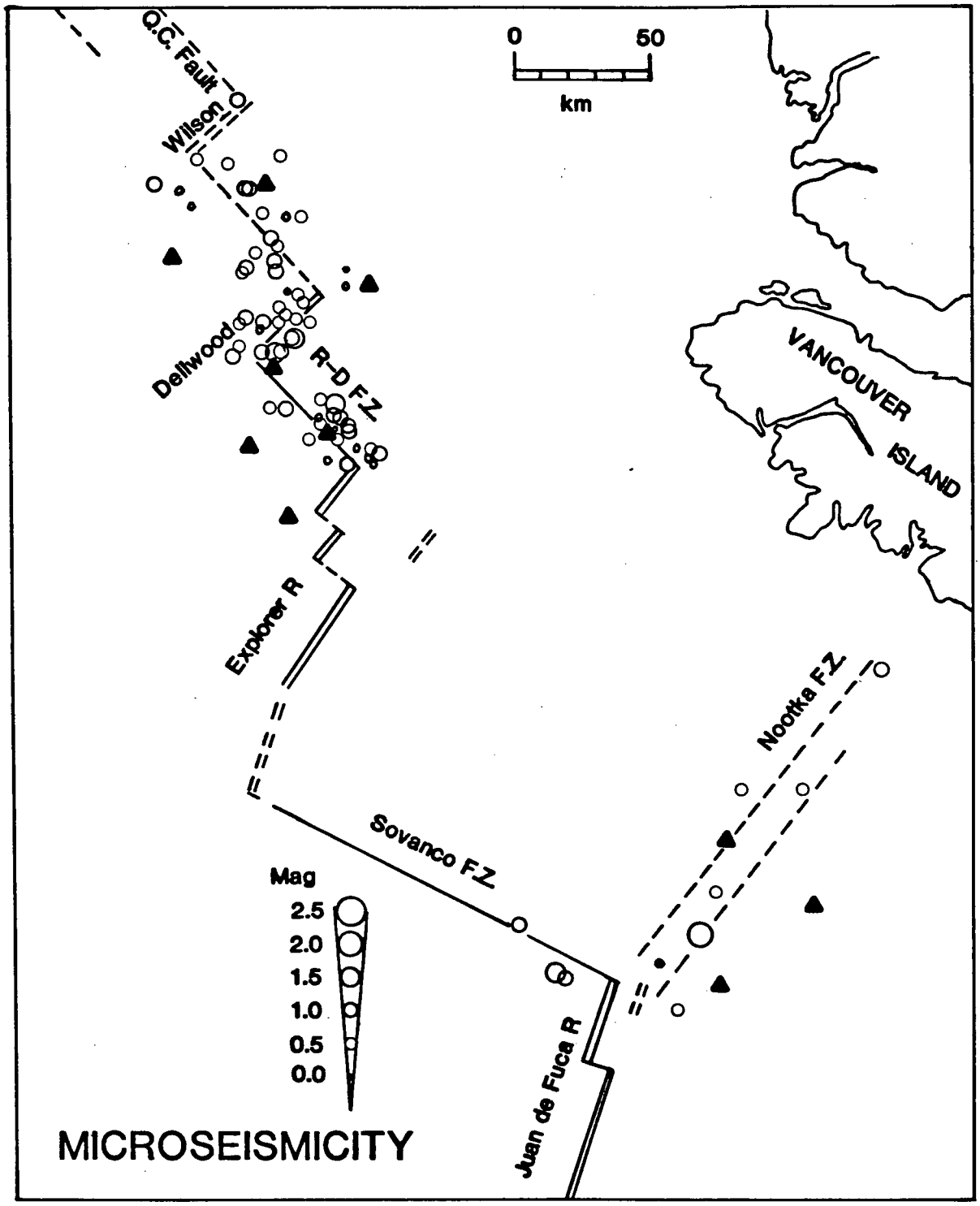

Figure 26: Microseismicity of the Explorer area from three ten-day ocean bottom seismometer surveys. Filled triangles mark OBS sites. Epicentral uncertainty approximately 10 km. From Keen and Hyndman (1979).

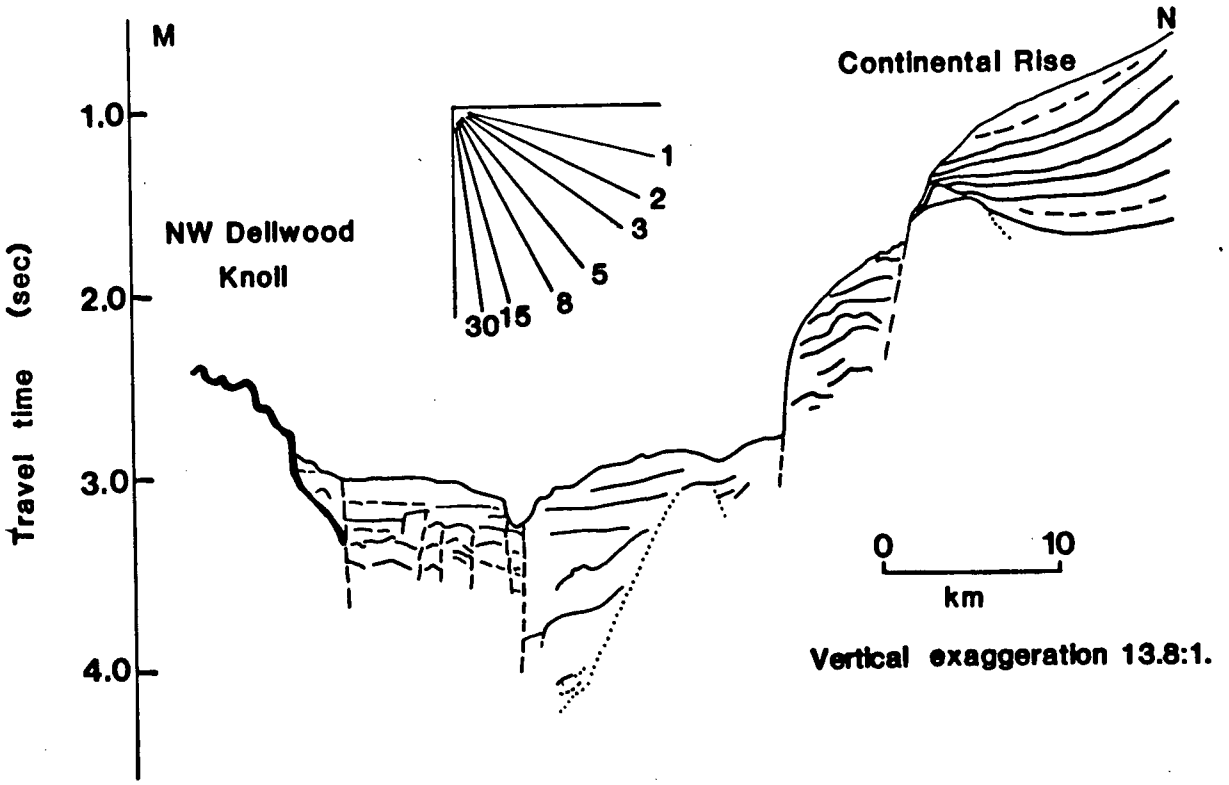

Figure 27: Southwest-northeast CSP profile across the continental rise from the NW Dellwood Knoll. Heavy line is oceanic basement, light lines are sedimentary reflectors, dashed lines are inferred faults (Bertrand, 1972).

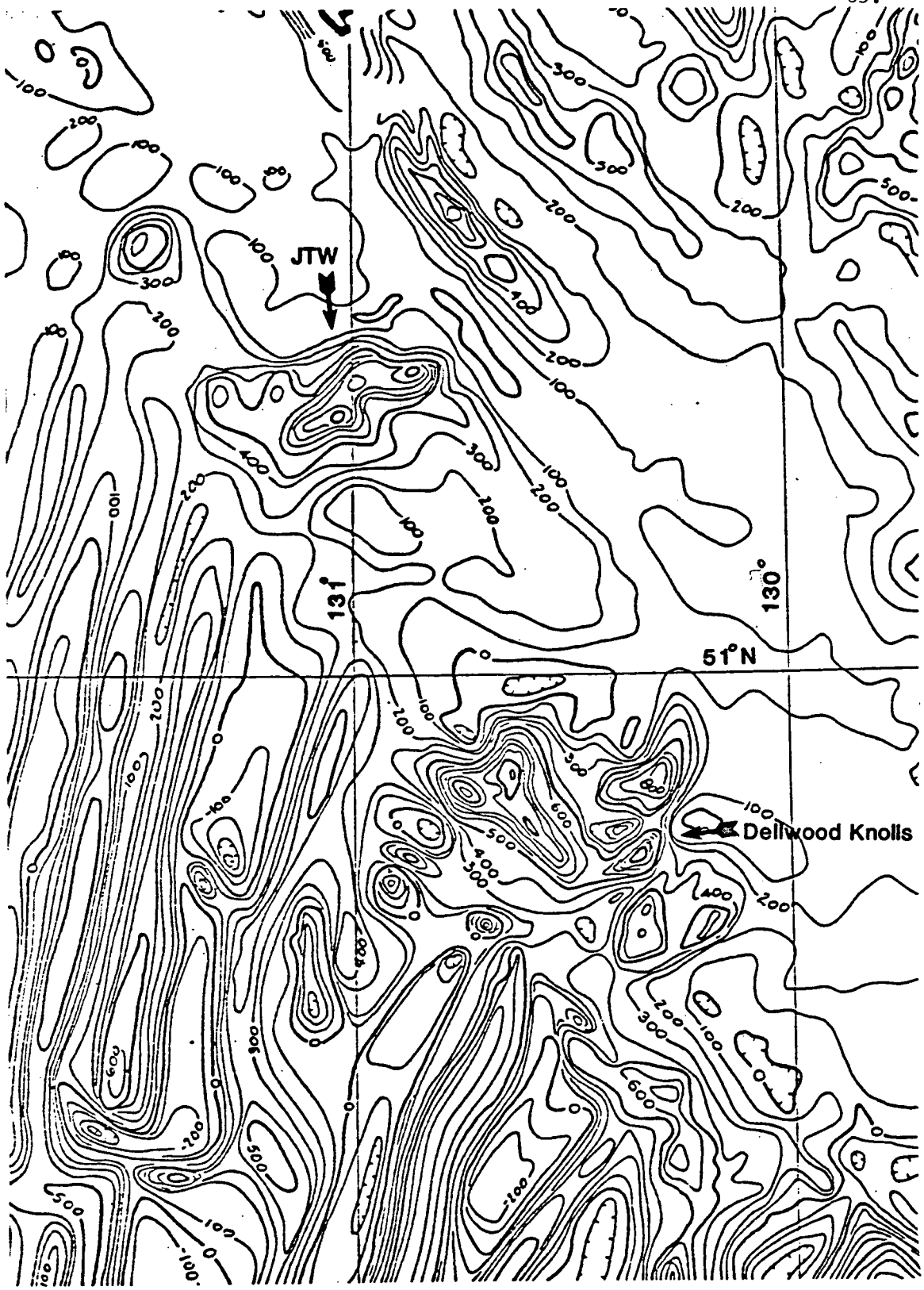

Figure 28: Magnetic anomaly map of JTW and Dellwood area. From Currie, R.G., and Seeman, D., 1980, Marine magnetic anomaly map-west coast of British Columbia, GSC Open File 724 (revised).

Charlotte transform fault. It is possible that the JTW microplate, along with the Dellwood segment and the Winona Basin, are now locked to the American Plate, and are moving with it (Davis and Riddihough, 1982).

Bathymetrically, the JTW Knolls do not have the typical conical shape of seamounts (Can. Hydrographic Service Map 19410-A, 2nd Ed., 1980), which is associated with most ocean islands. Instead, the southwest Knoll is more triangular in shape, with a steep, linear northwest face, while the northeast Knoll is elongated in a northeast-southwest direction. The direction of elongation of the seamounts is parallel to the proposed spreading axis.

However, chemically there is no evidence of typical ocean ridge volcanism at the JTW Knolls. The alkali basalts are distinctly non-MORB, and are too extremely alkaline to be the product of mixing of a plume magma with MORB, as is seen on the Reykjanes Ridge. It is likely that spreading has "jumped" to the JTW area because the plume created a weak spot in the crust, and readily tapped the magma source. The proposed ridge segment is only 25-30 km long, much smaller than the presumed size of the plume itself (Figure 23). This situation may be similar to that of Iceland, where the plume on the ridge produces all the magma necessary for spreading, and no typical MORB is produced.

Other newly initiated spreading centers in similar tectonic environments, such as the Gulf of California and the Gulf of Aden, are not similar chemically to the JTW Knolls (Terrell et al., 1979; Barberi and Varet, 1977; Barberi et al., 1980). Both areas of spreading are characterized by alkali-rich tholeiite (K_2O= 0.3-0.6%), but also exhibit LREE depletion (La/Sm_{ef}= 0.60-0.75). J.-G. Schilling (personal communication) reports a fresh olivine tholeiite dredged from a single volcanic cone on the spreading ridge in the Gulf of Tadjura (Afar area) with a La/Sm_{ef} ratio of 4.5. However, this cone is anomalous, and other tholeiites from the ridge exhibit LREE depletion. Schilling attributes the anomalous enrichment of the cone basalt to a smaller degree of partial melting, since it has a similar $^{87}Sr/^{86}Sr$ ratio to the rest of the ridge.

Thus, due to the lack of similar analyses from other spreading ridges, it seems unlikely that the JTW Knolls are only the result of a spreading ridge. The chemical evidence points to a mantle plume origin for the JTW basalts, and it is likely that these two tectonic features are simultaneously influencing the morphology of the JTW area.

Speculatively, there is also the possibility of contamination of JTW magmas if they come in contact with the continental crust at depth. No seismic refraction studies have been done in the area to ascertain the fashion in which the continental crust extends beyond the Queen Charlotte Fault, or even if it does. At present, no geophysical or petrographic evidence exists to suggest that such contamination is occurring, such as xenoliths of continental material.

CONCLUSIONS

The five ridge segments of the Explorer spreading area, from the Southern Explorer Ridge north to the Dellwood Knolls and the J. Tuzo Wilson Knolls, show significant variations in basalt chemistry which cannot be explained by crystal fractionation alone. Explorer Deep basalts are enriched in all the incompatible trace elements, such as K, Rb, Zr, Nb, and the LREE, which may reflect the presence of a weak hotspot beneath Explorer Deep. The nearby segments, Explorer Rift and the Southern Explorer Ridge, are erupting both incompatible element enriched and depleted basalts, which could result from a heterogeneous mantle source, or from intermittent injection of magma from the postulated hotspot beneath Explorer Deep into areas producing normal MORB. Sr isotope data do not indicate that two radiogenically distinct mantle sources exist (one hotspot, one typical ocean ridge). The Dellwood Knolls display a considerable chemical difference between the two knolls, which has previously been attributed to fractionation. However, new rare earth element and Sr isotope data suggest that the history of the Knolls is more complex, and that the southeast Knoll had a more radiogenic and trace-element-enriched mantle source than does the presently active northwest Knoll.

The three Explorer segments produce basalts with relatively high iron contents (Fe_2O_3*= 11 to 14%), which are classified as ferrobasalts. This basalt type occurs in areas with high amplitude magnetic anomalies. The magnetic traces of "pseudofaults" in the Explorer area, and the occurrance of high Fe-Ti basalts at the ends of the ridge, suggest that propagating rifts, similar to those currently active on the Juan de Fuca and Galapagos Ridges, exist along the Explorer system.

The J. Tuzo Wilson Knolls were thought to be the present-day expression of the Pratt-Welker plume. In terms of major elements, trace elements, and rare earth element patterns, the Knolls are chemically similar to other sea-

mounts in the chain. The JTW basalts are even more large ion lithophile element enriched. Geochronology disputes the hypothesis that the plume responsible for the latest stage of volcanism on Bowie Seamount is also the source of the JTW basalts. The existence of a second mantle plume, 300 km southeast of Bowie Seamount at the JTW Knolls, would explain the minor chemical and physiographical differences between the JTW Knolls and the other Pratt-Welker Seamounts, as well as the observed two-phase volcanic history of the southeastern part of the chain.

Recent geophysical evidence suggests that the JTW Knolls are the newest, most northerly segment of the Explorer-Dellwood system. Although JTW hawaiites are atypical for ocean ridge magmas, the situation appears to be similar to other ocean ridges where a ridge lies on a hotspot.

BIBLIOGRAPHY

Abbey, S., 1980, Studies in "standard samples" for use in the general analsis of silicate rocks and minerals, Geological Survey of Canada Paper 80-14, 26 p.

Barberi, F., and Varet, J., 1977, Volcanism of Afar: small scale plate tectonic implications, Geol. Soc. Am. Bull. 88, p. 1251-1260.

Barberi, F., Civetta, L., and Varet, J., 1980, Sr isotopic composition of Afar volcanics and its implications for mantle evolution, Earth Planet. Sci. Lett. 50, p. 247-259.

Barr, S.M., and Chase, R.L., 1974, Geology of the northern end of Juan de Fuca Ridge and sea-floor spreading, Can. Jour. Earth Sci. 11, p. 1384-1406.

Basaltic Volcanism Study Project, 1981, Basaltic Volcanism on the Terrestrial Planets, Pergamon Press Inc., New York, 1286 p.

Bertrand, W.G., 1972, A geological reconnaissance of the Dellwood Seamount Area, northeast Pacific Ocean, and its relationship to plate tectonics, unpublished M.Sc. thesis, University of British Columbia, 151 p.

Brown, G.C., Hughes, D.J., and Esson, J., 1973, New XRF data retrieval techniques and applications to USGS standard rocks, Chem. Geol. 11, no. 3, p. 223-229.

Byerly, G., 1980, The nature of differentiation trends in some volcanic rocks from the Galapagos Spreading Center, J. Geophys. Res. 85, p. 3797-3810.

Bryan, W.B., 1972, Morphology of quench crystals in submarine basalts, J. Geophys. Res. 77, p. 5812-5819.

Chase, R.L., 1977, J. Tuzo Wilson Knolls: Canadian hotspot, Nature 266, p. 344-346.

Clague, D.A., and Bunch, T.E., 1976, Formation of ferrobasalt at East Pacific Midocean Spreading Centers, J. Geophys. Res. 81, p. 4247-4256.

Clague, D.A., Frey, F.A., Thompson, G., and Rindge, S., 1981, Minor and trace element geochemistry of volcanic rocks dredged from the Galapagos spreading center: role of crystal fractionation and mantle heterogeneity, J. Geophys. Res. 86, p. 9569-9481.

Currie, R.G., and Seeman, D., 1980, Marine magnetic anomaly map- west coast of British Columbia, Geological Survey of Canada Open File 724 (revised).

Dalrymple, G.B., Silver, E.A., and Jackson, E.D., 1973, Origin of the Hawaiian Islands, American Scientist 61, no. 3, p. 294-308.

Davis, E.E., and Riddihough, R.P., 1982, The Winona Basin: structure and tectonics, Can. Jour. Earth Sci., in press.

Engel, A.E.J., and Engel, C.E., 1964, Composition of basalts from the mid-Atlantic Ridge, Science 144, p.1330-1333.

Engel, A.E.J., Engel, C.E., and Havens, R.G., 1965, Chemical characteristics of oceanic basalts and the upper mantle, Geol. Soc. Am. Bull. 76, p.719-734.

Erlank, A.J., and Kable, E.J.D., 1976, The significance of incompatible elements in mid-Atlantic Ridge basalts from 45°N with particular reference to Zr/Nb, Contrib. Mineral. Petrol. 54, p. 281-291.

Feather, C.E., and Willis, J.P., 1976, A simple method for background and matrix correction of spectral peaks in trace element determination by X-ray flourescence spectrometry, X-Ray Spectrometry 5, p. 41-48.

Flanagan, F.J., 1973, Description and analyses of eight new USGS rock standards, USS. Geol. Sur. Prof. Paper 840, 192 p.

Forbes, R.B., and Hoskin, C.M., 1969, Dredged trachyte and basalt from Kodiak Seamount and the adjacent Aleutian trench, Science 166, p. 502-504.

Forbes, R.B., Dugdale, R.C., Katsura, T., Matsumoto, H., and Haramura, H., 1969, Dredged basalt from Giacomini Seamount, Nature 221, p. 849--850.

Forbes, R.B., and others, 1982, Geochemistry of the Pratt-Welker Seamount Chain, manuscript in press.

Herzer, R.H., 1971, Bowie Seamount, a recently active, flat-topped seamount in the northeast Pacific Ocean, Can. J. Earth Sci. 8, p. 676 -687.

Hey, R.N., 1977, A new class of pseudofaults and their bearing on plate tectonics: a propagating rift model, Earth Planet. Sci. Lett. 37, p. 321-325.

Hey, R.N., Duennebier, F.K., and Morgan, J.W., 1980, Propagating rifts on mid-ocean ridges, J. Geophys. Res. 85, p. 3647-3658.

Howarth, R.J., and Thompson, M., 1976, Duplicate analyses in geochemical practice, Analyst 101, p. 690-709.

Hyndman, R.D., Rogers, G.C., Bone, M.N., Lister, C.R.B., Wade, U.S., Barrett, D.L., Davis, E.E., Lewis, T., Lynch, S., and Seeman, D., 1978, Geophysical measurements in the region of Explorer Ridge off Western Canada, Can. J. Earth Sci. 15, p. 1508-1525.

Irvine, T.N., and Barragar, W.R.A., 1971, A guide to the chemical classification of the common volcanic rocks, Can. J. Earth Sci. 8, p. 523 -545.

Kay, R.W., Hubbard, M.J., and Gast, P., 1970, Chemical characteristics and origins of oceanic ridge volcanic rocks, J. Geophys. Res. 75, p. 1585-1613.

Keen, C.E., and Hyndman, R.D., 1979, Geophysical review of the continental margins of eastern and western Canada, Can. Jour. Earth Sci. 16, p. 712-747.

Liias, R.A., Rhodes, J.M., Delaney, J.R., and Johnson, H.P., 1981, Trace element variation along the Juan de Fuca Ridge, abstract, EOS 62, no. 45, p. 1067.

MacDonald, G.A., and Katsura, T., 1964, Chemical composition of Hawaiian lavas, J. Petrol. 5, p. 82-135.

Malacek, S.J., and Clowes, R.M., 1978, Crustal structure near Explorer Ridge from a deep marine survey, J. Geophys. Res. 83, p. 5899-5912.

Melson, W.G., Vallier, T.L., Wright, T.L., Byerly, G., and Nelen, J., 1976, Chemical diversity of abyssal volcanic glasses erupted along Pacific, Atlantic, and Indian sea-floor spreading centers, Am. Geophys. Union Monograph 19, p. 351-365.

Minster, J.B., Jordan, T.H., Molnar, P., and Haines, E., 1974, Numerical modelling of instantaneous plate tectonics, Geophys. J. R. Astr. Soc. 36, p. 541-576.

Miyashiro, A., Shido, F., and Ewing, M., 1970, Crystallization and differentiation in abyssal tholeiites and gabbros from mid-ocean ridges, Earth Planet. Sci. Lett. 7, p. 361-365.

Moore, J.G., 1970, Water content of basalts erupted on the sea floor, Contrib. Mineral. Petrol. 28, p. 272-279.

Nixon, G.T., and Armstrong, R.L., 1980, Chemical and Sr-isotopic composition of igneous rocks from the Deep Sea Drilling Project Legs 59 and 60, in Kroenke, L., Scott, R., et al., 1980, Initial Reports of the Deep Sea Drilling Project, Volume LIX, Washington (U.S. Government Printing Office), p. 719-727.

O'Hara, M.J., 1977, Geochemical evolution during fractional crystallization of a periodically refilled magma chamber, Nature 266, p. 503-507.

Osborne, E.F., and Tait, D.B., 1952, The system diopside-forsterite -anorthite, Am. J. Sci. Bowen Volume 250A, p. 413-433.

Pearce, J.A., and Cann, J.R., 1973, Tectonic setting of basic volcanic rocks, Earth Planet. Sci. Lett. 19, p. 290-300.

Presnall, D.A., Dixon, J.R., O'Donnell, T.H., and Dixon, S.A., 1979, Generation of mid-ocean ridge tholeiites, J. Petrol. 20, p. 3-35.

Raff, A.D., and Mason, R.G., 1961, Magnetic survey off the west coast of North America, 40°N to 52°N, Geol. Soc. Am. Bull. 72, p. 1267-1270.

Riddihough, R.P., 1977, A model for recent plate interactions off Canada's west coast, Can. J. Earth Sci. 14, p. 384-396.

Riddihough, R.P., Currie, R.G., and Hyndman, R.D., 1980, The Dellwood Knolls and their role in the triple junction tectonics off northern Vancouver Island, Can. J. Earth Sci. 17, p. 577-593.

Sato, H., 1977, Nickel content of basaltic magmas: identification of primary magmas and a measure of the degree of olivine fractionation, Lithos 10, p. 113-120.

Schilling, J.-G., 1971, Sea-floor evolution: rare earth evidence, Phil. Trans. Roy. Soc. Lond. 268A, p. 663-706.

Schilling, J.-G., 1973, Iceland mantle plume: a geochemical study of the Reykjanes Ridge, Nature 242, p. 565-571.

Schilling, J.-G., 1975, Azores mantle blob: rare earth evidence, Earth. Planet. Sci. Lett. 25, p. 103-115.

Schilling, J.-G., Anderson, R.N., and Vogt, P., 1976, Rare-earth, Fe, and Ti variations along the Galapagos spreading center, and their relationship to the Galapagos mantle plume, Nature 261, p. 108-113.

Silver, E.A., von Huene, R., and Crouch, J.K., 1974, Tectonic significance of the Kodiak-Bowie Seamount Chain, northeast Pacific, Geology 2, no. 3, p. 147-150.

Srivastava, S.P., Barrett, D.L., Keen, C.E., Manchester, K.S., Shih, K.G., Tiffin, D.L., Chase, R.L., Thomlinson, A.G., Davis, E.E., and Lister, C.R.B., 1971, Preliminary analysis of geophysical measurements north of Juan de Fuca Ridge, Can. J. Earth Sci. 8, p. 1265-1281.

Sun, S.S., 1980, Lead isotopic study of young volcanic rocks from midocean ridges, ocean islands, and island arcs, in: The Evidence for Chemical Heterogeneity in the Earth's Mantle, Phil. Trans. Roy. Soc. Lond. A297, p. 179-202.

Sun, S.S., Nesbitt, R.W., and Sharaskin, A.Y., 1979, Geochemical characteristics of mid-ocean ridge basalts, Earth Planet. Sci. Lett. 44, p. 119-138.

Terrell, D.J., Pal, S., Lopez M, M., and Perez R, J., 1979, Rare earth elements in basalt samples, Gulf of California, Chem. Geol. 26, p. 267-275.

Thompson, G., Bryan, W.B., and Melson, W.G., 1980, Geological and geophysical investigation of the mid-Caymen Rise spreading center, J. Geol. 88, p. 41-55.

Tiffin, D.L., and Seeman, D., 1975, Bathymetric map of the western Canadian continental margin, Geological Survey of Canada publication.

Turner, D.L., Jarrard, R.D., and Forbes, R.B., 1980, Geochronology and origin of the Pratt-Welker Seamount Chain, Gulf of Alaska: a new pole of rotation for the Pacific Plate, J. Geophys. Res. 85, p. 6547-6556.

van der Heyden, P., 1982, Tectonic and stratigraphic relations between the Coast Plutonic Complex and Intermontane Belt, west central Whitesail Lake area, British Columbia, unpublished M. Sc. thesis, Univ. of British Columbia.

Vine, F.J., 1968, Magnetic anomalies associated with mid-ocean ridges, in Phinney, R.A. (ed.), The History of the Earth's Crust, Princeton Univ. Press, p. 73-89.

Vine, F.J., and Wilson, J.T., 1965, Magnetic anomalies over a young oceanic ridge off Vancouver Island, Science 150, p. 485-489.

Vogt, P., and Byerly, G.R., 1976, Magnetic anomalies and basalt composition in the Juan de Fuca-Gorda Ridge area, Earth Planet. Sci. Lett. 33, p. 185-207.

Wakeham, S.E., 1977, Petrochemical patterns in young pillow basalts dredged from Juan de Fuca and Gorda Ridges, unpublished M. Sc. thesis, Univ. of Oregon, 94 p.

Wilson, J.T., 1965, Transform faults, oceanic ridges, and magnetic anomalies southwest of Vancouver Island, Science 150, p. 482-485.

White, W.M., and Schilling, J.-G., 1978, The nature and origin of geochemical variations in mid-Atlantic Ridge basalts from the central North Atlantic, Geochim. Cosmochim. Acta 42, p. 1501-1516.

White, W.M., Schilling, J.-G., and Hart, S.R., 1976, Evidence for the Azores mantle plume from strontium isotope geochemistry, Nature 263, p. 659-661.

APPENDIX 1

Petrographic Descriptions

Abbreviations

Phenocrysts: Plag - plagioclase
Ol - olivine
Px - pyroxene

Matrix: f-s - fan-sherulites
plag micro - plagioclase microlites
op - opaque minerals

Remarks: vesic - vesicular
glomero - glomeroporphyritic
skel - skeletal phenocrysts
op - opaque minerals
Mn - manganese
r. - rare

PETROGRAPHIC DESCRIPTIONS

SAMPLE NO.	FRAGMENT TYPE	TEXTURE	PHENOCRYSTS	MATRIX	ALTERATION	REMARKS
J. Tuzo Wilson Knolls						
73-26-2-1	glassy pillow	intersertal	Plag, r. Ol.	glass & f-s	none	vesic., op common
73-26-5-1	glassy pillow	hyalophitic	Ol, Plag	glass & f-s	none	vesic.
"73"	glassy pillow		Plag		none	glomeroporphyritic
Dellwood Knolls and Seamounts						
70-25-2D-8	glassy pillow	hyalophitic	Plag, Ol	glass, f-s, op, pl micro.	Ol rims	vesic, glomero.
70-25-3D-1	glassy pillow	hyalopilitic	Plag	glass, f-s, pl micro.	high Fe^{3+}/Fe^{2+}	vesic, Mn crust
70-25-8D-121	glassy pillow	hyalopilitic	Ol, Plag	glass, f-s, pl micro.	minor	oxide crust
70-25-9D-1	glassy pillow	hyalopilitic	Ol, Plag	glass, f-s, pl micro.	none	magnetic
Explorer Rift						
71-15-77-5	glassy pillow	hyalophitic	r. Plag	f-s, plag micro	none	
71-15-77-6	glassy pillow	hyalopilitic	r. Plag	f-s, op, plag micro.	none	
70-25-4-49	glassy pillow	hyalopilitic	Ol, r. Plag	glass, f-s, plag micro.	none	glomero, skel. ol
70-25-4-62/64	glassy lava tubes	hyalopilitic	Ol, Plag	glass, f-s, plag micro	none	skel. ol.
70-25-16-1	glassy pillow	hyalophitic	Ol, r. Plag	f-s	fracs Fe-stained	skel. phenos, glomero.

SAMPLE NO.	FRAGMENT TYPE	TEXTURE	PHENOCRYSTS	MATRIX	ALTERATION	REMARKS
70-25-16-4	block lava	intersertal	Plag, Ol, tr.Px	f-s, op.	none	vesic, magnetic, skel. ol.
70-25-16-7	block lava	intergranular	Plag, Px, Ol	f-s, Px, plag micro	3mm Fe-stained rim	
77-14-33A	glassy pillow	hyalophitic	Plag, Ol	f-s, plag micro	none	skel. ol.,plag resorbed on rims
77-14-33B	glassy pillow	intersertal	Plag, Ol	f-s, op, m. granular Px	Ol fracs	skel. phenos.
Paul Revere Ridge Fracture Zone						
70-25-11-2	block lava	hyalopilitic	none	f-s, minor plag micro	weathered rim	
71-15-92-8	block lava	hyalophitic	Plag, Px	f-s, op., plag micro	weathered rim	
71-15-92-10	glassy pillow	hyalophitic	Plag, Ol	glass, f-s, op.	none	skel phenos.
71-15-91-1	block lava	holocrystalline			Ol rims and fracs.	
72-22-7-1	glassy pillow	hyalopilitic	Ol, Plag	glass, m. f-s	none	skel. ol.; dark and magnetic
70-25-6-14	block lava	hyalophitic	Plag, Ol	glass, f-s, plag micro	Ol serp.	
Explorer Deep						
70-25-17-1	block lava	intersertal, hyalophitic areas	Ol.	plag micros, f-s, glass	none	glomero.
79-6-32-39	glassy pillow	hyalophitic	Ol.	plag micro, f-s	none	
79-6-32-41	glassy pillow	hyalopilitic	Ol.	glass, f-s	none	glomero.
79-6-32-42	glassy pillow	hyalopilitic	Ol.	glass, f-s, plag micro	none	glomero.

SAMPLE NO.	FRAGMENT TYPE	TEXTURE	PHENOCRYSTS	MATRIX	ALTERATION	REMARKS
Southern Explorer Ridge						
77-14-36-X	block lava	hyalophitic	Ol, Plag	f-s, plag micro	none	skel. ol; vesic; glomero.
77-14-36-G	block lava	hyalophitic	Ol, Plag, r.Px.	f-s, glass, plag micro	none	skel ol; glomero.
77-14-36-8	glassy pillow	hyalophitic	Plag, Ol	f-s	none	vesic; microlites in radial clusters
77-14-36-13	block lava	hyalopilitic	Plag, Ol, Px	glass, f-s	none	glomero; skel ol.
77-14-36-32	block lava	hyalopilitic	Plag, Ol	glass, f-s	none	vesic;skel ol; glomero.
77-14-36-35	block lava	intergranular-holocrystalline		minor glass	none	large ol. crystals
77-14-36-36	block lava	fan-spherulitic		opaques	none	
73-26-13-3	block lava	intersertal	none	plag micro, glass, Px	none	
73-26-13-4	block lava	intersertal	none	plag micro, glass, Px	none	
70-25-15-3	glassy pillow	intersertal	none	plag and ol micro, f-s, glass	none	
70-25-15-8	glassy pillow	hyalophitic	Plag, Ol	glass, f-s, op.	none	phenos small
70-25-15-29	glassy pillow	hyalophitic to intersertal	r. Plag	plag micro, f-s, glass	none	
71-15-70-8	block lava	hyalopilitic	Ol.	f-s, plag micro.	weathered rim	

APPENDIX 2

Major element, trace element, precisions, and CIPW normative compositions for the J. Tuzo Wilson Knolls, Dellwood Knolls and Seamounts, and the Explorer Spreading Area.

(i) Total iron is reported as $Fe_2O_3^*$.

(ii) Normative compositions calculated assuming an $Fe^{3+}/(Fe^{3+}+Fe^{2+})$ ratio of 0.16 . The magnesium ratio is calculated on the same basis.

(iii) Volcanic rock classification (Class.) is after the method of Irvine & Baragar, (1971).

(iv) A blank indicates that no data was collected. A dash indicates a value of zero.

	Bowie Seamount	J. Tuzo Wilson Knolls			
	67-6-12†	73-26-2-1A	73-26-2-1B	73-26-2-1C	73-26-5-1A
SiO_2	45.4	48.41	48.75	49.66	51.24
TiO_2	2.60	2.51	2.40	2.43	1.78
Al_2O_3	18.50	15.22	15.87	16.03	16.08
Fe_2O_3*	11.90	9.77	9.28	9.29	7.83
MnO	0.19	0.17	0.16	0.16	0.19
MgO	5.90	6.04	5.06	5.17	6.82
CaO	8.5	8.18	8.00	8.17	8.76
Na_2O	3.8	4.87	5.18	5.02	4.99
K_2O	1.9	2.22	2.46	2.41	2.08
P_2O_5	0.70	0.67	0.66	0.71	0.62
H_2O+	0.30	1.37	0.93	0.31	0.13
CO_2 etc.	0.1	1.13	1.84	1.12	
Ba			361		
Ce			172		
Cr	335	25			
Nb		86	87	87	74
Nd			60		
Ni	86	52	38	33	101
Rb	41	55	36	38	48
Sr	679	593	590	599	567
V		232			
Y	32	30	31	31	27
Zr	338	376	396	372	410
La/Sm_{ef}		4.61	4.59		
Zr/Nb		4.4	4.8	4.3	5.5
Sr^{87}/Sr^{86}	.70272	.70255			
	.70258	.70250			
Qtz	-	-	-	-	-
Ne	7.38	7.31	6.86	6.57	8.42
Or	11.12	13.35	14.71	14.34	13.33
Ab	18.86	29.00	31.96	30.85	26.98
An	28.08	13.21	12.79	14.07	15.29
Di	8.26	13.31	9.18	12.19	19.57
Hy	-	-	-	-	-
Ol	17.59	13.03	12.27	11.29	11.04
Ilm	5.02	4.85	4.61	4.65	3.39
Mag	1.62	1.93	1.82	1.81	1.53
Ap	1.68	1.58	1.55	1.66	1.44
$100(Mg/Mg+Fe^{2+})$	52.43	57.63	54.54	55.05	65.71
Class.	Alkali Basalt	Hawaiite	Mugearite	Hawaiite	Hawaiite

†- Major element analysis by Geological Survey of Canada (Herzer, 1971).

	J. Tuzo Wilson Knolls			Dellwood Knolls	
	73-26-5-1B	73-26-5-1C	"73"	70-25-2D-8	70-25-3D-1**
SiO_2	50.12	50.46	50.00	47.33	51.25
TiO_2	1.73	1.74	1.79	1.30	2.33
Al_2O_3	16.16	16.00	15.62	16.91	15.60
Fe_2O_3*	7.62	7.73	9.02	10.23	10.47
MnO	0.17	0.16	0.16	0.16	0.16
MgO	6.78	6.55	6.37	9.50	5.00
CaO	8.57	8.54	9.12	12.36	11.95
Na_2O	4.95	4.92	4.30	2.29	3.24
K_2O	2.02	2.03	1.78	0.22	0.58
P_2O_5	0.58	0.57	0.53	0.09	0.28
H_2O^+	1.17	1.18	1.04	0.80	0.84
CO_2 etc	0.62	0.51	0.80		
Ba		274	291	42	
Ce		180	156		
Cr		105	85	342	177
Nb	75	75	63	4	
Nd		68	56	11	
Ni	90	91	76	206	66
Rb	48	48	41	4	7
Sr	575	565	576	182	345
V		193	201	212	
Y	26	27	30	22	34
Zr	402	378	323	101	164
La/Sm_{ef}	5.13		4.50	0.81	1.49
Zr/Nb	5.4	5.1	5.1	25.2	
Sr^{87}/Sr^{86}					.70267***
			.70256	.70240	.70290
			.70262		.70279
Qtz	-	-	-	-	-
Ne	7.52	6.84	3.14	0.19	-
Or	12.10	12.17	10.66	1.31	3.43
Ab	28.79	29.81	31.28	19.38	27.92
An	16.01	15.69	18.20	35.28	26.07
Di	15.55	16.35	15.46	20.86	25.82
Hy	-	-	-	-	8.98
Ol	12.39	11.76	12.94	18.29	0.66
Ilm	3.33	3.35	3.45	2.48	4.43
Mag	1.50	1.52	3.14	1.99	2.03
Ap	1.36	1.34	1.24	0.21	0.65
100 (Mg/ $Mg+Fe^{2+}$)	66.19	65.09	60.85	67.14	51.25
Class.	Hawaiite	Hawaiite	Hawaiite	Alkali Basalt	Olivine Tholeiite

**- Major element analysis by Japan Analytical Research Chemistry Institute (Bertrand, 1972).

***- Leached sample.

	Dellwood Seamounts		Explorer Rift		
	70-25-8D-121	70-25-9D-1	71-15-77-5	71-15-77-6	70-25-4-49
SiO_2	49.51	48.59	48.43	48.33	46.07
TiO_2	1.62	1.64	1.70	1.69	1.07
Al_2O_3	15.68	14.18	13.32	13.33	15.45
Fe_2O_3*	10.14	11.80	12.49	12.56	12.25
MnO	0.18	0.16	0.20	0.20	0.18
MgO	6.86	8.15	9.02	9.02	11.71
CaO	12.54	11.94	12.30	12.34	12.00
Na_2O	3.29	2.59	2.57	2.47	1.93
K_2O	0.27	0.33	0.21	0.21	0.07
P_2O_5	0.17	0.16	0.15	0.16	0.08
H_2O^+	0.40	1.30	0.25	0.40	0.36
CO_2 etc			0.17	0.22	0.09
Ba	36	37		63	
Ce				2	
Cr	284			436	
Nb	7	6	8	9	3
Nd	8	7		20	
Ni	70	73	65	65	265
Rb	6	8	5	5	3
Sr	154	179	146	150	143
V	267			271	
Y	29	28	29	29	20
Zr	103	113	106	109	72
La/Sm_{ef}		1.04	1.11	1.13	
Zr/Nb	14.8	18.8	11.8	13.6	24.0
Sr^{87}/Sr^{86}					
Qtz	-	-	-	-	-
Ne	1.34	-	-	-	0.14
Or	1.61	1.98	1.25	1.25	0.41
Ab	25.79	22.46	22.06	21.24	16.33
An	27.28	26.41	24.23	24.75	33.26
Di	27.92	26.68	28.32	28.34	20.51
Hy	-	5.42	3.97	4.95	-
Ol	10.57	11.18	13.64	13.03	24.54
Ilm	3.10	3.16	3.25	3.23	2.04
Mag	1.98	2.32	2.43	2.45	2.34
Ap	0.40	0.38	0.35	0.37	0.19
100 (Mg/ $Mg+Fe^{2+}$)	59.28	60.31	61.38	61.24	67.78
Class.	Alkali Basalt	Olivine Tholeiite	K-poor Ol. Bas.	K-poor Ol. Bas.	Picrite Basalt

Explorer Rift

	70-25-4-62G	70-25-4-62W	70-25-4-64	70-25-4-104	70-25-4-119
SiO_2	46.03	46.03	46.16	46.41	46.20
TiO_2	1.09	1.06	1.06	1.06	1.08
Al_2O_3	15.19	15.65	15.62	16.23	15.37
Fe_2O_3*	12.27	12.23	11.99	11.88	12.33
MnO	0.19	0.19	0.19	0.18	0.19
MgO	12.20	11.74	11.92	10.98	11.76
CaO	12.00	11.94	11.96	11.92	12.07
Na_2O	1.87	1.97	1.95	2.19	1.92
K_2O	0.06	0.07	0.07	0.12	0.07
P_2O_5	0.08	0.09	0.08	0.08	0.08
H_2O^+	0.25	0.18	0.13	0.18	0.12
CO_2 etc	0.03	0.14	0.12	0.05	0.08
Ba	8				
Ce					
Cr	500				
Nb	4	3	3	3	3
Nd	6				
Ni	270	275	265	248	261
Rb	3	3	3	3	3
Sr	144	146	149	142	145
V	183				
Y	20	13	19	20	20
Zr	70	73	74	72	72
La/Sm_{ef}	0.59			0.61	
Zr/Nb	17.5	24.3	24.7	24.0	24.0
Sr^{87}/Sr^{86}	.70232				
Qtz	-	-	-	-	-
Ne	0.25	0.28	0.17	1.06	0.12
Or	0.36	0.41	0.41	0.71	0.41
Ab	15.59	16.37	16.39	16.83	16.23
An	32.82	33.55	33.55	33.98	33.01
Di	21.10	19.62	19.82	19.71	20.93
Hy	-	-	-	-	-
Ol	25.18	24.84	24.85	23.10	24.48
Ilm	2.07	2.01	2.01	2.01	2.05
Mag	2.38	2.37	2.32	1.06	2.38
Ap	0.19	0.21	0.19	0.19	0.19
100 (Mg/ $Mg+Fe^{2+}$)	68.63	67.87	68.63	67.07	67.73
Class.	Picrite Basalt	Picrite Basalt	Picrite Basalt	Ankaramite	Picrite Basalt

Explorer Rift

	70-25-16-1	70-25-16-4	70-25-16-7	77-14-33-A	77-14-33-B
SiO_2	46.85	48.79	48.73	47.99	47.87
TiO_2	1.31	1.79	1.82	1.26	1.28
Al_2O_3	14.70	15.29	15.06	15.18	15.32
Fe_2O_3*	11.53	10.89	10.92	10.65	10.46
MnO	0.22	0.18	0.18	0.18	0.17
MgO	11.69	7.88	7.89	10.17	10.06
CaO	11.95	11.82	11.92	12.91	13.13
Na_2O	2.02	3.46	3.52	1.79	1.88
K_2O	0.18	0.28	0.32	0.27	0.27
P_2O_5	0.11	0.21	0.21	0.13	0.14
H_2O^+	0.47	0.12	0.11	0.21	0.27
CO_2 etc	0.09	0.16	0.19	0.30	0.22
Ba				44	
Ce					
Cr		374		575	
Nb	7	8	8	11	12
Nd				12	
Ni	275	84	72	204	150
Rb	4	6	6	8	6
Sr	160	210	212	150	153
V		257		229	
Y	21	23	26	22	20
Zr	95	114	121	84	83
La/Sm_{ef}	0.81	1.19		1.69	1.73
Zr/Nb	13.6	14.3	15.1	7.6	6.9
Sr^{87}/Sr^{86}				.70246	
Qtz	-	-	-	-	-
Ne	-	2.43	3.09	-	-
Or	1.07	1.66	1.90	1.54	1.60
Ab	17.36	25.14	24.42	15.33	16.11
An	30.54	25.29	24.27	32.59	32.53
Di	22.38	25.31	26.39	23.31	24.58
Hy	1.71	-	-	10.00	6.24
Ol	21.74	13.79	13.42	11.78	13.63
Ilm	2.50	3.41	3.47	2.40	2.44
Mag	2.24	2.11	2.17	2.07	2.03
Ap	0.26	0.49	0.49	0.30	0.32
100 (Mg/ $Mg+Fe^{2+}$)	69.05	61.42	61.39	67.76	67.91
Class.	Average Tholeiite	Alkali Basalt	Alkali Basalt	K-rich Tholeiite	K-rich Tholeiite

Paul Revere Ridge (F.Z.)

	70-25-11-2	71-15-92-8W	71-15-92-8G	71-15-92-10	71-15-91-1Ψ
SiO_2	46.70	48.43	48.28	48.43	45.43
TiO_2	1.28	1.95	1.94	1.78	0.86
Al_2O_3	16.37	13.94	13.28	13.28	14.38
Fe_2O_3*	11.21	13.00	13.25	12.83	12.96
MnO	0.15	0.22	0.22	0.22	0.24
MgO	9.12	7.69	8.12	8.73	14.34
CaO	10.68	11.61	11.59	12.17	8.74
Na_2O	2.41	3.10	2.88	2.30	1.54
K_2O	0.18	0.26	0.27	0.21	0.09
P_2O_5	0.10	0.21	0.20	0.18	0.10
H_2O^+	0.77	0.13	0.43	0.41	0.49
CO_2 etc	1.13	0.33	0.41	0.35	2.03
Ba			25		
Ce			11		
Cr			336		
Nb	5	11	13	11	
Nd			20		
Ni	275	94	100	97	
Rb	4	5	6	5	2
Sr	138	152	143	135	100
V			296		
Y	24	36	35	32	
Zr	81	136	132	125	
La/Sm_{ef}	0.60		1.00		0.59
Zr/Nb	16.2	12.4	10.2	11.4	
Sr^{87}/Sr^{86}					
Qtz	-	-	-	-	-
Ne	-	-	-	-	-
Or	1.07	1.54	1.61	1.25	0.48
Ab	20.77	26.60	24.79	19.75	17.63
An	33.43	23.37	22.58	25.39	25.76
Di	4.64	25.42	25.75	26.13	-
Hy	21.92	0.92	4.57	11.94	17.24
Ol	2.45	3.72	3.71	8.37	27.78
Ilm	2.45	3.72	3.71	3.41	1.39
Mag	2.19	2.52	2.58	2.50	3.22
Ap	0.23	0.49	0.47	0.42	0.16
100 (Mg/ $Mg+Fe^{2+}$)	64.16	56.55	57.42	59.97	75.20
Class.	K-poor Tholeiite	Alkali Basalt	K-poor Tholeiite	K-poor Tholeiite	Picrite Basalt

Ψ- Weathered sample. Not included in diagrams in text.

	Paul Revere Ridge		Explorer Deep		
	72-22-7-1	70-25-6-14	70-25-17-1	79-6-32-39	79-6-32-41
SiO_2	48.24	50.09	49.32	49.11	48.64
TiO_2	3.53	1.42	1.76	1.75	1.78
Al_2O_3	10.69	16.78	15.10	13.44	12.99
Fe_2O_3*	19.33	8.80	11.51	12.27	12.23
MnO	0.30	0.13	0.19	0.20	0.22
MgO	5.44	7.10	7.81	8.95	10.05
CaO	8.38	13.78	11.43	11.29	11.50
Na_2O	2.79	2.58	2.44	2.23	1.96
K_2O	0.53	0.10	0.45	0.43	0.40
P_2O_5	0.39	0.16	0.21	0.20	0.20
H_2O^+	1.10		0.50	0.42	0.63
CO_2 etc	0.37		0.08	0.46	0.20
Ba	21		106	102	
Ce	76		17	14	
Cr	171	267	334	393	
Nb	19		15	20	18
Nd	36		20	22	
Ni	147	347	163	136	145
Rb	10	3	10	9	9
Sr	133	153	161	155	163
V	400		274	283	
Y	65	38	32	26	28
Zr	280	90	144	137	124
La/Sm_{ef}	1.18		1.54	2.03	
Zr/Nb	14.7		9.6	6.9	6.5
Sr^{87}/Sr^{86}	.70254			.70252	
Qtz	1.60	-	-	-	-
Ne	-	-	-	-	-
Or	3.19	0.59	2.68	2.56	2.39
Ab	24.35	22.10	20.99	19.17	16.89
An	15.24	33.75	29.06	25.53	25.65
Di	18.59	27.15	21.37	21.74	23.83
Hy	24.59	6.06	13.96	19.05	17.24
Ol	-	5.67	5.66	4.66	4.57
Ilm	6.84	2.69	3.37	3.35	3.41
Mag	3.78	1.71	2.25	2.39	2.39
Ap	0.92	0.37	0.49	0.47	0.47
100 (Mg/ $Mg+Fe^{2+}$)	38.24	63.97	59.89	61.61	64.39
Class.	K-poor Tholeiite	K-poor Tholeiite	Average Tholeiite	Average Tholeiite	K-rich Tholeiite

	Explorer Deep	Southern Explorer Ridge			
	79-6-32-42	77-14-36-X	77-14-36-G	77-14-36-8	77-14-36-13
SiO_2	48.68	48.72	48.66	49.12	48.89
TiO_2	1.79	1.62	1.63	1.58	1.58
Al_2O_3	12.94	13.57	13.25	13.57	13.32
Fe_2O_3*	12.41	12.71	12.67	12.81	13.00
MnO	0.21	0.21	0.22	0.20	0.21
MgO	9.85	8.87	9.40	8.63	8.68
CaO	11.55	12.12	12.04	11.93	11.88
Na_2O	2.03	2.26	2.19	2.15	2.14
K_2O	0.40	0.19	0.17	0.21	0.23
P_2O_5	0.20	0.14	0.13	0.14	0.13
H_2O^+	0.49	0.22	0.22	0.26	0.32
CO_2 etc	0.24	0.22	0.27	0.21	0.44
Ba				28	51
Ce				4	
Cr				285	329
Nb	19	7	7	8	8
Nd				14	14
Ni	165	78	84	75	80
Rb	11	5	4	5	5
Sr	163	122	123	118	120
V				281	278
Y	30	26	28	27	28
Zr	126	100	100	99	105
La/Sm_{ef}		0.96		0.92	
Zr/Nb	6.6	14.3	14.4	14.9	13.1
Sr^{87}/Sr^{86}		.70254			
Qtz	-	-	-	-	-
Ne	-	-	-	-	-
Or	2.38	1.13	1.01	1.25	1.37
Ab	17.47	19.40	18.80	18.47	18.40
An	25.16	26.39	25.89	26.85	26.17
Di	24.20	25.92	25.75	24.89	24.14
Hy	16.47	12.30	13.37	17.32	18.35
Ol	7.44	8.45	5.20	4.89	4.70
Ilm	3.43	3.09	3.11	3.02	3.02
Mag	2.42	2.47	2.46	2.49	2.53
Ap	0.47	0.33	0.30	0.33	0.30
$100\ (Mg/Mg+Fe^{2+})$	63.59	60.56	62.01	59.72	59.50
Class.	K-rich Tholeiite	K-poor Tholeiite	K-poor Tholeiite	Average Tholeiite	Average Tholeiite

Southern Explorer Ridge

	77-14-36-32	77-14-36-35	77-14-36-36	73-26-13-3	73-26-13-4
SiO_2	48.41	49.32	48.73	49.27	49.02
TiO_2	1.61	1.42	1.70	1.56	1.52
Al_2O_3	13.06	15.28	14.25	14.28	14.34
Fe_2O_3*	13.17	10.78	11.98	12.71	12.12
MnO	0.23	0.18	0.19	0.21	0.20
MgO	9.27	8.44	9.58	7.03	7.50
CaO	11.97	12.39	10.84	11.80	12.16
Na_2O	2.06	2.45	2.47	2.58	2.58
K_2O	0.21	0.24	0.18	0.42	0.35
P_2O_5	0.13	0.16	0.20	0.18	0.16
H_2O^+	0.48	0.15	0.47	0.64	0.56
CO_2 etc	0.27	0.06	0.23	0.14	0.33
Ba					8
Ce					4
Cr					213
Nb	8	3	10	6	9
Nd					15
Ni	79	112	251	78	107
Rb	6	6	4	11	7
Sr	123	121	127	110	110
V					275
Y	29	22	33	28	27
Zr	101	86	118	104	100
La/Sm_{ef}					0.86
Zr/Nb	12.6	28.7	11.8	17.3	11.1
Sr^{87}/Sr^{86}					
Qtz	-	-	-	-	-
Ne	-	-	-	-	-
Or	1.25	1.42	1.07	2.51	2.09
Ab	17.74	20.98	21.24	22.24	22.21
An	25.91	29.97	27.38	26.32	26.64
Di	25.63	24.58	19.51	25.27	25.43
Hy	15.00	8.48	14.57	11.02	9.25
Ol	4.61	9.25	5.99	6.41	7.97
Ilm	3.08	2.70	3.25	2.99	2.91
Mag	2.57	2.09	2.34	2.48	2.36
Ap	0.30	0.37	0.47	0.42	0.36
100 (Mg/ $Mg+Fe^{2+}$)	60.77	63.27	63.76	54.90	57.66
Class.	Average Tholeiite	Average Tholeiite	K-poor Tholeiite	Average Tholeiite	Average Tholeiite

Southern Explorer Ridge

	70-25-15-3	70-25-15-8	70-25-15-29	71-15-70-1	71-15-70-8
SiO_2	49.06	49.24	48.95	48.07	48.23
TiO_2	1.77	1.80	1.79	1.98	2.11
Al_2O_3	13.35	13.54	13.62	13.99	13.32
Fe_2O_3*	12.14	12.39	12.12	13.30	13.47
MnO	0.19	0.20	0.20	0.21	0.22
MgO	8.33	8.30	8.13	8.38	9.27
CaO	11.81	11.70	11.94	10.44	10.61
Na_2O	2.58	2.33	2.64	2.55	2.36
K_2O	0.38	0.37	0.40	0.50	0.30
P_2O_5	0.19	0.20	0.19	0.20	0.22
H_2O^+	0.60	0.50	0.46	0.83	0.37
CO_2 etc	0.35	0.20	0.35	0.44	0.39
Ba			29	34	33
Ce				3	25
Cr				398	393
Nb	12	12	13	8	10
Nd				17	22
Ni	55	90	82	243	218
Rb	8	7	9	11	6
Sr	158	180	162	145	129
V				290	308
Y	29	30	29	39	39
Zr	137	136	141	155	154
La/Sm_{ef}	1.35				0.87
Zr/Nb	11.4	11.3	10.8	19.4	15.4
Sr^{87}/Sr^{86}	.70249				
Qtz	-	-	-	-	-
Ne	-	-	-	-	-
Or	2.27	2.21	2.38	2.99	1.79
Ab	22.19	20.05	22.71	22.04	20.31
An	23.89	25.54	24.23	25.45	24.97
Di	25.93	24.84	26.12	18.67	19.68
Hy	10.67	15.62	8.21	13.08	16.96
Ol	8.02	4.93	9.30	9.86	8.21
Ilm	3.40	3.45	3.43	3.81	4.04
Mag	2.37	2.42	2.35	2.60	2.62
Ap	0.44	0.47	0.44	0.47	0.51
!00 (Mg/ $Mg+Fe^{2+}$)	60.16	59.58	59.61	58.11	60.23
Class.	Average Tholeiite	Average Tholeiite	Average Tholeiite	Average Tholeiite	Average Tholeiite

PRECISIONS OF STANDARDS AND UNKNOWNS

FOR EACH ELEMENT

	Percent Mean Deviations From Recommended Values For Standards (Abbey, 1980).	Howarth and Thompson 95% Confidence Limits From Precision Plots.
SiO_2	1.5%	1%
TiO_2	2.3%	7%
Al_2O_3	3.4%	3%
Fe_2O_3*	2.9%	3%
MnO	2.5%	5%
MgO	2.8%	5%
CaO	2.4%	2%
Na_2O	9.7%	10%
K_2O	2.7%	5%
P_2O_5	15.0%	8%
	One Standard Deviation, Based On Fits To Working Curves	
Ba	±2 ppm	60%
Ce	±21 ppm	60%
Cr	±17 ppm	5%
Nb	±1 ppm	15%
Nd	±2 ppm	22%
Ni	±5 ppm	15%
Rb	±2 ppm	15%
Sr	±5 ppm	6%
V	±15 ppm	4%
Y	±5 ppm	15%
Zr	±5 ppm	7%

Final Data for Standards Used in Construction of Working Curves for Major Element Analysis

EXPLORER RIDGE MAJOR ELEMENTS

STANDARDS

IDENT	SiO_2	Al_2O_3	Fe_2O_3	MgO	CaO	Na_2O	K_2O	TiO_2	MnO	P_2O_5	H_2O	CO_2	TOTAL	
AGV1	60.13	15.18	7.05	1.77	5.33	4.11	2.91	1.15	0.10	0.50	0.78	0.02	99.03	FINAL VALUE
	60.73	15.33	7.12	1.79	5.38	4.15	2.94	1.16	0.10	0.50	0.78	0.02		NORM. VALUE
	59.61	17.19	6.81	1.52	4.95	4.32	2.92	1.06	0.10	0.51	0.78	0.02	99.79	RECCOM. VALUE
	1.12	-1.86	0.31	0.27	0.43	-0.17	0.02	0.10	0.00	-0.01	0.0	0.0		NORM.-RECC.
JB1	53.01	14.61	9.04	7.55	9.12	2.32	1.45	1.40	0.16	0.31	1.01	0.18	100.16	FINAL VALUE
	52.93	14.59	9.02	7.54	9.10	2.31	1.45	1.40	0.16	0.30	1.01	0.18		NORM. VALUE
	52.60	14.62	9.04	7.76	9.35	2.79	1.42	1.34	0.15	0.26	1.01	0.18	100.52	RECCOM. VALUE
	0.33	-0.03	-0.02	-0.22	-0.25	-0.48	0.03	0.06	0.01	0.04	0.0	0.0		NORM.-RECC.
BCR1	55.13	13.14	12.77	3.43	6.83	3.43	1.70	2.21	0.18	0.39	0.67	0.02	99.88	FINAL VALUE
	55.20	13.15	12.78	3.43	6.84	3.44	1.70	2.21	0.18	0.39	0.67	0.02		NORM. VALUE
	54.53	13.72	13.42	3.48	6.97	3.30	1.70	2.26	0.18	0.36	0.67	0.02	100.61	RECCOM. VALUE
	0.67	-0.57	-0.64	-0.05	-0.13	0.14	-0.00	-0.05	-0.00	0.03	0.0	0.0		NORM.-RECC.
MRG1	40.42	8.57	18.21	13.50	14.77	0.37	0.20	3.74	0.17	0.10	0.98	1.00	102.04	FINAL VALUE
	39.61	8.40	17.84	13.23	14.48	0.36	0.20	3.67	0.17	0.10	0.98	1.00		NORM. VALUE
	39.32	8.50	17.89	13.49	14.77	0.71	0.18	3.69	0.17	0.06	0.98	1.00	100.76	RECCOM. VALUE
	0.29	-0.10	-0.05	-0.26	-0.29	-0.35	0.02	-0.02	-0.00	0.04	0.0	0.0		NORM.-RECC.
NIMN	51.41	16.92	9.73	7.35	11.92	2.24	0.28	0.21	0.19	0.05	0.33	0.10	100.74	FINAL VALUE
	51.03	16.79	9.66	7.30	11.84	2.23	0.28	0.21	0.19	0.05	0.33	0.10		NORM. VALUE
	52.64	16.50	8.90	7.50	11.50	2.46	0.25	0.20	0.18	0.03	0.33	0.10	100.59	RECCOM. VALUE
	-1.61	0.29	0.76	-0.20	0.34	-0.23	0.03	0.01	0.01	0.02	0.0	0.0		NORM.-RECC.
W1	51.86	15.13	11.32	6.45	10.99	2.04	0.69	1.06	0.17	0.20	0.53	0.06	100.50	FINAL VALUE
	51.60	15.05	11.27	6.42	10.94	2.03	0.69	1.05	0.17	0.20	0.53	0.06		NORM. VALUE
	52.72	15.02	11.09	6.63	10.98	2.15	0.64	1.07	0.17	0.14	0.53	0.06	101.20	RECCOM. VALUE
	-1.12	0.03	0.18	-0.21	-0.04	-0.12	0.05	-0.02	-0.00	0.06	0.0	0.0		NORM.-RECC.
BHVO	49.74	14.37	11.86	7.35	11.28	2.60	0.48	2.67	0.17	0.23	0.0	0.0	100.75	FINAL VALUE
	49.37	14.27	11.78	7.30	11.19	2.58	0.47	2.65	0.16	0.23	0.0	0.0		NORM. VALUE
	49.90	13.70	12.14	7.20	11.40	2.30	0.53	2.70	0.17	0.28	0.0	0.0	100.32	RECCOM. VALUE
	-0.53	0.57	-0.36	0.10	-0.21	0.28	-0.06	-0.05	-0.01	-0.05	0.0	0.0		NORM.-RECC.

APPENDIX 3

Precision plots for major and trace element precision analysis, after the method of Howarth & Thompson (1976).

(i) Inset on each plot are the duplicate data pairs used in the Precision analysis.

(ii) The upper and Lower precision lines are the 99% and 90% precision lines, respectively.

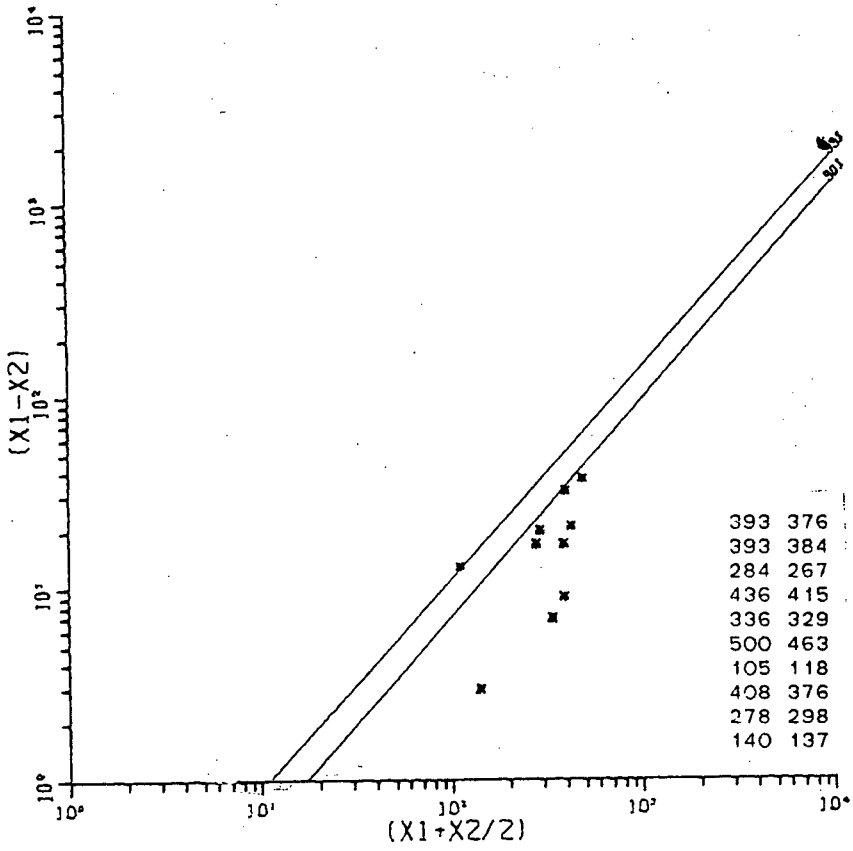

CHROMIUM PRECISION **5%**

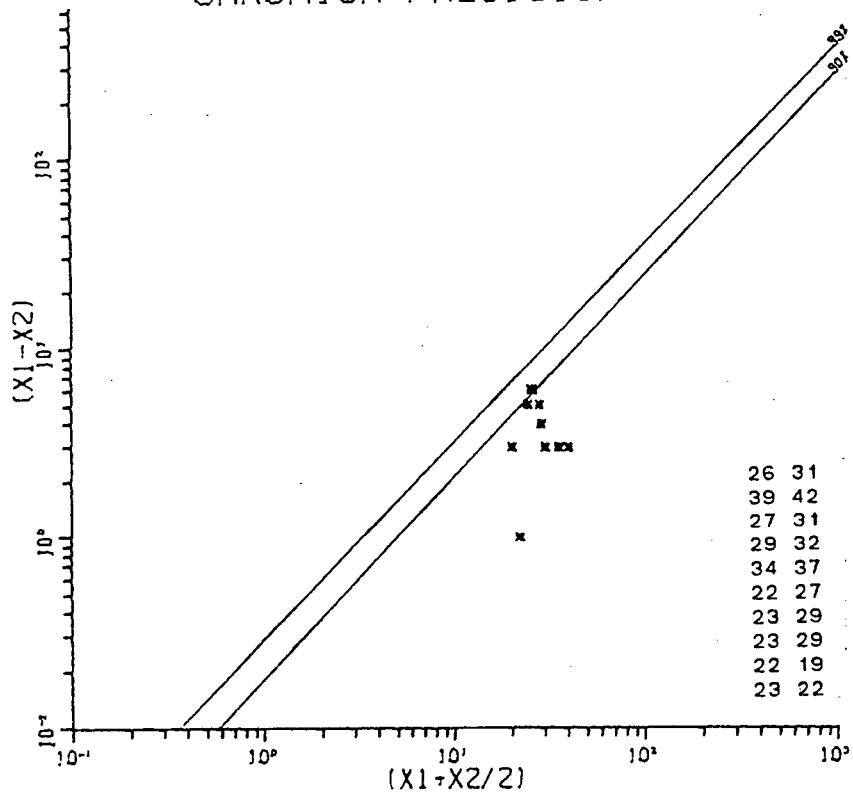

YTTRIUM PRECISION **15%**

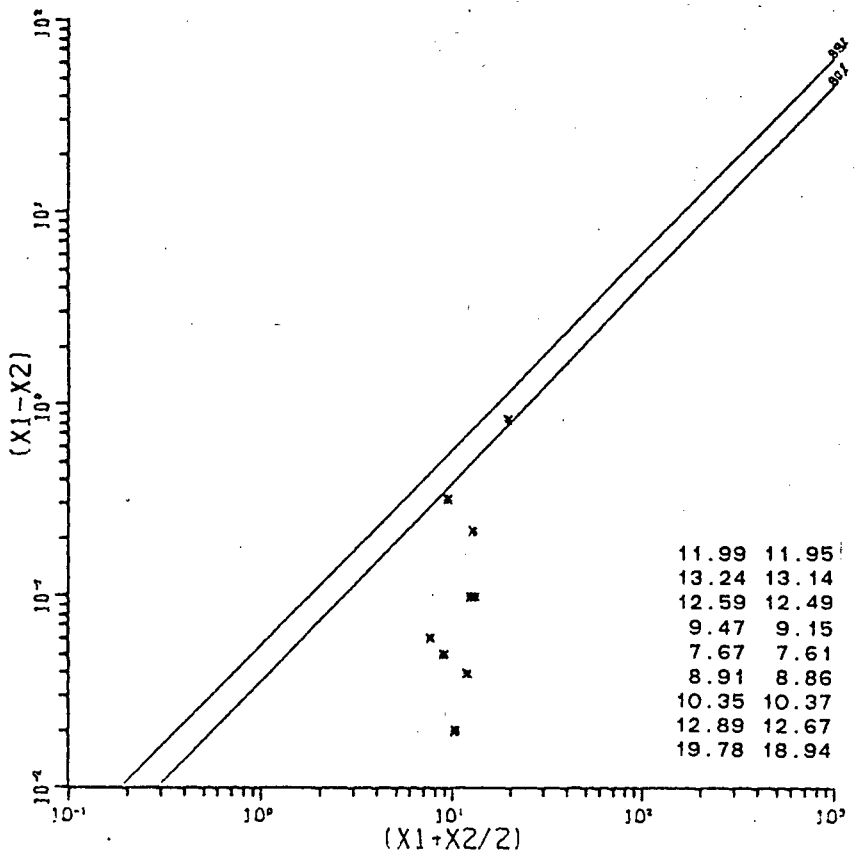

IRON PRECISION **3%**

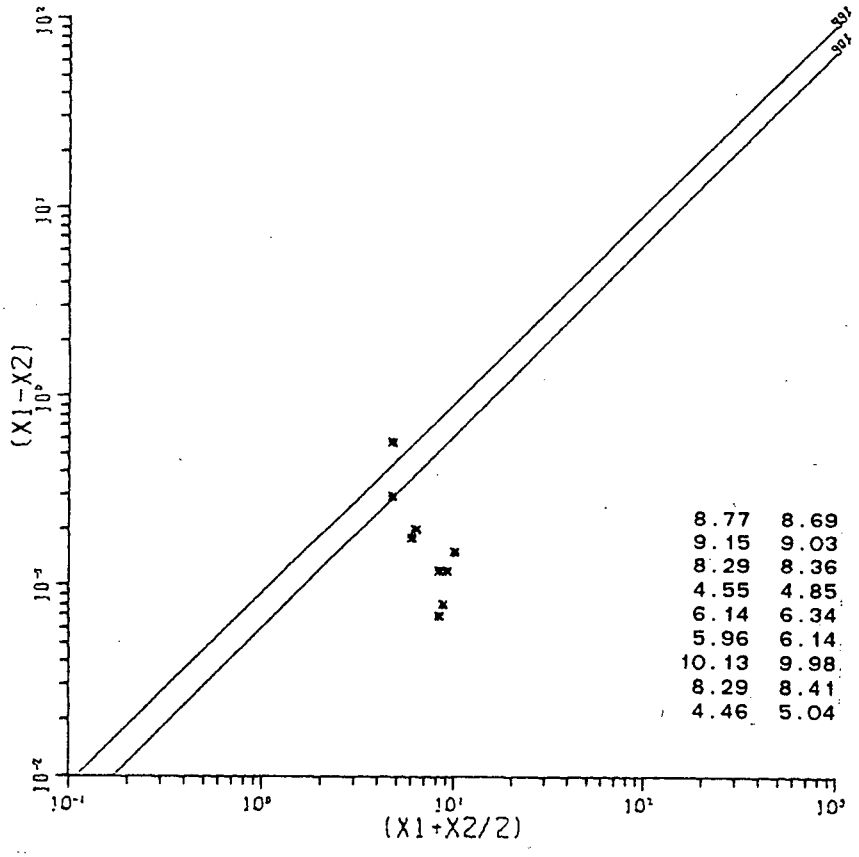

MAGNESIUM PRECISION **5%**

APPENDIX 4

Phillips PW-1410 X-ray fluorescence spectrometer operating conditions for major element and trace element analysis, and description of computer program action used in the reduction of major element XRF data.

ELEMENT	Fe	Fe bkg	Ti	Ti bkg	Ca	Ca bkg	K	K bkg	Si	Si bkg
LINE	Kα	→	→	→	→	→	→	→	→	→
2θ	57.54	56.00	86.25	91.00	113.17	110.40	136.75	132.15	109.14	113.30
TARGET	Cr	—	—	—	—	—	—	—	—	→
CRYSTAL	LiF 200	—	—	—	—	—	—	→	PET	→
kV/mA	50/35	—	—	→	50/16	→	50/35	→	50/40	→
COLLIMATOR	F	—	—	—	—	—	—	—	—	→
COUNTER	F	—	—	—	—	—	—	—	—	→
VACUUM	ON	—	—	—	—	—	—	—	—	→
GAIN	128	—	—	—	—	—	—	—	—	→
COUNTER kV	8.01 x 2	—	—	—	—	—	—	—	—	→
LOWER LEVEL	150	—	—	—	—	—	—	—	—	→
WINDOW	700	—	—	—	—	—	—	—	—	→
COUNT TIME	10 sec	—	—	—	—	—	—	—	—	→

XRF
PRESSED PELLET
ANALYSES

ELEMENT	Al	Al bkg	P	P bkg	Mg	Mg bkg	Na	Na bkg	Mn	Mn bkg
LINE	Kα	→	→	→	→	→	→	→	→	→
2θ	145.19	139.00	89.61	92.60	45.01	44.00	54.96	53.30	63.00	65.00
TARGET	Cr	—	—	—	—	—	—	→	W	→
CRYSTAL	PET	—	—	→	TLAP	—	—	→	LiF 200	→
kV/mA	50/40	—	—	—	—	—	—	—	—	→
COLLIMATOR	C	—	—	—	—	—	—	→	F	→
COUNTER	F	—	—	—	—	—	—	—	—	→
VACUUM	ON	—	—	—	—	—	—	—	—	→
GAIN	128	→	61	→	128	—	—	—	—	→
COUNTER kV	8.01 x 2	—	—	—	—	—	—	—	—	→
LOWER LEVEL	150	→	140	→	150	→	150	—	—	→
WINDOW	700	→	220	→	470	→	700	—	—	→
COUNT TIME	10 sec	—	—	→	100 sec	10 sec	100 sec	10 sec	20 sec	→

COMMENTS

Due to d-spacing temperature dependance of PET crystal 2θ must be determined for each run.

XRF Major Element Analysis Machine Conditions.

MAJOR ELEMENT ANALYSIS

Data Reduction Program Action

(i) Intensity ratios for the standards are regressed against their known chemical analyses and the resulting quadratic equation is applied to the intensity ratios for all standards and unknowns to obtain the first approximate results.

(ii) Total mass absorption coefficients for the standards are calculated from the known chemical analyses and mass absorption coefficients, and are used to generate corrected standard intensity ratios, which are then fitted against the known chemical analyses to derive a new set of quadratic regression line coefficients.

(iii) First approximate results from (i) are used in conjunction with known mass absorption coefficients to generate total approximate mass absorption coefficients for standards and unknowns. A series of ratios, crudely corrected for mass absorption, is then derived for standards and unknowns. The regression coefficients obtained in (ii) are applied to these crudely corrected ratios to obtain a new analytical result, which is then recycled iteratively to generate new mass absorption corrected intensity ratios and a further refined analysis, until successive results (totals) for each sample converge to a difference of less than 0.001 weight % oxide.

(iv) The final, mass absorption corrected analyses for the standards derived in (iii) are regressed against their known chemical analyses. This fit should give straight lines of unit gradient for each element, but minor deviations often occur. Therefore:

(v) Final analytical results are generated by applying the quadratic function of regression from (iv) to the iterated analyses from (iii). In this way, wet chemical discrepancies are smoothed out and each standard is effectively "standardized" against the remainder of the standard block.

For a more detailed program description, and a listing of the program, see van der Heyden (1982).

XRF TRACE ELEMENT ANALYSIS MACHINE CONDITIONS

ELEMENT	SR/RB Sr	Rb	Compton Peak	CE/ND bkg	Ce	Nd	bkg	BA Ti	Ba	bkg
LINE	$K\alpha_1$	$K\alpha_1$			$L\beta_1$	$L\alpha_1$		$K\alpha_1$	$L\alpha_1$	
2θ	25.11	37.93	30.13	Ce-.85	71.62	72.13	Nd+1.3	86.09	87.17	Ba+4.0
TARGET	Molybdenum			Molybdenum				Chromium		
CRYSTAL	LIF(200)	LIF(220)	LIF(220)	LIF(200)				LIF(200)		
kV/mA	60/40			60/40				50/40		
COLLIMATOR	fine			fine				fine		
COUNTER	Scintillation			Flow Proportional and Scintillation				Flow Proportional		
VACUUM	off			on				on		
GAIN	128			128				128		
COUNTER kV	10.9			FPC: 8.4 Sc: 9.5				8.7		
LOWER LEVEL	280			200				360		
WINDOW	420			500				320		
COUNT TIME	3 x 10 secs			40 s.	100 s.	100 s.	40 s.	10 s.	10 s.	10 s.
REDUCTION	Feather and Willis			Berman				Berman		
REMARKS	Duplicates done using Berman method.							Ti correction on Ba.		

	NI			CR/V					
ELEMENT	bkg	Ni	bkg	bkg	Cr	bkg	bkg	V	Ti
LINE		$K\alpha_1$			$K\alpha_{1,2}$			$K\alpha_1$	$K\beta_{1,3}$
2θ	Ni-.63	48.67	Ni+1.37	Cr-2.20	69.36	Cr+1.5	V-1.86	76.89	77.27
TARGET	Molybdenum			Molybdenum					
CRYSTAL	LIF(200)			LIF(200)					
kV/mA	60/40			60/40					
COLLIMATOR	coarse			- - - - - coarse - - - -			- - - -	fine	- - - - -
COUNTER	Flow Proportional and Scintillation			Flow Proportional and Scintillation					
VACUUM	on			on					
GAIN	128			128					
COUNTER kV	FPC: 8.6 Sc: 10.8			FPC: 8.6 Sc: 10.8					
LOWER LEVEL	300			280					
WINDOW	300			440					
COUNT TIME	20 secs.	40	20	40 secs.	100	40	40	100	40
REDUCTION	Berman			Berman					
REMARKS	Use aluminium filter.			Ti interference on V corrected using Ti-spiked pellet. Cr corrected for V interference.					

NB/ZR/Y/SR/RB

ELEMENT	bkg	Nb	Zr	bkg	Y	bkg	Sr	bkg	Rb	bkg
LINE		$K\alpha_1$	$K\alpha_1$		$K\alpha_1$		$K\alpha_1$		$K\alpha_1$	
2θ	Nb-.35	21.36	22.51	Y-.25	23.76	Sr-.70	25.11	Rb-.74	26.58	Rb+.50
TARGET	Tungsten									
CRYSTAL	LIF(200)									
kV/mA	50/40									
COLLIMATOR	fine									
COUNTER	Flow Proportional and Scintillation									
VACUUM	on									
GAIN	128									
COUNTER kV	FPC: 8.6 Sc: 10.95									
LOWER LEVEL	300									
WINDOW	450									
COUNT TIME	20 secs.	40	40	20	40	20	40	20	40	20
REDUCTION	Berman									
REMARKS	Rb interference on Y, Sr interference on Zr corrected using Sr-Rb-spiked pellet.									